APPLICATION OF PHOTOGRAMMETRY FOR MONITORING SOIL SURFACE MOVEMENT

by

ARJAN POUDEL

THESIS

Submitted in partial fulfillment of the requirements for the degree
of Master of Science in Civil Engineering at
The University of Texas at Arlington
MAY, 2023

Arlington, Texas

Copyright © by Arjan Poudel 2023

All Rights Reserved

ACKNOWLEDGEMENTS

I extend my sincere gratitude to Dr. Xinbao Yu, my academic advisor, and supervisor, for entrusting me with the opportunity to conduct this research project. I am grateful for his unwavering support, guidance, and valuable insights that have significantly contributed to the success of this thesis. I also extend my sincere appreciation to the members of my graduate committee, Dr. Nick Fang, and Dr. Md Azijul Islam, for their invaluable feedback and time devoted to reviewing my work.

I would like to sincerely thank my colleague, Mehran Azizian, for his exceptional guidance and support during my research project. His extensive knowledge and experience in the application of photogrammetry in soil have been invaluable. I am also thankful to post-doctoral research associate Dr. Gang Lei for his guidance and assistance throughout my research at the University of Texas at Arlington.

I extend my sincere appreciation to the Texas Department of Transportation (TxDOT) for providing financial support for my research. I am grateful for their support, which has enabled me to pursue my academic and research goals.

I am deeply grateful to my parents, my brother, and my girlfriend for their unconditional love and support. Their unwavering encouragement has been a constant source of inspiration throughout my academic journey. I also extend my heartfelt thanks to my uncles and their wives for their continuous support during my stay and study here in the United States. Last but not least, I owe a debt of gratitude to my friends for making this place feel like a second home.

May 2023

To Mom, My Family, and My Frie

TABLE OF CONTENTS

LIST OF FIGURES

Figure Page

LIST OF TABLES

ABSTRACT

Application of Photogrammetry for Monitoring Soil Surface Movement

Arjan Poudel, MS

The University of Texas at Arlington

Supervising Professor: Dr. Xinbao Yu

Understanding slope behavior and forecasting failure requires accurate soil surface movement measurements. Research gaps and constraints remain despite the development of diverse methods. Recently, photogrammetry has become a promising method for detecting soil surface movement. This method involves setting coded targets and ground points on the soil surface, taking photographs before and after the movement, and using photogrammetric software to measure accurately. However, past studies have mostly used high-end cameras with excellent resolution and geotagging, which may not have been available in all contexts. Thus, this study compares the accuracy and precision of geotechnical soil surface measurement with a consumer-grade DSLR camera. The study shows how photogrammetry with a consumer-grade camera can measure soil surface movement.

This paper presents a study in which photogrammetry was used to measure heave in clayey soil during a pullout test in the lab. The study details the procedures involved in the test, including the placement of the targets and the use of digital dial gauges to obtain measurements. The results show that the photogrammetric approach was successful in obtaining accurate and consistent measurements of heave. This information can be valuable in understanding the behavior of the soil under different conditions and aid in predicting potential soil heave.

In addition, this study also applied photogrammetry in the field to monitor the movement of a particular slope over a period of several months. A 3D model of the slope was built by processing images captured using a consumer-grade camera, and reliable accuracy was achieved. Ground points were observed over a period to monitor the slope. The field results showed that there was no significant movement in the slope during the three-month observation period. The successful application of photogrammetry in this field test demonstrates its potential as a valuable tool for monitoring and analyzing soil surface movement in natural environments.

CHAPTER 1

INTRODUCTION

1.1 Overview

Slope monitoring is a critical process used to evaluate the stability of natural and man-made slopes to ensure the safety of people and infrastructure situated on or near them. Current slope monitoring practices involve various techniques, including field observations, remote sensing, and instrumentation-based monitoring. Field observations entail visually inspecting the slope surfaces, while remote sensing techniques, such as satellite monitoring, use imagery to detect any changes in slope behavior (Osasan & Afeni, 2010). On the other hand, instrumentation-based monitoring requires the installation of devices, such as tiltmeters and piezometers, to measure slope deformation and water pressure. However, each method has its limitations, such as subjectivity in field observations, limited resolution in remote sensing, and cost and specialized expertise requirements in instrumentation-based monitoring (Maloo & Thaker, 2022). Therefore, to ensure stable slopes and minimize potential risks, it is recommended to utilize a combination of these techniques to obtain a comprehensive understanding of slope behavior (Francioni et al., 2014).

Slope stability refers to the ability of a slope to resist sliding and maintain its stability. Driven anchors are commonly used in geotechnical engineering to provide stability and support to structures by transferring loads to the soil. Pullout tests are commonly used to determine the pullout capacity of soils in embedded and driven anchors. In most cases, heave surface movement is measured to assess the performance of anchors using extensometers, displacement transducers, or

settlement plates in laboratory settings, while surveying tools are used in field conditions. However, these methods have limitations as the results only provide an average heave measurement, and sensors can only be placed in a limited number of locations and require skilled surveyors (Asfaw et al., 2023; Matsuoka et al., 2003). Therefore, there is a need for a reliable technique that can measure the entire heave area and provide precise measurements. Texas is one of the states in the United States that is plagued with problems of expansive soils due to severe weather conditions that contribute to the swell-shrink phenomenon. The soil swell and shrinkage affect the safety of public infrastructure like pavement and the foundations of private and corporate buildings (Gautam et al., 2019). Engineers and construction professionals can improve their understanding of soil characteristics and design structures that are better suited to local conditions by measuring the swell heave, highlighting the need for continuous soil surface monitoring to better understand the swelling properties of the heave and shrink in the soil. To achieve this, novel and reliable methods for measuring and monitoring heave include remote sensing techniques like satellite-based interferometry, laser scanning, and photogrammetry, as well as geophysical methods such as ground-penetrating radar and electrical resistivity imaging.

Among these methods, close-range photogrammetry has become a highly precise tool for measuring and analyzing soil surfaces. It provides accurate topographic data and high-resolution 3D models that are useful in agriculture, environmental monitoring, and geosciences. Photogrammetry involves reconstructing 3D models of soil surfaces from overlapping images taken by aerial or ground-based cameras. In the geotechnical field, these models can be used to measure slopes, surface roughness, heave, soil erosion, and other vital parameters essential for the conservation, management, and monitoring of slopes (Eboigbe, 2021; Javadnejad & Gillins, 2016; Luhmann et al., 2013; Shahbazi et al., 2015). Modern cameras equipped with geotagging

capabilities and tracking systems are now easily accessible in the market. These cameras capture images with superior resolution, which can be processed effectively using photogrammetric software to generate 3D models (Štroner et al., 2021). However, research on the application of consumer-grade cameras for this purpose is still limited, which would be particularly suited for small-budget projects.

1.2 Problem Statement

Photogrammetry has been used in geotechnical engineering primarily for creating ground surface contour maps and charting topographic features, with specialized software to produce precise 3D terrain models. However, the process was expensive, time-consuming, and required special tools and knowledge. Furthermore, manually analyzing photographs to produce precise 3D models was prone to errors, making it less useful for routine geotechnical engineering applications.

Recent advancements in computer processing speed and digital imaging have made photogrammetry more widely available and affordable. The use of unmanned aerial vehicles (UAVs) equipped with high-resolution cameras has made it possible to quickly and efficiently record vast terrain areas. Modern software can also analyze the images to produce highly accurate, detailed 3D models. This has made photogrammetry more useful for geotechnical engineering applications.

Although consumer-grade cameras are more accessible and affordable than specialized photogrammetry cameras, their lower resolution and image quality have limited their use in geotechnical engineering. Additionally, the software available to process consumer-grade images may not be optimized for their use. However, as consumer-grade drones and cameras gain

popularity, more researchers are exploring their potential for photogrammetric applications in geotechnical engineering. As such, the current study aims to investigate the feasibility of using consumer-grade cameras for photogrammetric applications in geotechnical engineering and to develop a methodology to improve their accuracy and usability.

1.3 Objective

The primary aim of this study is to investigate the feasibility of utilizing close-range photogrammetry in geotechnical applications, specifically to measure soil surface movements with consumer-grade cameras. The specific objectives can be listed below:

- Measure heave measurement during pullout tests of soil anchors in the laboratory for different embedment depths using images and photogrammetric software.
- Create a 3D model of a river slope using images and photogrammetric software.
- Generate digital elevation models of the ground surface within different periods to detect slope movement.

1.4 Thesis Structure

This thesis consists of five chapters. Chapter 1 of the thesis is an introduction that provides an overview of the research topic, outlines the objectives of the study, and presents an outline of the thesis.

Chapter 2 is a literature review that covers some of the key terms and concepts in photogrammetry, including an introduction to the components of photogrammetry and the

analytical process. The chapter also includes a brief overview of photogrammetric software and previous studies on photogrammetric applications in soil movement.

Chapter 3 is the methodology section which details the methods used to perform laboratory tests and field tests. It provides a comprehensive explanation of the testing procedures and materials used in the study.

Chapter 4 is the result and analysis section. It presents all the results obtained from the laboratory and field tests, compares the findings, and explains the results through illustrations and explanations.

Finally, Chapter 5 is the summary and conclusion section which provides an overview of the study's results and draws conclusions based on the observations made in the laboratory and field. It also provides recommendations for future research.

CHAPTER 2

LITERATURE REVIEW

2.1 Introduction

This thesis uses several terms to discuss photogrammetry, namely, obtaining measurements and data about physical objects and the environment through photographic images and other phenomena. The objectives of this chapter are to provide a clear understanding of these terms. In addition, the different types of photogrammetry, including terrestrial, aerial, and close-range, are briefly discussed. Furthermore, this chapter will also summarize current practices related to slope monitoring and heave measurement in laboratory and field settings. It is essential to understand these practices as they will be referenced throughout the thesis concerning photogrammetry.

The main objective of this chapter is to provide a comprehensive overview of the components necessary for photogrammetry, including image processing, error detection, error elimination, processing stages, geometrical transformations, and other related concepts.

2.2 Slope Stability and Monitoring

Slope monitoring is essential for assessing the stability of natural and human-made slopes to ensure the safety of people and infrastructure. Various types of soil movement are common and can be observed on most river slopes including falling (Hagerty et al., 1981), toppling (Zhu et al., 2020), sliding, flowing, or a combination of these. Different techniques can be used to monitor slope behavior, including visual inspection, inclinometers, ground-based radar, GPS, LiDAR, crack meters, tiltmeters, and vibrating wire piezometers (Jaboyedoff et al., 2012; Kane & Beck,

2000; Racek et al., 2021; Yang et al., 1997). Each method has its strengths and limitations, and the selection of an appropriate method depends on various factors, such as slope characteristics, monitoring objectives, and available resources.

Ground stabilization techniques are necessary to ensure the longevity and safety of structures. Micro-piling, soil nailing, sheet piling, and anchor plate installation are commonly used for this purpose. Percussion-driven earth anchors (PDEAs), as shown in *Figure 1*, are a cost-effective and efficient alternative to other ground anchoring methods, particularly in soft soils. PDEAs can be installed quickly and easily, have a smaller environmental impact, and are highly versatile. Research has shown that PDEAs are highly effective in stabilizing slopes and soil masses, particularly in soft soils, and they are a reliable and cost-effective ground anchoring method for ensuring soil and slope stability in various applications (Asfaw et al., 2023; Asfaw et al., 2023; Baker & Konder, 1966).

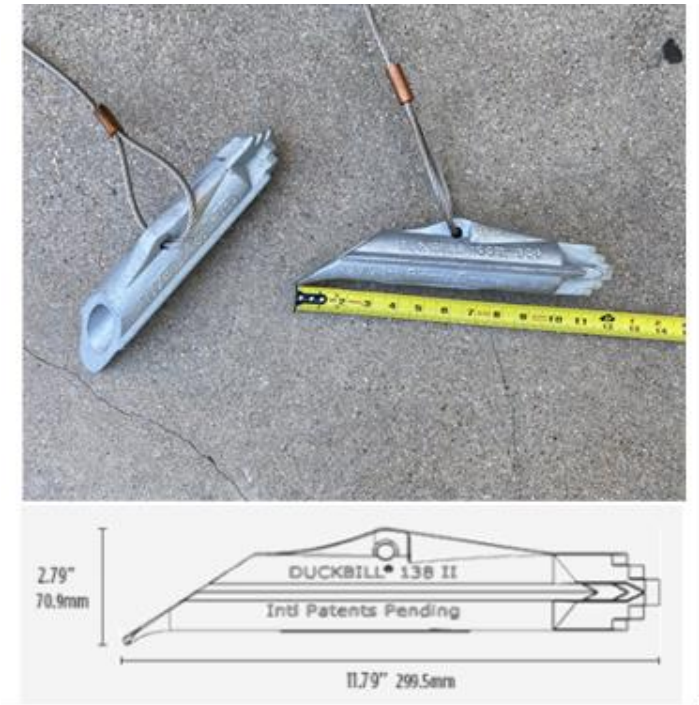

Figure 1: Duckbill 138 II earth anchor (Asfaw et al., 2023)

PDEAs are simple and effective, lightweight, corrosion-resistant products that are suitable for a range of design life requirements. They offer immediate quantifiable loads, making them ideal for temporary and permanent situations. PDEAs have a low environmental impact since they do not require grout, resulting in no curing time, no mess, and no contamination. Therefore, they are a cost-effective and sustainable alternative to traditional anchoring techniques (McWilliam & Paramaguru, 2017).

2.3 Heave Measurement

In geotechnical engineering and geo-environmental engineering applications, heave measurement is a critical factor in anchor pullout tests, which is important for designing stable foundations, retaining walls, and other structures that rely on anchoring. Heave refers to the upward movement or swelling of the soil, and it can increase the resistance to anchor pullout, leading to an overestimation of the soil's pullout capacity. This can result in the selection of an undersized anchor for the required load capacity, which could compromise the stability and safety of the structure.

To prevent heave and ensure accurate pullout capacity measurements, engineers use different methods, such as soil columns with scales or displacement transducers, surveying, remote sensing, and tiltmeters. Tiltmeters are devices that can detect changes in the angle of a structure or object and can be used to measure heave by monitoring the angle of a structure embedded in the soil. Overall, determining the pull-out capacity of soil and measuring heave during anchor pullout tests are crucial in selecting the appropriate anchor type, size, and spacing to ensure sufficient

resistance to pullout forces, which helps ensure the safety and longevity of the structure (Matsuoka et al., 2003; Tang et al., 2009). However, measuring heave can be a challenging task due to limitations in instrumentation and project budget, and photogrammetry may offer a powerful alternative tool for geotechnical applications.

2.4 Photogrammetry

According to Wolf et al. (2014), photogrammetry is a multidisciplinary field combining art, science, and technology to obtain reliable information about physical objects and the environment through recording, measuring, and interpreting photographic images and patterns of recorded radiant electromagnetic energy and other phenomena. To gather measurements and data about an object, photogrammetry analyzes the change in position from at least two different images, using techniques such as perspective, advanced processing software, and photo analysis, both on the ground and from the air. Taking photos from various locations and angles can make precise calculations using methods such as photo interpretation and geometric relationships. Analysts can create shapes, maps, and 3D models of real-world scenes with the data obtained through photogrammetry.

Photogrammetry has been widely used in various fields, such as geology, archaeology, architecture, and civil engineering, to collect and analyze data. For example, in geology, photogrammetry has been used to study geological formations and measure the topography of the earth's surface (Honarmand & Shahriari, 2021). In archaeology, photogrammetry has been used to create 3D models of ancient sites and artifacts (Howland et al., 2014). Finally, in architecture and civil engineering, photogrammetry has been used to create accurate as-built drawings and models, assess building damage, and plan renovations (Maas & Hampel, 2006; Shashi & Jain, 2007). The

advancements in photogrammetry technology have led to the development of new techniques and tools, such as unmanned aerial vehicles (UAVs) and laser scanning, which have improved the accuracy and efficiency of photogrammetric data collection and analysis (Puliti et al., 2020). In addition, photogrammetry has been integrated with other technologies, such as geographic information systems (GIS), to create accurate and detailed maps and data visualizations (Jensen et al., 2009).

Furthermore, photogrammetry has been used in disaster response and management to assess the damage, create damage assessment maps, and plan recovery efforts (Mandirola et al., 2021). In agriculture, photogrammetry has been used to monitor crop growth and yields and to create digital elevation models of fields for irrigation management (Ballesteros et al., 2015; Zhang et al., 2018). The versatility and applicability of photogrammetry make it a valuable tool in a wide range of fields and industries.

2.4.1 Types of Photogrammetry

Photogrammetry can be broadly categorized into aerial photogrammetry and terrestrial photogrammetry. Aerial photogrammetry is a commonly used method for mapping and surveying large areas whereas, terrestrial photogrammetry is a form of photogrammetry that involves capturing images of objects or structures from a stationary position on the ground using a camera.

2.4.1.1 Aerial Photogrammetry

Aerial photogrammetry is a widely used method for mapping and surveying large areas. The process involves capturing aerial images of the ground using cameras mounted on aircraft or

drones. These images are then processed using specialized software to create detailed maps and 3D models of the area. With the advent of unmanned aerial vehicles (UAVs) and drones, aerial photogrammetry has become more accessible and cost-effective for various applications (Westoby et al., 2012).

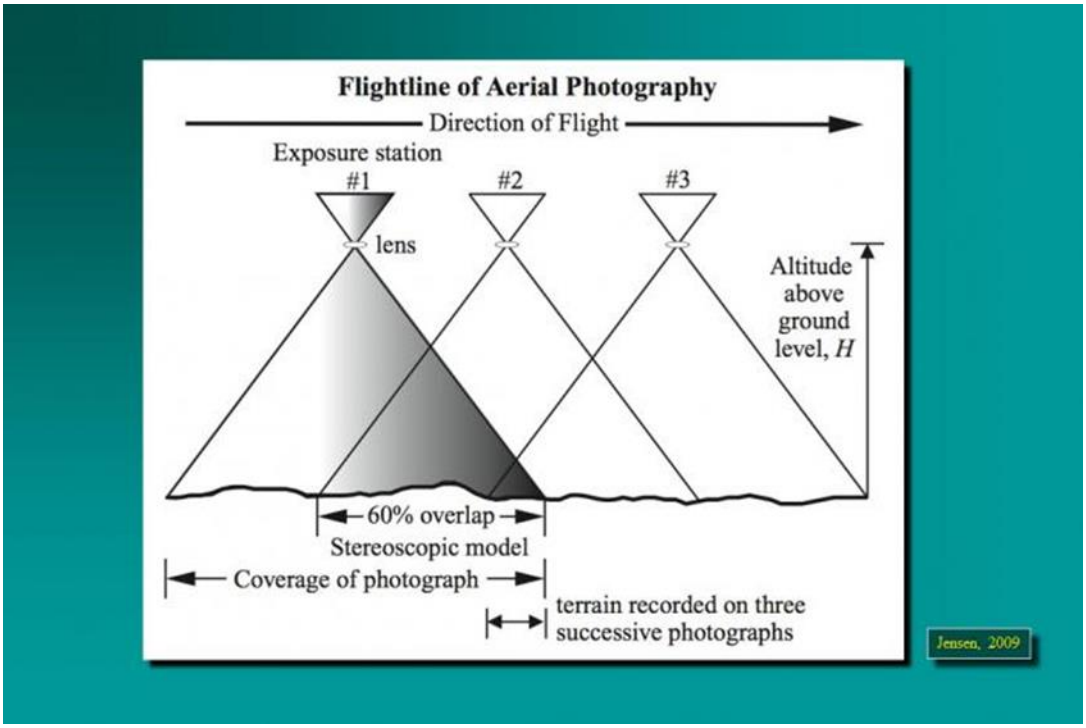

Figure 2: Aerial photogrammetry, Jensen 2009

Aerial photogrammetry has been applied in various fields, such as disaster management (Mandirola et al., 2021), environmental monitoring (Ballesteros et al., 2015; Puliti et al., 2020), urban planning (Balsa-Barreiro & Fritsch, 2018; Shashi & Jain, 2007), and agriculture (Ballesteros et al., 2015). By providing high-resolution and up-to-date information, aerial photogrammetry offers a valuable tool for decision-making in these fields.

Aerial photogrammetry is closely related to remote sensing, which involves the collection

of data from a distance using sensors mounted on aircraft, satellites, or other platforms. Remote sensing and aerial photogrammetry are complementary techniques, with remote sensing providing broader spatial coverage and aerial photogrammetry offering higher spatial resolution and accuracy (Jensen et al., 2009). A flight line of aerial photography with overlapping images is shown in *Figure 2*.

2.4.1.2 Terrestrial Photogrammetry

Terrestrial photogrammetry is a form of photogrammetry that involves capturing images of objects or structures from a stationary position on the ground using a camera. It has been used in various applications, including architecture, engineering, and cultural heritage preservation (Balsa-Barreiro & Fritsch, 2018). The images captured are processed using specialized software to create 3D models and maps of the object or structure. Terrestrial photogrammetry offers high accuracy and flexibility, allowing for precise measurement and documentation of complex shapes and details (Bolognesi et al., 2014). In addition, it has become more accessible with low-cost cameras and software, making it a cost-effective alternative to traditional measurement methods.

Terrestrial photogrammetry has been used in various fields, such as archaeology, geology, and industries (Bolognesi et al., 2014; Fraser & Brown, 1986; C. Wang et al., 2015). By providing accurate and detailed information, terrestrial photogrammetry offers a valuable tool for visualization, analysis, and decision-making in these fields.

2.4.2 Close-Range Photogrammetry

Close-range photogrammetry, also a special case of terrestrial photogrammetry, involves

collecting and processing photogrammetric data at a close distance from the object of interest. While terrestrial photogrammetry is often used to produce maps and land features, close-range photogrammetry is typically limited to smaller objects and areas(Bolognesi et al., 2014). According to Luhmann (2010), close-range photogrammetry refers to measurements taken at distances of less than 200 feet. However, the use of the close range is expanded even to slope monitoring (Stylianidis et al., 2003). This method is commonly used for industrial measurement, cultural heritage documentation, and medical imaging (Luhmann et al., 2013) as shown in *Figure 3*.

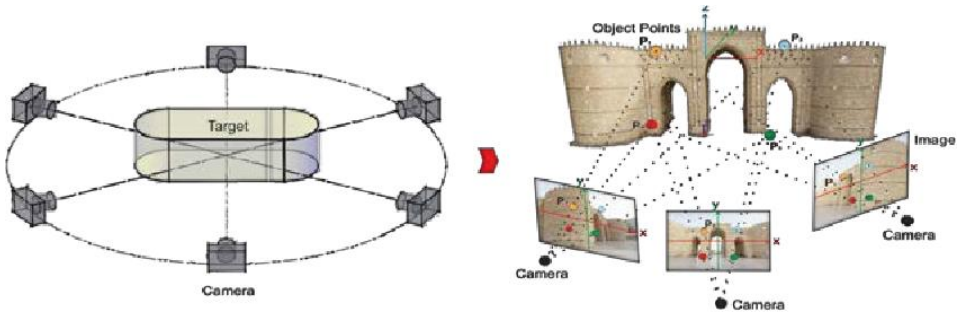

Figure 3: Close range photogrammetry (Luhmann et al., 2013)

The primary goal of close-range photogrammetric measurements is to reconstruct an object in either digital or graphical form, with accuracy levels ranging from under 0.1mm in the manufacturing industry to around 1cm in the construction industry(Luhmann, 2010). Additionally, this technique has strong ties to digital image processing, geographic information systems (GIS), mapping, computer graphics and computer vision, computer-aided design (CAD), and digital image processing. A typical flow diagram of photogrammetry is presented below in *figure4*.

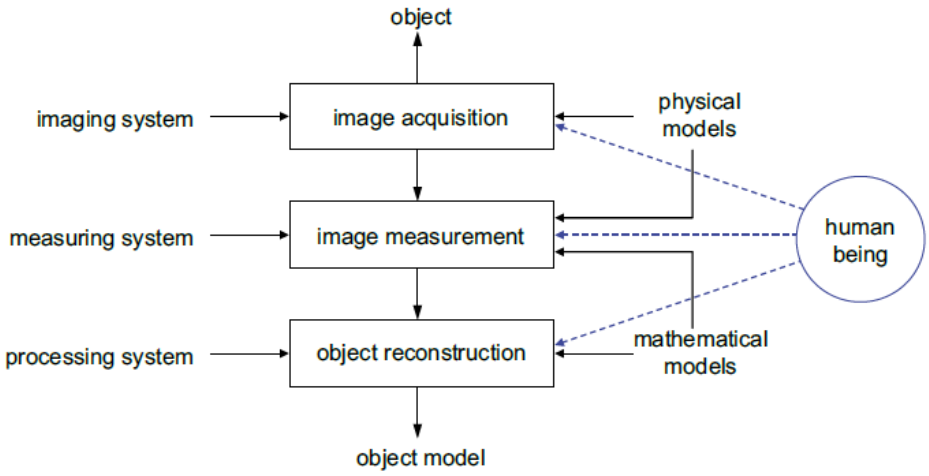

Figure 4: Photogrammetric process (Luhmann et al., 2013)

2.4.3 Camera, Sensor, and Lens

A camera is an electronic device that captures images by recording light onto a physical medium such as a sensor or film, with the lens playing a crucial such in close-range measurement, collecting and focusing light from the scene onto the image capture mechanism.

2.4.3.1 Camera and Sensor

A camera captures images by recording light onto a physical medium such as a sensor or film, with the lens playing a crucial role in focusing light onto the image capture mechanism. The quality and type of lens used can significantly impact image quality, with high-quality lenses offering better sharpness, contrast, and overall image quality (Adams, 2018; Baxter et al., 2009). In digital cameras, as shown in *Figure 5*, the image is recorded onto a sensor, which consists of tiny photosites that capture light and convert it into digital information for processing by the camera's electronics (Luhmann et al., 2016).

Figure 5: Canon 850D DSLR

Camera sensors, such as CCD and CMOS, convert light into electrical charges or digital signals, respectively, and have their strengths and weaknesses. CCD sensors are generally better suited to low-light environments, while CMOS sensors offer better overall performance and lower power consumption(Waltham, 2013). The size of the sensor is an essential factor in determining image quality, with larger sensors having larger photosites, resulting in higher resolution and better overall image quality due to their ability to capture more light with less noise and better dynamic range (Luhmann et al., 2016; Parulski, 1985) noted that a camera sensor comprises of millions of tiny photosites that are sensitive to light and record what is being seen through the lens.

2.4.3.2 Lens and Optical Terminologies

Close-range measurement and imaging technologies are crucial in the measurement process as they impact object preparation, image acquisition, and image content analysis. The lens is a crucial component of imaging technologies for close-range measurement, collecting and focusing light from the scene onto the image capture mechanism. High-quality lenses significantly impact image quality, and understanding lens properties, such as focal length, aperture, depth of field, and distortion, is critical to achieving better results in photogrammetric applications. Lens

aberrations, such as chromatic and spherical aberration, can affect image quality, but these aberrations can be overcome with complex optical arrangements and coatings(Baxter et al., 2009; Luhmann et al., 2013; Ricolfe-Viala & Sánchez-Salmerón, 2010).

To understand the lens, some basic terms related to the lens are discussed. The center of curvature of a lens is the center of the sphere of which a lens is a part, denoted as C1 and C2 for concave and convex lenses respectively. The focus is the point where light rays converge after passing through a lens, and the optical center is the lens's central point where light rays pass through without deviation. The principal axis is an imaginary straight line that passes through the center of curvature of a lens, dividing it into two symmetrical halves, and the radius of curvature is the distance between the center of the lens and the point at which parallel light rays converge after passing through the lens. Focal length, the distance between the lens's optical center and the camera's image sensor, as shown in *Figure 6*, determines a lens's angle of view and magnification (Adams, 2018).

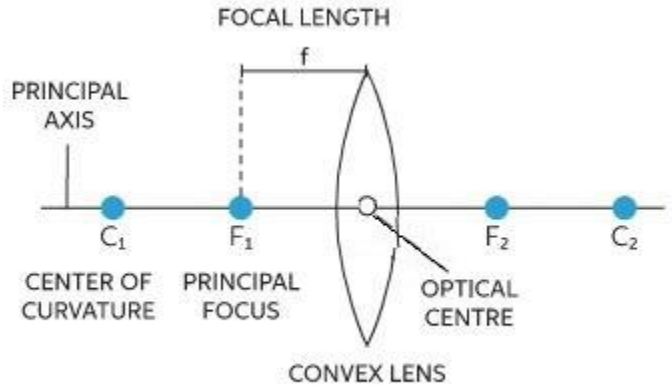

Figure 6: Convex lens diagram

Aperture, depth of field, ISO, and shutter speed are collectively known as the "exposure triangle" in photography. These four elements work together to control the amount of light that enters the camera and ultimately determine the exposure of the image as shown in *Figure 7-9*.

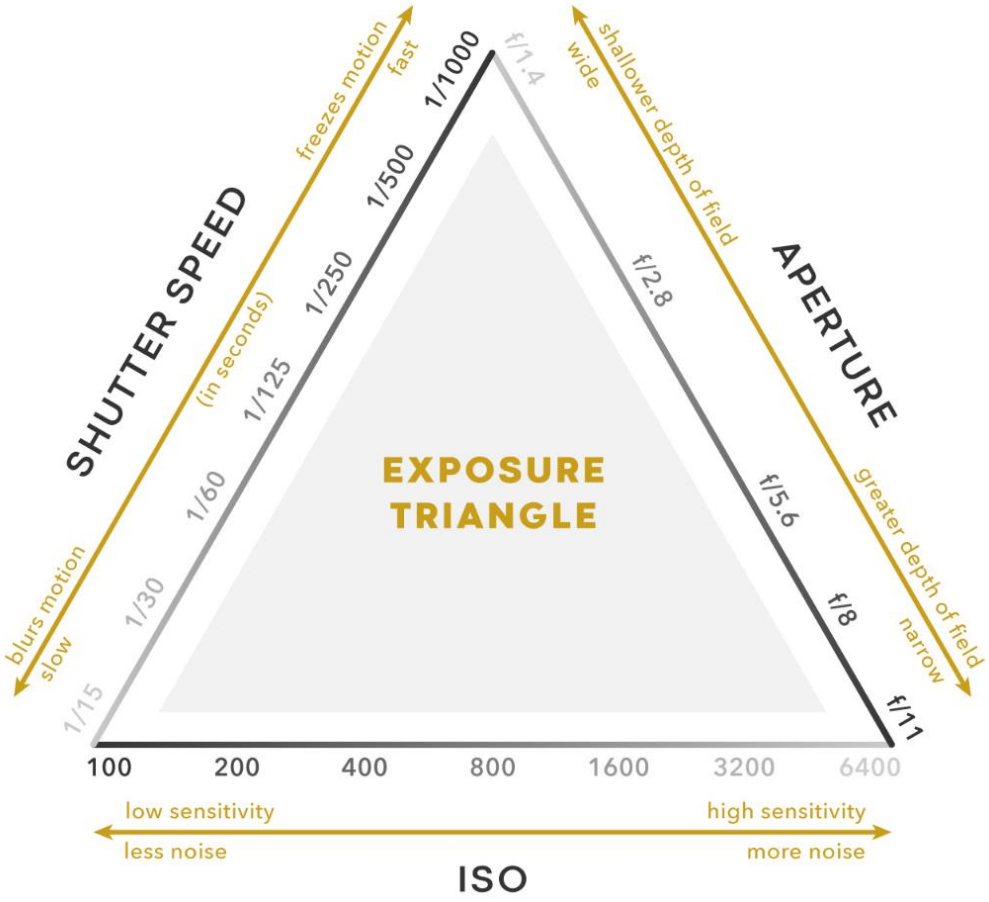

Figure 7: Exposure Triangle. Source: Polarpro.com

Aperture is a term used in photography that describes the opening of a lens's diaphragm, which controls the amount of light that passes through the lens. The aperture can be adjusted to add depth to photos and to control the exposure of an image, making it brighter or darker. Using higher f-numbers, denoting small aperture size, can produce sharper images with a high depth of field, capturing details in the foreground and the background. However, this can result in darker

photos, requiring a slower shutter speed. Conversely, lower f-numbers can create a blurred background effect (Westoby et al., 2012).

The depth of field is the distance range that appears in focus in a scene and is influenced by the aperture, focal length, and distance to the subject. Larger apertures result in a shallower depth of field, while smaller apertures result in a deeper depth of field. Longer focal lengths tend to produce a shallower depth of field, while shorter focal lengths produce a deeper depth of field. The relation of depth of field with varying aperture size is explained in the figure.

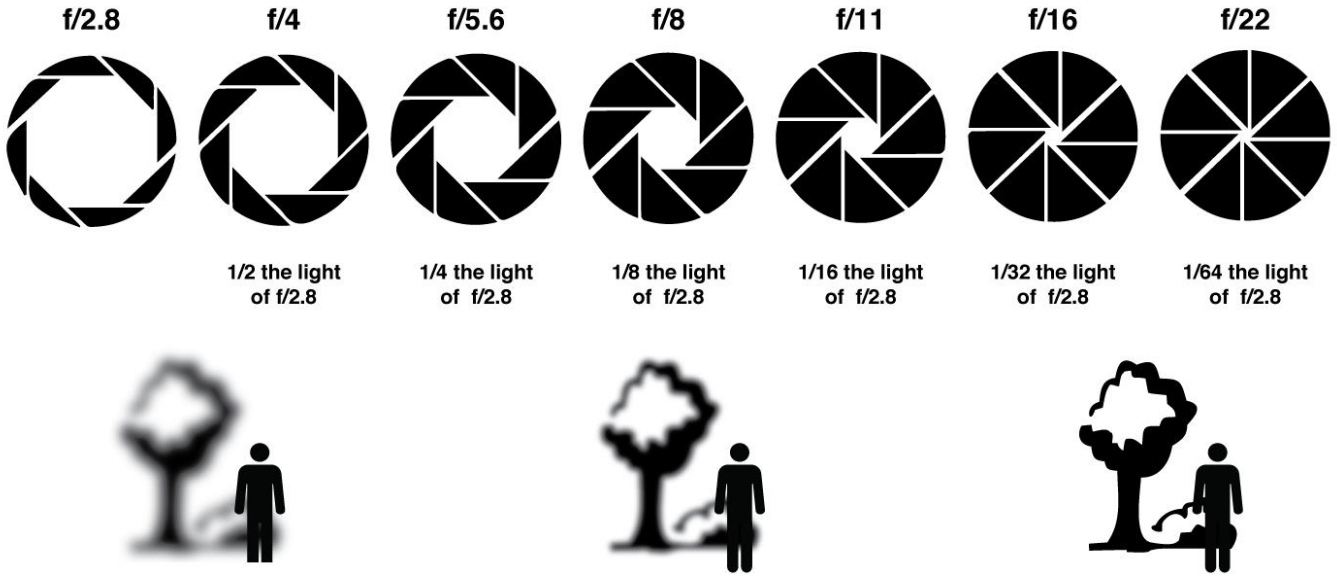

Figure 8: Aperture size and Image quality, Source: facweb.cs.depaul.edu

ISO is the camera's sensitivity to light as it pertains to either film or a digital sensor. A lower ISO value means less sensitivity to light, while a higher ISO means more sensitivity. ISO is simply a camera setting that will brighten or darken a photo (Nex & Remondino, 2014) Optimally, you should always try to stick to the base ISO (lower ISO) to get the highest image quality as higher ISO values produce more noise.

In photography, the shutter speed refers to the length of time that the camera's shutter remains open when taking a picture, which helps control the amount of light that is captured and allows for motion to be either frozen or blurred. Typically measured in fractions of a second, a slower shutter speed allows more light to be captured and produces motion blur, while a faster shutter speed captures less light and freezes movement as shown in the figure. Slow shutter speeds are commonly used in low-light conditions or to capture motion blur, while fast shutter speeds are preferred for photographing fast-moving subjects (Sagers & Patterson, 2012).

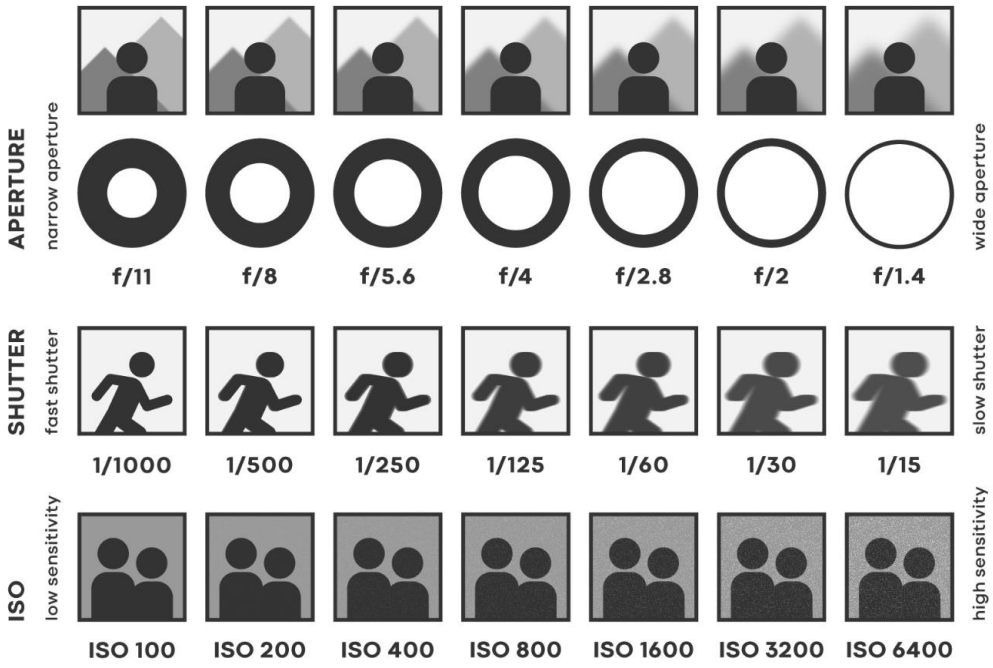

Figure 9: Variability of Images with Aperture, Shutter Speed and ISO. Source: Polarpro.com

2.4.3.3 Image Settings for image acquisition

To ensure proper image matching and reconstruction, it is recommended to capture more photos than necessary with sufficient overlap. The object of interest should occupy a large portion of the image, with missing parts captured in other images. Good lighting is important, but flash should be avoided, and ground control points should be evenly spread in aerial photogrammetry for proper geo-referencing. To minimize camera movement and ensure image consistency, a tripod or stabilizer should be used, and calibration pattern sets may be necessary for close-range photogrammetry. Textured, shiny, highly reflective or transparent objects, unwanted foregrounds, moving objects within the scene, and flat objects or scenes should be avoided. The camera should be set to take images at the maximum possible resolution, with the lowest ISO to reduce noise. The aperture value should be high enough to capture sharp photos with sufficient focal depth, while the shutter speed should not be too slow to avoid blur (Luhmann et al., 2013; Nex & Remondino, 2014; Rottensteiner et al., 2014; Szeliski, 2010; Westoby et al., 2012).

2.4.3.4 Distortion and Camera Calibration

Distortion in photogrammetry refers to the alteration of the image shape or size compared to the original scene, caused by lens design, manufacturing, or alignment issues. Camera calibration is a crucial step in photogrammetry to determine the intrinsic and extrinsic parameters of the camera, including focal length, the position of the principal point, and lens distortion (Ricolfe-Viala & Sánchez-Salmerón, 2010). Calibrating the camera is essential to ensure the accurate reconstruction of 3D models from the captured images. Without proper calibration,

images may have varying characteristics that can lead to inaccurate results, such as perspective distortion, radial distortion, and chromatic aberration. The calibration process involves capturing images of a calibration target with known dimensions and using specialized software like Agisoft Metashape Professional to determine the camera's intrinsic and extrinsic parameters. Once calibrated, the camera can be used to capture images for photogrammetric processing with increased accuracy and consistency (Lin & Shih-Hong, 2012; Luhmann et al., 2016; Manual, 2022).

2.4.4 Targets

Using targets in photogrammetry is a crucial step for obtaining accurate and reliable measurements. According to the literature, defining a set of points to track and fixing a target in correspondence with each point is essential to ensure stability during the entire observation period (Balsa-Barreiro & Fritsch, 2018). Targets with a unique shape or pattern aid in automatic recognition and measurement in images, especially for identifying specific features of the object being measured, which may be challenging to locate due to low contrast and variability in appearance (Elkhrachy, 2021). Targets also serve as control points for geodetic measurement and can improve accuracy, particularly when using multiple cameras observing an object from different viewing directions, by providing more tie points to the object being measured (Q. Wang et al., 2022). Additionally, the use of targets reduces the time and effort required for manual identification and measurement (Maas & Hampel, 2006). Targets can have different shapes and patterns, such as circular, spherical, patterned, coded, or even probes and hidden-point devices (Q. Wang et al., 2022). The selection of a target type depends on the application and the characteristics of the object being measured. Two different types of targets are shown in *Figure 10*.

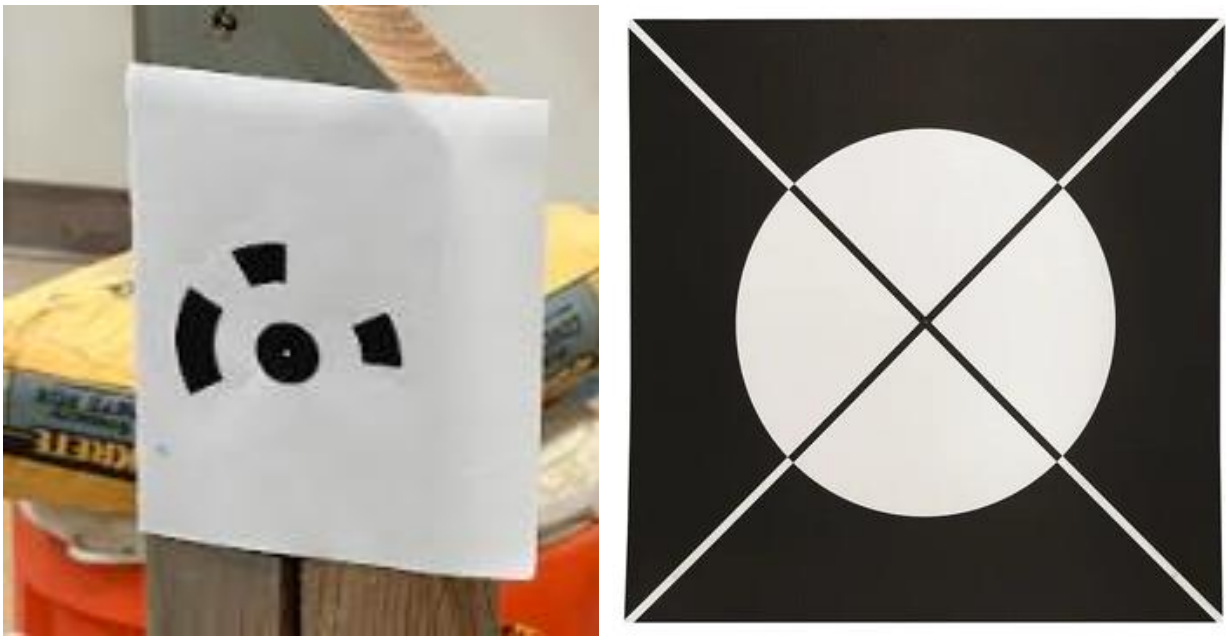

(a) (b)

Figure 10: (a) Schneider centripetal circle coded target and (b) Ground control target

2.4.5 Image Transformation

One of the fundamental aspects of photogrammetry is the establishment of an accurate and reliable coordinate system, which enables precise measurements of features and objects within the images. This involves the application of mathematical concepts such as triangulation, which allows the determination of the location of an object in 3D space based on the angles between the object and two or more known points. The coordinate system is essential for accurate measurement and mapping, and it is used to define the position and orientation of the camera relative to the objects being imaged (Luhmann et al., 2016).

In addition to the coordinate system, photogrammetry also involves the use of mathematical methods to transform the images into useful data. This process includes rectifying

the images to account for distortions caused by the camera lens, as well as calculating age resolutions and scales (Guindon, 1997; Ricolfe-Viala & Sánchez-Salmerón, 2010). To ensure the accuracy of the resulting data, photogrammetric methods also incorporate error calculations and bundle adjustments using least square methods(Fryer & Kniest, 1985; Lin & Shih-Hong, 2012). These calculations help to identify and correct any errors or discrepancies in the measurements, ensuring that the final product is as accurate and reliable as possible.

2.4.5.1 Coordinate System

Photogrammetry uses different coordinate systems to establish a relationship between images, cameras, and objects. The pixel coordinate system, as shown in *Figure 11*, stores digital image data in rows and columns, and is a left-handed system with its origin at the upper left element. The image coordinate system is a two-dimensional right-handed rectangular Cartesian coordinate system, with its origin set at the center of the image as shown in the figure. Extending the image coordinate system with a z-axis perpendicular to the image plane leads to the establishment of the camera coordinate system, which is a 3D coordinate system that originates at the perspective center O'. These coordinate systems enable establishing relationships between the image plane, the camera, and the object being measured.

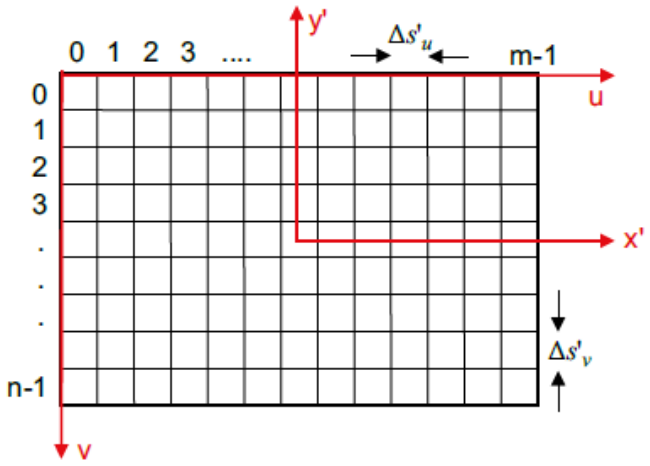

Figure 11: Pixel coordinate system (Luhmann et al., 2013)

The model coordinate system describes the relative position and orientation of two or more images' image coordinate systems. Its origin is usually at the perspective center of one of the images. The object coordinate system, also known as the world coordinate system, is defined by the object's reference points in a spatial Cartesian coordinate system XYZ. Each of these coordinate systems serves a unique purpose in photogrammetry and is essential for establishing accurate and reliable measurements (Luhmann et al., 2013).

Homogeneous coordinates, utilized in computer graphics and photogrammetry, are an extension of Cartesian coordinates that represent 3D points in space. In this system, each point in 3D space is represented as a four-dimensional vector, [X, Y, Z, W], where X, Y, and Z are the spatial coordinates and W is a scaling factor. The scaling factor is used to represent the point at infinity, which is not possible in Cartesian coordinates. Homogeneous coordinates make it possible to use matrix transformations, including translation and rotation, through the multiplication of the point's coordinates by a transformation matrix. This simplifies calculations and transformations on sets of points (Grussenmeyer & Khalil, 2002).

$$X = \begin{bmatrix} x \\ y \\ z \\ 1 \end{bmatrix} = \lambda \begin{bmatrix} x \\ y \\ z \\ w \end{bmatrix}$$

2.4.5.2 Transformation of coordinates

Transformation of coordinates is essential in photogrammetry as it enables the integration of data from different sources, such as images from multiple cameras or surveying data, into a unified coordinate system. By transforming coordinates between different coordinate systems, it is possible to align data accurately and create a consistent and reliable 3D model. This is crucial for various applications in photogrammetry, including mapping, surveying, and modeling of objects or landscapes.

In photogrammetry, there are different types of coordinate transformation methods used to transform points from one coordinate system to another. Similarity transformation preserves the ratio of distances between points and the angles between lines in the original coordinate system. It includes scaling, rotation, and translation but does not include shearing or distortion. Similarity transformations are useful when dealing with 2D images, especially for orientation purposes. They are commonly used in the alignment of two or more images, image matching, and image registration. It involves four parameters, consisting of two for translation, one for rotation, and one for scaling factor. The matrix notation can be expressed as:

$$\mathrm{X} = \mathrm{m} \cdot \mathrm{R} \cdot \mathrm{x} + \mathrm{X0}$$

$$\begin{bmatrix} X \\ Y \end{bmatrix} = m. \begin{bmatrix} Cos\ \alpha & -Sin\ \alpha \\ Sin\ \alpha & Cos\ \alpha \end{bmatrix} \begin{bmatrix} x \\ y \end{bmatrix} + \begin{bmatrix} X_o \\ Y_o \end{bmatrix}$$

Similarly, for the reverse transformation of coordinates from the target system into the source system (to obtain x in previous equation):

$$x = \frac{1}{m} R^{-1}.(X - X_o)$$

$$\begin{bmatrix} x \\ y \end{bmatrix} = \frac{1}{m} \begin{bmatrix} Cos\ \alpha & Sin\ \alpha \\ -Sin\ \alpha & Cos\ \alpha \end{bmatrix} \begin{bmatrix} X - X_o \\ Y - Y_o \end{bmatrix}$$

On the other hand, affine transformations are linear transformations that preserve parallelism, ratios of distances, and include translation. They also include stretching, shearing, and reflection. Affine transformations can be represented by a matrix multiplication of the original coordinates and a transformation matrix. They are useful in image rectification, image warping, and feature extraction from images. In matrix notation the affine transformation is written as:

$$X = A.x + a$$

$$\begin{bmatrix} X \\ Y \end{bmatrix} = \begin{bmatrix} m_x Cos\ \alpha & -m_y Sin\ (\alpha + \beta) \\ m_x Sin\ \alpha & m_y Cos\ (\alpha + \beta) \end{bmatrix} \begin{bmatrix} x \\ y \end{bmatrix} + \begin{bmatrix} X_o \\ Y_o \end{bmatrix}$$

For the reverse transformation from coordinates in the target system to coordinates in the source system:

$$x = A^{-1}.(X - a)$$

In addition, Polynomial transformations are non-linear transformations that can correct image distortion caused by various factors. They are based on a mathematical model that uses polynomial functions to map image coordinates to new coordinates using control points. Polynomial transformations are more flexible than affine transformations and can correct more

complex distortions, such as barrel and pincushion distortions in images captured with wide-angle lenses, preserving object shape better. For two-degree polynomial n=2,

$$X = a00 + a10 \cdot x + a11 \cdot y + a20 \cdot x2 + a21 \cdot x \cdot y + a22 \cdot y2$$

$$Y = b00 + b10 \cdot x + b11 \cdot y + b20 \cdot x2 + b21 \cdot x \cdot y + b22 \cdot y2$$

Finally, Projective transformations, shown in *Figure 12*, also known as homography transformations, are non-linear transformations used to map points between two projective spaces. They are used in 3D reconstruction and perspective distortion correction. After linearization of the equation of the transformation model, we get:

$$a_0 + a_1x + a_2y - X - c_1xX - c_2yX = 0$$

$$b_0 + b_1x + b_2y - Y - c_1xY - c_2yY = 0$$

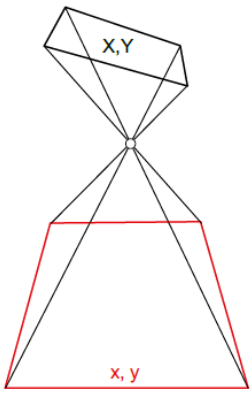

Figure 12: Projective Transform

2.4.5.3 Rotation of coordinates

In photogrammetry, rotation is a crucial operation that helps to align multiple images of the same object or scene. To accurately measure the position and shape of an object, its images

from different angles must be oriented and transformed into a common reference system. This process requires the application of spatial rotations to align the images, which involves changing their orientation relative to each other.

Rotations are based on the principle of transforming a coordinate system in three-dimensional space by rotating it about one or more axes. The three axes of rotation, x, y, and z are defined relative to the object's position and orientation as shown in *Figure 13*. The rotation can be described using Euler angles or rotation matrices, which specify the amount and direction of the rotation about each axis. These rotations can be performed successively to achieve the desired transformation.

Spatial rotations are essential in photogrammetry because they allow the images to be aligned and corrected for differences in position and orientation. This alignment is necessary to create accurate 3D models of objects or scenes from multiple images. Additionally, rotation is used in image stabilization to correct for camera motion and in feature detection algorithms to identify and track objects in images.

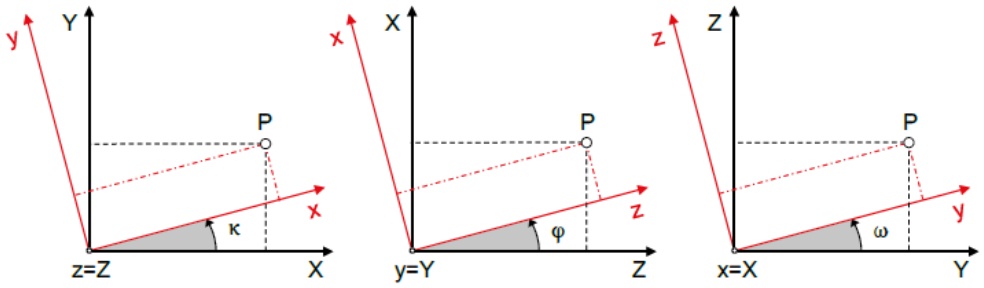

Figure 13: Rotation in Each Axes

2.4.6 Analytical Methods

To identify the image of an object point, it is essential to use image interpretation and measurement techniques that allow the identification of the object's form, brightness, or color distribution. To obtain values for each image point, radiometric and geometric data in terms of intensity, grey value, color value, and position in the image are necessary. To achieve this, measurement systems with appropriate geometric and optical quality must be used. Once these measurements are obtained and a mathematical transformation between the image and object space is established, it becomes possible to model the object accurately (Luhmann et al., 2013). In close-range photogrammetry, the analysis process can be broken down into several stages (Wolf et al., 2014).

The first stage involves providing information about the object being studied, such as reference points, distances, and other geometric elements. The second stage involves measuring image points for orientation, which provides information about the image coordinates. The third stage involves calculating orientation parameters, including both interior and exterior orientation. Finally, the object can be reconstructed from the oriented images, resulting in new points and geometric elements.

Overall, close-range photogrammetry involves a complex and multi-stage analysis process that requires careful attention to object and image data to generate accurate reconstructions Two commonly used analytical methods in photogrammetry are bundle adjustment and image feature matching.

2.4.6.1 Bundle adjustment for close-range photogrammetry

According to J. Y. Lin & Shih-Hong, 2012, bundle adjustment is a widely used method in analytical photogrammetry, which utilizes the least squares method to solve redundant observation equations and calculates object coordinates and exterior orientation parameters from overlapped and unlimited numbers of images. In close-range photogrammetry, bundle adjustment is commonly used to handle the tilted and infinite number of images as seen in *Figure 14*. It involves refining the 3D coordinates, the parameters of the relative motion, and the optical characteristics of the camera employed to acquire the images, given a set of images depicting several 3D points from different viewpoints. Bundle adjustment is a simultaneous process that combines all these parameters, resulting in a more accurate and reliable reconstruction of the object being imaged. The general equation for bundle adjustment can be expressed as follows:

$$Minimize: \Sigma_i \Sigma_j |x_{ij} - P(X_j, R_i, t_i|^2$$

Where:

- i indexes the images
- j indexes the points
- x_{ij} is the observed 2D projection of the j-th point in the i-th image
- P is the projection function that maps a 3D point X_j into the i-th image plane, given the camera parameters R_i (rotation matrix) and t_i (translation vector)
- $|x_{ij} - P(X_j, R_i, t_i|^2$ denotes the squared Euclidean distance between the observed point and the projected point.

The objective of bundle adjustment is to find the optimal values of the camera parameters R_i and t_i and the 3D point coordinates X_j that minimize the sum of squared reprojection errors over all image observations. This is typically solved using nonlinear least squares optimization algorithms.

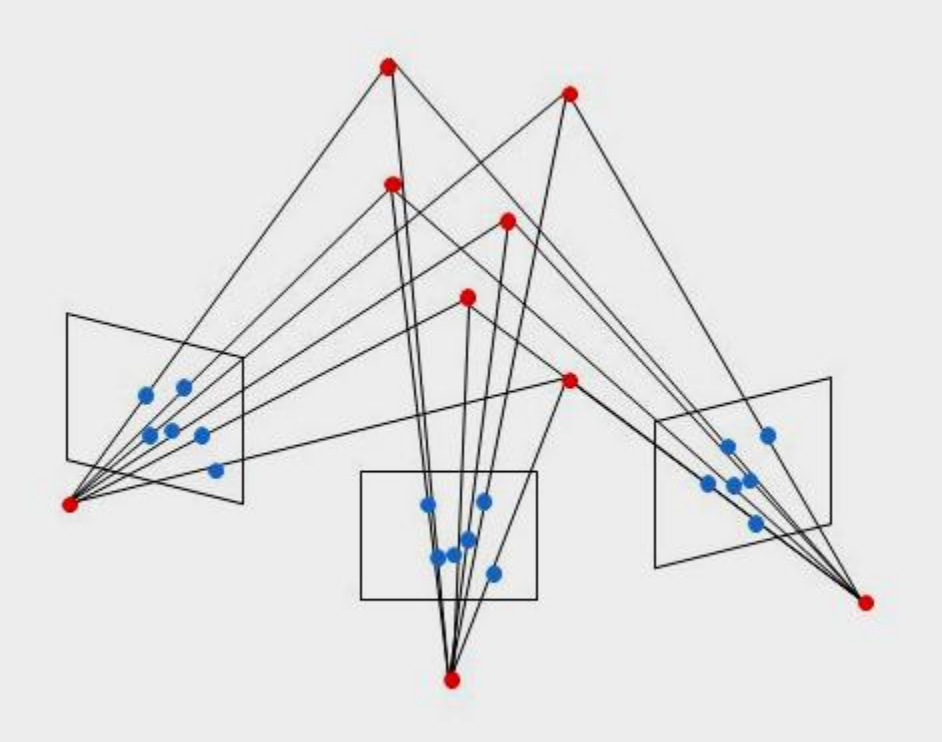

Figure 14: Bundle adjustment

The least squares technique involves finding the line or curve of best fit that accurately represents a set of data points by minimizing the sum of the squared offsets (residuals) between the points and the curve. This process, also known as regression analysis, quantitatively measures the trend of the results when establishing a relationship between two variables. This technique can be used for both estimation and error calculation in photogrammetry. Typically, a linear method is used, but if the problem is not linear, it can be linearized using the Gaussian method (Fryer & Kniest, 1985; Grau et al., 2021).

Different strategies can be employed to optimize the imaging configuration and improve the accuracy of the results to perform bundle adjustment. One such strategy is a simulation, where a priori accuracy estimation is provided by simulating object points like the actual measurement in terms of number and distribution. Another strategy is divergence, where bundle adjustments that do not converge can be prevented by controlled program abortion after the first iteration and pre-correction of image coordinates by known distortion values. Finally, gross errors can be eliminated in complex imaging configurations through manual or automatic methods, where only one blunder should be eliminated per program run, usually the one with the largest normalized correction (Luhmann et al., 2013).

2.4.6.2 Feature Matching

Feature matching is a popular analytical method in photogrammetry that involves identifying and matching distinctive points or features in multiple images taken from different viewpoints or at different times. This method is particularly useful for applications such as stereo matching, image registration, change detection, and creating 3D models. The distinctive points or features are detected using various algorithms such as Scale-Invariant Feature Transform (SIFT), Speeded Up Robust Features (SURF), or Oriented FAST and Rotated BRIEF (ORB) (Stanier et al., 2016).

Once the key points or interest points are identified in the images, they are matched based on their characteristics such as scale, orientation, and location as shown in *Figure 15*. The matching process is typically done using techniques such as nearest-neighbor matching, geometric verification, or RANSAC. The resulting matched points can then be used to calculate the 3D coordinates of the object or scene using techniques such as bundle adjustment or Structure from

Motion (SfM). The feature matching method has been widely used in aerial photogrammetry to create accurate digital elevation models and orthophotos, as well as in close-range photogrammetry for creating 3D models of objects and scenes (Cleveland & Wartman, 2006; Mandirola et al., 2021; Scaioni et al., 2015).

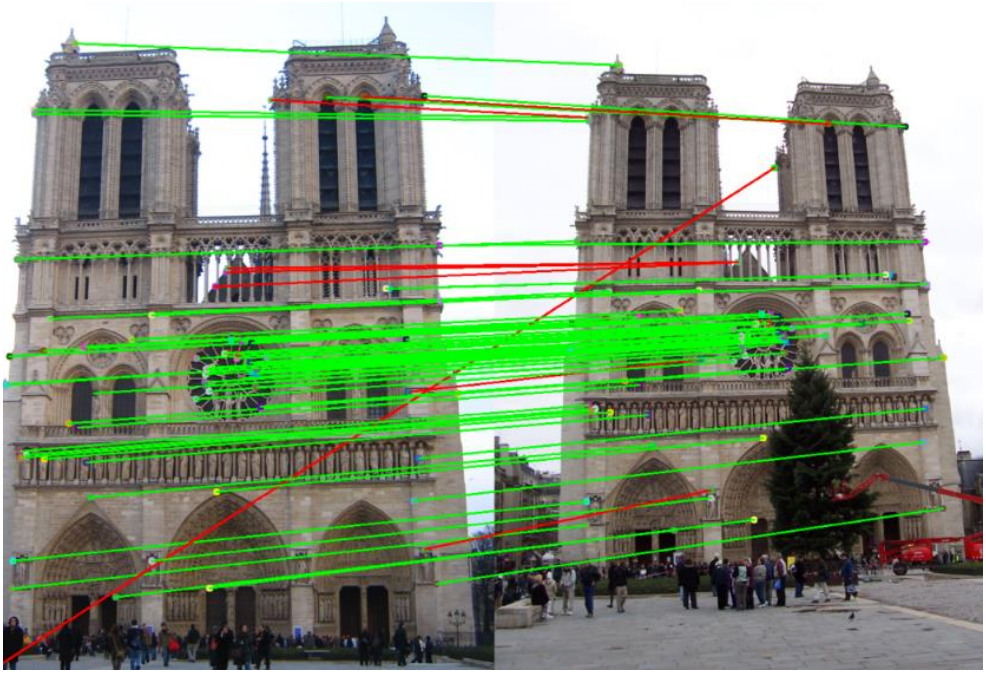

Figure 15: Feature Matching of a Building from Two Images

2.5 Previous Usage of Photogrammetry in Soils

Photogrammetry is commonly used in soil research for its non-destructive and efficient measurement and analysis of soil properties. It has been applied to measure soil erosion, monitor changes in soil structure and texture, assess soil moisture content, and map soil properties across large areas. By generating detailed three-dimensional models of soil surfaces through aerial or ground-based photography, photogrammetry provides precise measurements of soil parameters.

Previous studies have utilized photogrammetry in various applications related to soil surfaces, as summarized in the upcoming section.

2.5.1 3D reconstruction and volume-change measurement of soil samples (Xia et al., 2020)

In this paper, the authors propose a photogrammetric computer vision approach for 3D reconstruction and volume-change measurement of unsaturated soils. The proposed method involves capturing images of the soil samples from different angles, and then processing them using photogrammetric software to create a 3D model of the soil samples. The traditional methods of measuring soil deformation rely on manual measurements which are time-consuming, subjective, and inaccurate. The proposed approach involves capturing a series of images of the soil surface using a camera from multiple angles and processing them using photogrammetric techniques to generate a 3D model of the soil surface. Computer vision algorithms are then applied to the 3D model to calculate the volume change of the soil. The proposed approach was validated using laboratory experiments which demonstrated that it provides accurate and efficient measurements.

The proposed photogrammetric computer vision approach captures and processes many images in a relatively short time, reducing the need for manual measurements. The accuracy of the approach was also found to be superior to traditional methods. The test conducted in the experiments proved that the entire target IDs were correct, showing that the approach achieves nearly 100% accuracy in coded target detection

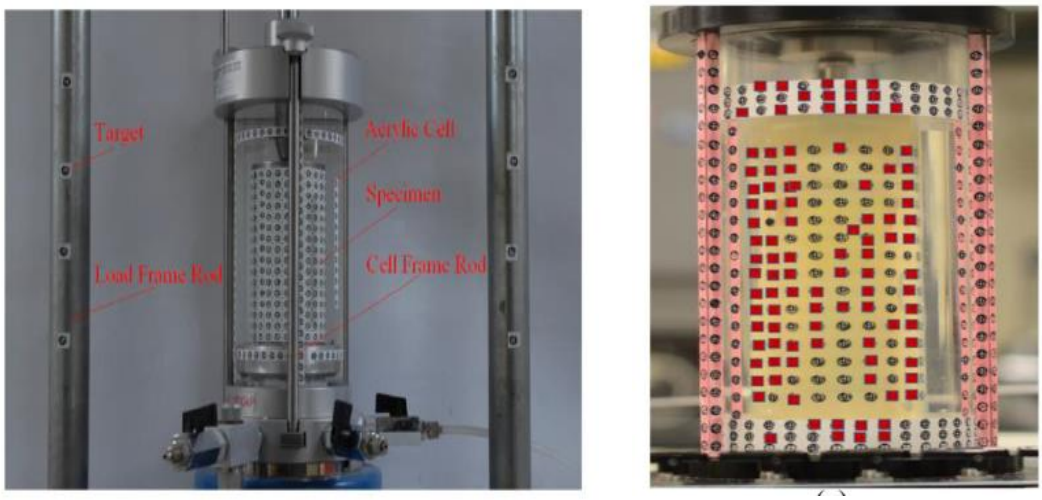

(a) (b)

Figure 16: (a) System setup and (b) Target detection using software

. Additionally, the results of 3D reconstruction using the software Photomodler demonstrated that the proposed 3D reconstruction method can reconstruct the 3D models of the triaxial cell and back-calculate the camera locations. The proposed photogrammetric computer vision approach provides an accurate and efficient method for measuring the volume change of unsaturated soils.

2.5.2 Ground movement monitoring using UAV (Javadnejad & Gillins, 2016)

The study aimed to investigate the use of unmanned aircraft systems (UAS) based photogrammetry for ground movement monitoring in trench settlement. The study used a DJI Phantom 2 Vision+ UAS to capture aerial photographs of a test site during the trench excavation and backfilling processes. The aerial images were processed using Agisoft Photoscan software to generate a digital surface model (DSM) and orthomosaic maps. The study found that UAS-based photogrammetry was a reliable and efficient method for ground movement monitoring in trench

settlement. The generated DSMs accurately showed the ground movement over time, and settlement volumes were calculated with high precision.

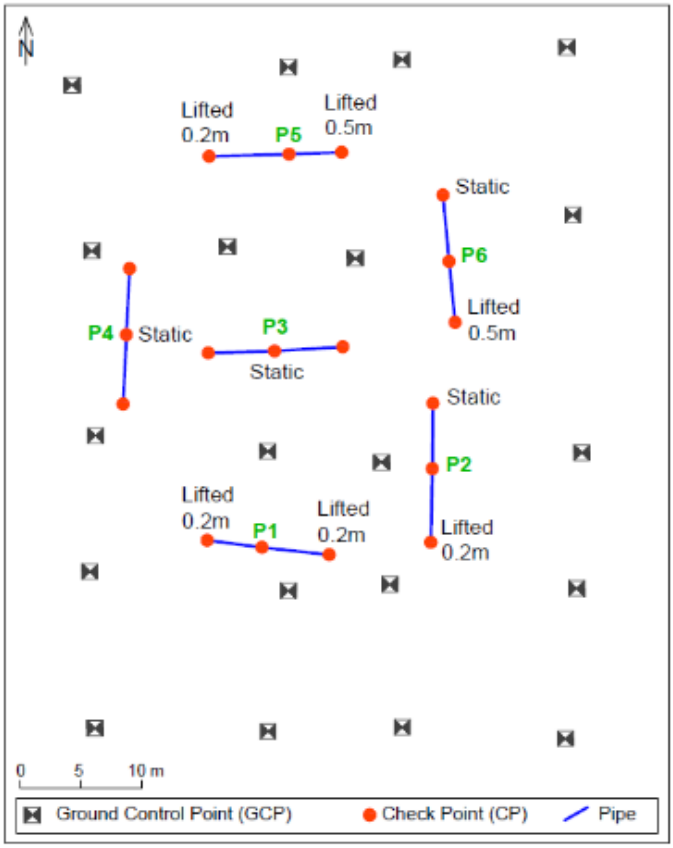

Figure 17: Placement of steel pipes and GCPs

The results suggest that UAS-based photogrammetry is a promising method for ground movement monitoring in civil engineering projects. It provides accurate and efficient measurements of ground movement and settlement volumes, making it a valuable tool for monitoring trench settlement. The study recommends that UAS-based photogrammetry can replace traditional surveying methods in similar civil engineering applications, resulting in significant time and cost savings.

2.5.3 DEM measurements of a gravel-bed surface (C. Wang et al., 2015)

This study explores the use of low-resolution imagery to create accurate digital elevation models (DEMs) of gravel-bed surfaces in comparison to high-resolution imagery. The study area was a gravel-bed river in China, where images were collected using two different scales: 1:4000 and 1:10000. The images were processed using photogrammetry software to create DEMs, which were then compared to a ground-based LiDAR survey for accuracy assessment. The study found that the DEMs created using the low-resolution 1:10000 images had an accuracy similar to those created using the high-resolution 1:4000 images. The accuracy of the DEMs improved with increasing point density and image resolution. The study concludes that low-resolution images can be used to create accurate DEMs of gravel-bed surfaces, which can be beneficial for large-scale surveys and monitoring.

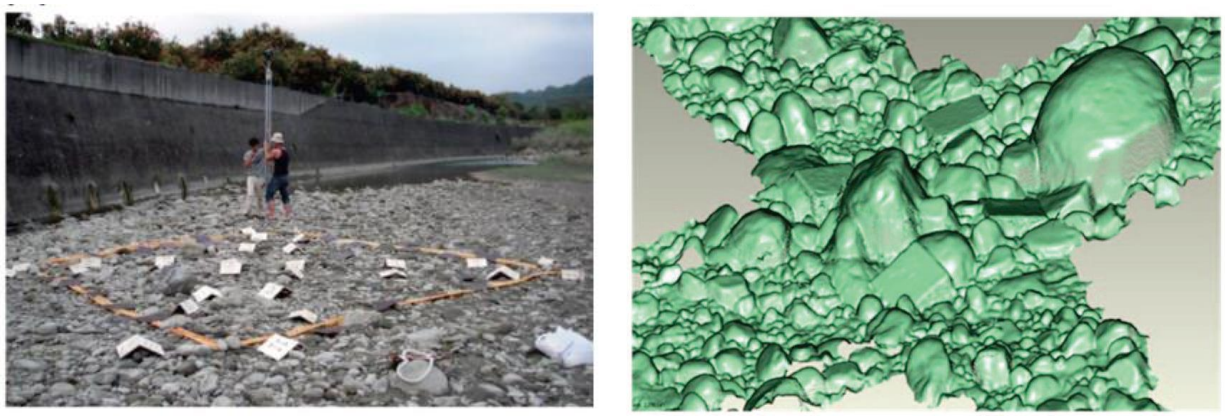

(a) (b)

Figure 18: (a) Testing scenario in the riverbank and (b) Output

The findings of this study provide a cost-effective and efficient method for creating high-quality DEMs of gravel-bed surfaces, showing that photogrammetry is a useful tool for studying

gravel-bed rivers. The study also highlights the importance of point density and image resolution for accurate DEM measurements. Overall, the study provides valuable insights into the potential use of photogrammetry in large-scale surveys and monitoring of gravel-bed rivers, which can help to better understand the surface morphology and hydrological processes of these environments.

2.6 Postprocessing Software

In photogrammetry, images can be transformed into detailed 3D models through specialized software. By scanning an object and creating millions of point clouds, which are points on a 3D coordinate system, a precise 3D model of the scan is generated, providing insight into the structure of the object. Photogrammetry software is used for a variety of applications, such as topography mapping, architectural reconstruction, and mechanical engineering. It can also be used in conjunction with drone analytics software to provide 3D visualizations of captured locations, including slope maps and digital surface models. Additionally, photogrammetry software can be integrated with other design tools, such as BIM software, CAD software, and building design tools (Alidoost & Arefi, 2017; Becker et al., 2018; Grussenmeyer & al Khalil, 2008). In our lab and field work we are using the Agisoft Metashape Professional. The commonly used photogrammetric software are Pix4Dmapper, Autodesk ReCap, RealityCapture, OpenDroneMap, VisualSFM, MicMac, COLMAP, and iWitness.

2.6.1 Agisoft Metashape Professional

Professional photogrammetry software called Agisoft Metashape processes digital photos for a variety of uses, including indirect measurements of objects of different scales, cultural heritage documentation, visual effects, and production. A few key capabilities allow Metashape to analyze multiple data types (including aerial and close-range imagery), output a point cloud, measure areas, volumes, and distances, and create 3D meshes that can subsequently be exported to several well-liked formats. Additionally, 4D models can be altered, allowing for the complete editing of 3D recordings of scenes (Alidoost & Arefi, 2017; Agisoft Manual, 2022) Agisoft Metashape licenses come in two versions, and the professional edition, and standard edition.

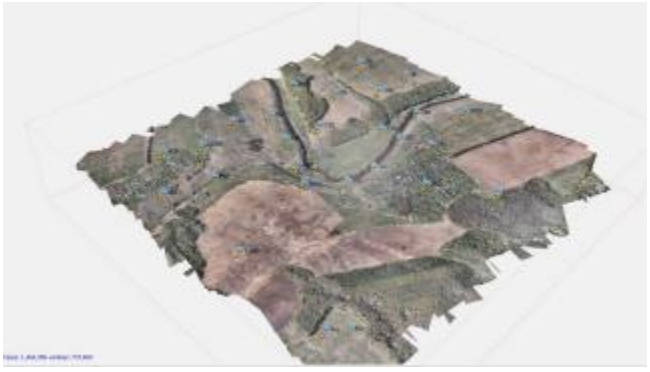

Figure 19: 3D model output of Metashape, Source: agisoft.com

2.6.2 iWitnessPRO

iWitness Pro is a cutting-edge photogrammetric software that revolutionizes the way photogrammetry is conducted in various industries such as forensic science, accident reconstruction, and engineering. With its advanced features and processing methods, iWitness Pro offers accurate and reliable measurement and analysis of objects, scenes, and images captured

from multiple viewpoints. The software's wide range of applications includes crime scene documentation, accident reconstruction, virtual scene reconstruction, and 3D modeling. It provides features such as image orientation, point cloud generation, surface modeling, and image rectification, and supports various data formats, making it accessible and versatile.

iWitness Pro offers user-friendly interfaces, intuitive workflows, and extensive documentation, making it suitable for both expert and novice users. It provides a comprehensive set of measurement and analysis tools, including distance, angle, area, volume, and trajectory measurements, as well as visualization and reporting capabilities. The software also offers robust error analysis and quality control features to ensure the accuracy and reliability of the measurements. Overall, iWitness Pro is a powerful and versatile photogrammetric software that is widely used in various industries for precise and efficient measurement and analysis tasks. Its advanced features, user-friendly interfaces, and extensive functionalities make it a valuable tool for professionals who require accurate and reliable photogrammetry results (Cronk et al., 2008).

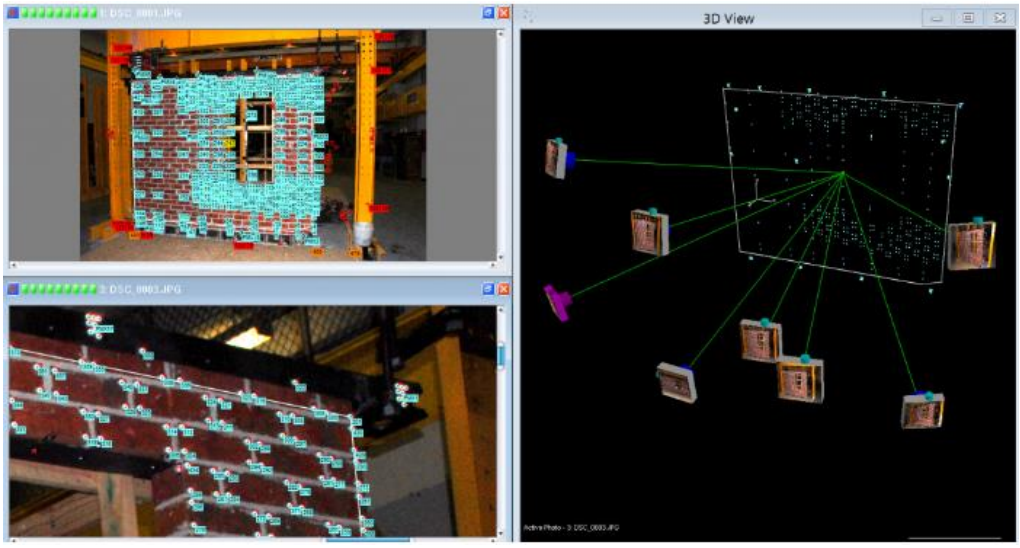

Figure 20: Monitoring the deformation of a brick wall structure under different load conditions using iWitnessPRO Source: Photometrix.com.au

CHAPTER 3

METHODOLOGY

This chapter provide a detailed overview of the procedures followed in both field and laboratory settings to research soil surface movement using photogrammetry. The study utilized a simple consumer-grade camera, the Canon 805D, to acquire images and test its applicability in the experiments.

In the field experiments, a novel technique for measuring ground movement using photogrammetry was employed. The approach involved capturing a series of photographs of the ground surface and creating a 3D model from these images. From the resulting 3D model, the accuracy of the site dimensions was checked, and the movement of the ground point near the inclinometer was known. To ensure the accuracy of the ground movement measurement, reference points and checkpoints were established using surveying techniques with a total station. The reference points served as control points, with their locations precisely measured and recorded. Checkpoints were then established in the columns of bridges, and their positions were calculated using the photogrammetry software Agisoft Metashape. The readings from the checkpoints were then compared with the measurements from the total station, allowing for a comparison of the photogrammetry data. Reflective targets and ground points were used as part of this process to ensure precise and accurate measurement of the ground movement.

In the laboratory experiments, the anchor pullout test was used to determine the pullout capacity of an anchor in a soil sample. The test involved measuring the heave, which refers to the upward movement of the soil surface, during the experiment. Photogrammetry was used to capture the soil surface before and after the test and create a DEM of the model of the soil surface using

Agisoft Metashape Professional. The resulting DEM was then used to calculate the amount of heave that occurred during the test. To assess the reliability and accuracy of photogrammetry, the results were compared with the traditional dial gauges, which are frequently used to measure heave in the laboratory.

3.1 Camera and Lights

The camera used in photogrammetry plays a vital role in capturing multiple images of an object or scene from various angles. These images are then processed to create a 3D model that can be analyzed or visualized. The camera must be of high quality with a high-resolution lens and low distortion to capture accurate and precise images. In addition to the quality of the camera, its setup and calibration are also critical in photogrammetry. The camera must be calibrated to ensure that the captured images have consistent characteristics like focal length, distortion, and perspective. Moreover, the camera's settings, such as exposure, aperture, shutter speed, and ISO, must be carefully set to ensure that all images have the same brightness and contrast.

The accuracy and reliability of the resulting 3D model depend largely on the quality, setup, and calibration of the camera used in photogrammetry. A high-quality camera with proper calibration and settings can produce high-resolution images that can be used to create detailed and accurate 3D models of objects and scenes. Photographers generally use high-end cameras with built-in geotagging systems with remote triggering. For our test, we used consumer-level Canon 850D digital single-lens reflex (DSLR) camera as shown in *Figure 21*.

The Canon 850D has several features that make it suitable for close-range photogrammetry. The camera's manual settings allow for precise control over the focal length, shutter speed, and

aperture settings, which are important parameters in photogrammetry. The Canon 850D is a flexible DSLR camera with features designed to satisfy both photographers' and videographers' needs. With its Dual Pixel CMOS AF, DIGIC 8 Image Processor, and 24.2 Megapixel APS-C CMOS sensor, it can produce high-quality photos and videos with quick and precise autofocus even in low-light conditions. Its built-in Wi-Fi and Bluetooth connectivity make image transfer and remote control from mobile devices simple, and its vari-angle touchscreen Display makes it simple to compose from various perspectives. It is a trustworthy camera for a variety of photography and videography tasks because of its continuous shooting speed of up to 7 frames per second and 4K UHD video recording capabilities at 24 frames per second.

Figure 21: Canon EOS850D camera used for test

For the lab work, we did the calibration of the camera using the checkerboard generated from Metashape (*Figure 22*) and imported the resulting calibration parameters (*Figure 23*) for processing the images. These calibration parameters were obtained after processing images of the chessboard:

f - Focal length measured in pixels (in pixels).

cx, cy - Principal point coordinates, i.e., coordinates of lens optical axis interception with sensor plane (in pixels).

b1, b2 - Affinity and non-orthogonality (skew) coefficients (in pixels).

k1, k2, k3, k4 - Radial distortion coefficients (dimensionless).

p1, p2 - Tangential distortion coefficients (dimensionless).

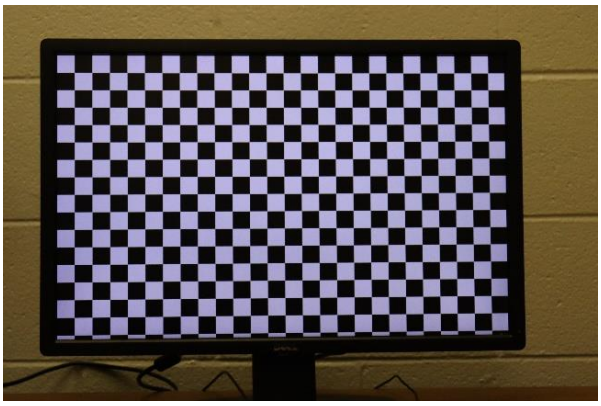

Figure 22: Chessboard generated by Metashape for camera calibration

		cx:	39.6652
f:	13401.3208	cy:	-175.042
k1:	0.0985268	p1:	0.00169209
k2:	-2.50829	p2:	-0.00257568
k3:	44.0094	b1:	-0.684428
k4:	-314.259	b2:	-1.04466

Figure 23: Calibration parameters

During the lab test, the camera was mounted on a tripod with adjustable height, which allowed us to capture images from different heights and angles. This was essential to ensure that we captured all the necessary details of the object. However, when we conducted the field test, we had to rely on handheld shots due to the steep terrain, which made it challenging to set up the tripod. While handheld shots are not ideal for photogrammetry, we took precautions to ensure that the images were as stable as possible by bracing the camera against our bodies and taking shots in short bursts.

One of the critical factors in capturing high-quality images for photogrammetry is adequate and uniform lighting. To ensure that the images had sufficient lighting, we used a light system that allowed us to manually adjust the intensity of light and move the height of the lights. This allowed us to achieve the desired lighting conditions for the images and improve the accuracy of the photogrammetric model. The processing software we used recommended specific lighting conditions for detecting feature points and markers accurately, and we made sure to adhere to these recommendations during the image acquisition process.

3.2 Laboratory Heave Measurement

In the geotechnical laboratory of UTA, four tests were conducted to examine the impact of different embedments of anchors. The tests were performed using excavated clayey soil obtained from the I-20 project site. To carry out the tests, a wooden box with metal bracing of dimensions 1m x 1m x 1m was constructed in the lab. The base of the box was fixed to the floor using a bolt. However, for our test, the width of the box was reduced to almost 30 cm so that Plexiglas could be installed to monitor the anchor movement. The box was attached and restrained with a metal beam in the base and a column on two sides where we could place and adjust the beam. This beam

acted as a platform to hold the hydraulic jack in the column.

3.2.1 Properties of Soil

Soil testing is a crucial step in any geotechnical analysis or engineering project that involves soil. The results of these tests can be used to determine the soil's properties and how it will behave under different conditions. In our case, understanding the index properties and compaction parameters of the concrete sand will help us to predict its pullout capacity and heave movement accurately. Additionally, classifying the soil based on USCS allows us to communicate its properties and characteristics effectively.

Clayey soil for the lab tests was obtained from the I-20 project site and various tests including Atterberg limits, proctor tests, UU tests, and index tests, and results are summarized in *Table 1*.

Table 1: Properties of Clayey Soil

Properties	Values
Liquid Limit (LL)	27%
Plastic Limit (PL)	19%
Plasticity Index (PI)	8%
Unit Weight	19.6 KN/m3
USCS classification	CL (Sandy Lean Clay)
Unconfined compression strength (UCS), qu	55.16 kN/m2
Unconfined Compression Strength (UCS), Cu	27.6 kN/m2
Maximum Dry Density	17.83 kN/m3
Optimum Moisture Content	14.20%

3.2.2 Test Setup and Surface Preparation

For heave measurement, the box was filled with clay taken from the IH-20 project site and compacted to the appropriate density. The soil surface was prepared by compacting it in layers of

10 cm using a hand rammer and ensuring the moisture content and compaction were appropriate. The desired moisture content was 11% with 95% of the maximum dry density. Each layer had a moist weight of about 60 kg and was first spread loosely before being compacted with the rammer. Moisture content for each layer was measured and recorded. After compaction, the surface was covered for at least one night to ensure even moisture distribution.

Figure 24: Placement of Dial Gauges on the surface

Four digital dial gauges were utilized to determine the heave of the surface as seen in *Figure 24*. The gauges were positioned at the center of the surface, with two on each side. The gauges were placed on printed targets from meta shape, which were situated on small cardboard to prevent them from penetrating the soil surface. To facilitate photogrammetric analysis, a marker was placed on top of the cardboard. The testing setup before placing the dial gauge is shown in *Figure 25*. Furthermore, an LVDT and a load cell were placed alongside a hydraulic jack, as shown in *Figure 25*, to record the anchor displacement and pull-out load. The hydraulic jack could displace a little less than 6 inches in every complete stroke. After each stroke, the jack was loosened, and

the process was repeated. The corresponding pull-out load was recorded in the load cell. The number of strokes for each embedment depth varied based on the displacement observed.

Figure 25: Test setup

To obtain uniform lighting and compensate for shadows in the lab test, additional lights were placed in the corners. While there are no strict requirements for lighting, it is important to achieve good lighting conditions that allow for clear detection of points with the camera. However, glare and reflections from surfaces should be avoided to ensure accurate results. The lighting setup

was carefully designed to meet these requirements and ensure that the images captured were of high quality and suitable for photogrammetric analysis.

3.2.3 Target Setup & Survey

To accurately georeferenced the images captured during the lab tests, targets were strategically placed along the metal column and on the surface of the soil as shown in *Figure 26*. Reflective targets measuring 6cm x 6cm were used in conjunction with smaller markers generated by meta shape and printed on plain paper. The smaller markers were placed on the soil surface while the reflective targets were used to determine local coordinates using a total station in non-prismatic mode.

Figure 26: Surveying in the Lab

This combination of targets and markers allowed for precise referencing of the images as seen in *Figure 26.* The placement of markers on the sand surface was particularly advantageous as the meta-shape software could automatically detect the coded targets. This saved time and effort in the post-processing phase, as manual identification of targets can be a time-consuming and

tedious process. The reflective targets ensured accurate measurement of local coordinates, providing a reference point for aligning the images in the photogrammetric software. By using a combination of reflective targets and coded markers, the accuracy and efficiency of the georeferencing process were greatly improved.

3.2.4 Image Settings

To ensure optimal image processing during image acquisition, it is recommended in the literature to adjust camera settings manually. Maintaining a constant focal length of approximately 50mm is advised, and a lower aperture value is preferred to achieve a higher field of view. In the geotechnical lab, where the subject of interest is often small, an aperture value of f/5.0 or lower is utilized.

In order to prevent camera shake or blur from subject movement, the shutter speed is adjusted to around 1/200. At the same time, the ISO is set to automatic mode with a maximum limit of 1600. This enables the camera to adapt the ISO level according to the lighting conditions available, while also preventing excessive noise in the resulting images.

3.2.5 Testing Schedule

In order to showcase the practical application of photogrammetry in geotechnical engineering, four pullout tests were conducted in the laboratory using clayey soil. To demonstrate the effectiveness of photogrammetry in measuring soil surface movement, different embedment depths were utilized during the tests. For each test, four coded targets were placed on the soil surface, with two on each side at varying locations. The testing schedule for each test

was summarized in *Table 2* detailing the embedment of anchor, pullout strokes, and moisture content of the soil. The test ID for each test is assigned based on the embedment depth.

Table 2: Testing Schedule

Test no	Anchor Embedment Depth, cm	Test ID	Moisture content, %	No of strokes
1	65	E65	11.2	2.4
2	75	E75	11.6	4
3	85	E85	11.4	4.3
4	55	E55	12	2

3.3 Field Demonstration for 3D modelling and Slope Monitoring

3.3.1 Site Location and Description

TxDOT is widening IH-20 over Lower Clear Fork Trinity River to add auxiliary lanes between Bryant Irvin Rd and Winscott Rd. The widening project, which includes stabilizing the riverbank slope and treating it with an erosion control system, is necessary to meet the Transportation Planning that requires widening the highway to eight lanes. Additionally, the city of Benbrook is built an emergency access bridge downstream of the TxDOT IH-20 bridge, affecting the overall hydrology of the Lower Clear Fork Trinity River watershed. The google earth map and the existing slope are shown in *Figure 27-29* along with the proposed drawing for the cross-section.

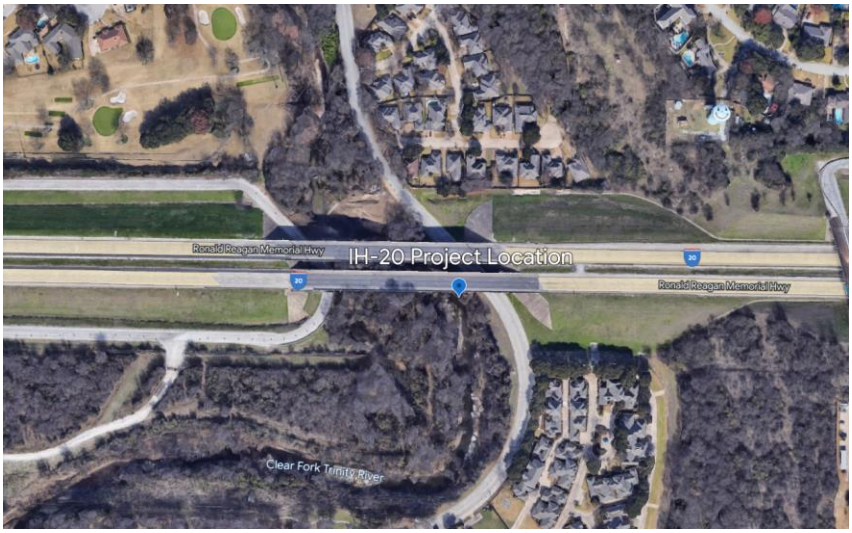

Figure 27: Project Location in Benbrook

Figure 28: Existing Channel condition that has been eroded and scoured

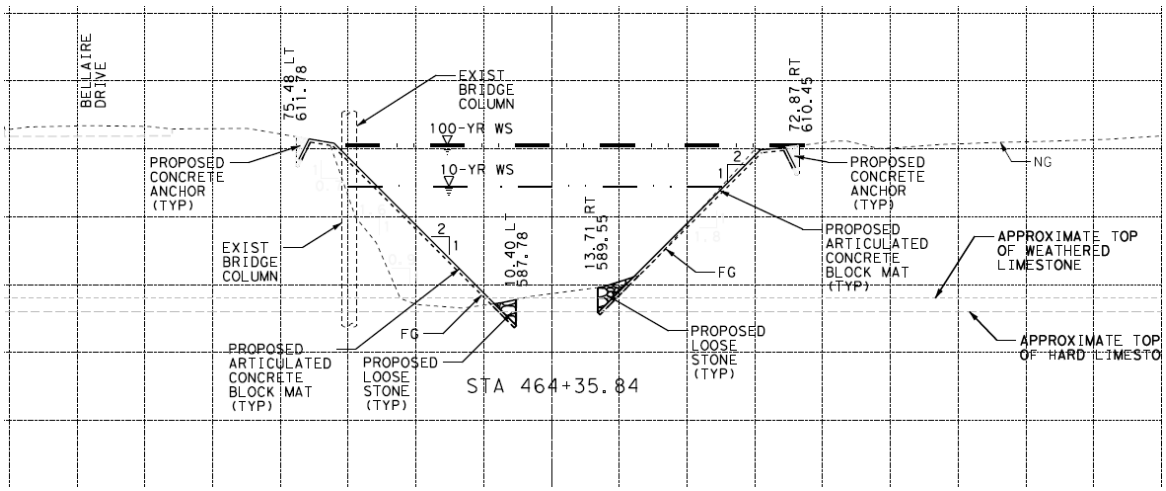

Figure 29: Existing/proposed Channel Cross-section

Starting from December 2022, the analysis has been underway, and during this time, the installation of articulated concrete blocks (ACBs) with PDEA was completed under the south bridge on both sides, and half of the north bridge on the east side was also completed. The final slope is proposed to be in the slope of 2:1 (H: V) or flatter if possible. The distance from the bottom of the bridge deck to the underpass accessway is estimated to be 25 ft, while the distance to the normal water level from the bottom of the bridge deck is 55 ft. On the south bridge, there are five columns on each side where ACB and PDEA installation is complete. In addition, for the northeast bridge, ACB installation has been completed for approximately three columns on the south side as seen in *Figure 30*. Therefore, assuming the stability of the bridge columns, we placed our control points within these columns.

Figure 30: Site Picture Taken from North Side indicating East and West Side

3.3.2 Target Setup

During the survey, Leica reflective survey targets measuring 6”x6” and black and white ground control points measuring 24” x24” were set up. To ensure accurate measurements, the targets were distributed evenly throughout the area of interest. By placing the targets in strategic locations, we obtained precise and reliable measurements of the column bases marked with targets.

Reflective Target surveying equipment included self-adhesive 3M Diamond Grade Reflective Tape with Prismatic retroreflective technology that can stick to most surfaces, but the glue was used to adhere them to column surfaces. The yellow-colored tape having a survey range of approximately 200 meters (650 feet) and provides high survey accuracy in both standard and

fast measurement modes, with 2mm 2 ppm and 5mm 2 ppm, respectively is used for the control points as shown in *Figure 31*. The reflective targets are manufactured by Reflective Target Canada.

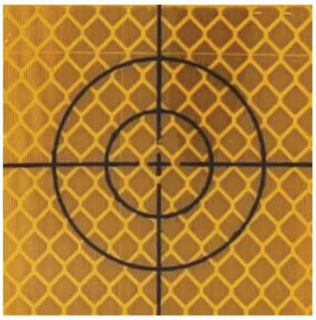

Figure 31: Reflective Targets

These Ground Control Points (GCPs) or Ground Points (GPs) used on site is the one generally used for drone mapping up to 400 feet altitude. GP used in the site is 24” x 24” in size, and they are made with lightweight, weatherproof mesh material as shown in *Figure 32*. The GCPs have a unique center-pass through design that allows pre-established survey markers to be inserted through the GCP for precise aerial mapping. The GCPs also have corner anchor points to prevent movement during mapping, and they are compatible with most photogrammetry software. The center flaps can cover the cutout for traditional mapping or can be opened for precise coordinate shooting. With 4 tie-down points, the GCPs are easy to keep in place during windy days and can be left in the field for repeated use.

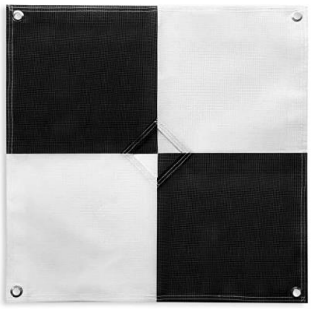

Figure 32: Ground Control Point

The east slope was found to be steeper and wider than the west side, to obtain accurate measurements four ground control points were used on the east side, while only two ground targets were used on the west side. This decision was made to ensure that we obtained accurate and reliable measurements in the challenging terrain of the east slope. By strategically placing the ground control points and targets, as shown in *Figure 33*, we were able to overcome the challenges presented by the terrain and obtain accurate measurements of the column bases marked with targets. Overall, we were able to complete the survey accurately and efficiently, thanks to the use of Leica reflective survey targets and the strategic placement of ground control points and targets.

(a) (b)

Figure 33: Placement of (a) GCPs and (b) Reflective targets in the site

3.3.3 Field Survey

Using a total station to survey the column bases marked with targets is a reliable method for obtaining accurate coordinates. The process involves setting up the total station, orienting it, measuring the targets, calculating the coordinates, verifying the measurements, and recording the final coordinates as shown in *Figure 34*. The accuracy of the measurements depends on the stability of the total station, the clear line of sight to the targets, and the correct orientation of the

total station. Therefore, it is crucial to follow a systematic approach to ensure accurate measurements. By following this process, we obtained precise coordinates of the column bases marked with targets.

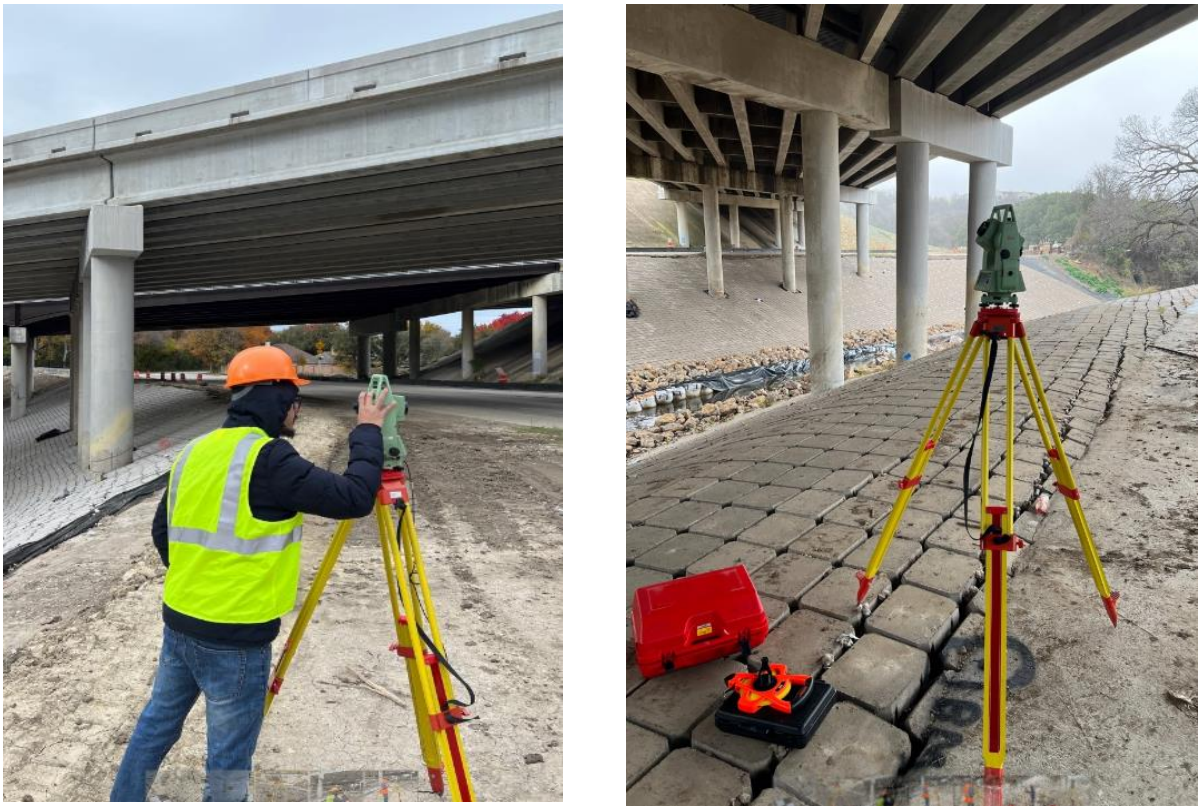

(a) (b)

Figure 34: (a) and (b) Surveying in the field

First, the total station was set up at a stable location with a clear line of sight to the targets on the column bases. Then, we use the total station's orientation function to align it with a known point or benchmark. This will ensure that the total station is correctly positioned and oriented, allowing for accurate measurements. Once the total station is set up and oriented, we use the measurement function to measure the location of the targets on the column bases. We record these measurements and calculate the X, Y, and Z coordinates of each target. Afterward, we performed

the verification measurements by taking additional measurements around the column bases and adjusting as necessary. Finally, we record the final coordinates of each target marker on the column bases.

3.3.4 Image Acquisition and Camera Settings

The perfect camera settings and weather conditions for capturing images for photogrammetry depend on various factors such as the subject being mapped, the type of camera being used, and the specific software being utilized. However, in general, it is recommended to use a high-resolution camera with a wide-angle lens and a fast shutter speed to minimize motion blur. The aperture should be set to a small value to increase the depth of the field and reduce distortion. A low ISO setting can help to minimize image noise. It is also recommended to capture images on an overcast day or during the early morning or late afternoon when the sun is at a low angle, as this can help to reduce harsh shadows and glare on the subject being mapped. Additionally, it is important to ensure consistent lighting and overlap between images to ensure accurate photogrammetric reconstruction.

The process of image acquisition involved capturing multiple sets of photos, with additional images taken of areas where the dense point cloud needed to be supplemented. To ensure uniform lighting, the imaging was conducted on a cloudy day. The camera settings were like those used during the lab tests, with slight modifications to ensure optimal image quality. Manual settings were used to adjust the focal length, which was set to approximately 50mm, based on the observation of the actual images which indicated a focal length of 49mm. The shutter speed was set to 1/200 sec to capture clear and sharp images, and the aperture was adjusted slightly above its lowest value to enable capturing wider images with greater depth of field, resulting in an aperture

setting of f/6.3. The ISO was set to automatic, with a maximum value of 1600, to ensure that the camera captured images at the optimal exposure level while minimizing image noise. These camera settings were selected to ensure high-quality images with minimal noise and accurate detail for photogrammetric reconstruction.

We revisited the site a few times to capture additional images of the southeast section near the inclinometer for a comparative analysis of two ground points with the earlier image data. We paid close attention to the weather conditions and chose a cloudy day to ensure uniform lighting in the captured images. To maintain consistency, the same image settings as before were used. By capturing images of the same location at different times and under similar conditions, we aimed to detect any changes in the terrain or surface features. The comparison of these images allowed us to assess deformation or movement in the southeast area of the slope.

3.4 Stages for Analysis

Agisoft Metashape is a photogrammetry software that can convert 2D images into 3D models. The output of image analysis using Metashape varies depending on the project objectives. In our test, we aimed to determine heave movement by comparing two sets of pictures taken in the lab. Meanwhile, in the field, we aimed to obtain a 3D model output and compare the movement of the area near the inclinometer. The basic steps involved in generating a 3D model and DEM with ortho mosaic are as follows:

Image Alignment: The first step is to import the 2D images into the software and align them using Metashape's image alignment feature. This process identifies common features in each

image and matches them with corresponding features in other images. As a result, a dense point cloud is created that represents the surface of the object in the images.

Dense Point Cloud Generation: After generating the point cloud, the next step is to filter and clean it up to remove any noise or outliers. This results in a denser point cloud that accurately represents the surface of the object.

Ground control point (GCP) tagging: To improve the accuracy of the DEM, ground control points (GCPs) can be added manually. These are marked points with known elevations used to adjust the elevation values of the point cloud.

3D Mesh Generation: Next, the denser point cloud is used to create a 3D mesh, which is a digital representation of the surface of the object. The mesh is made up of triangles that are connected to form a 3D surface.

DEM generation: From the dense point cloud, Metashape can create a DEM by either triangulating the point cloud to create a TIN (triangulated irregular network) or by using interpolation techniques to estimate the elevation of each pixel in the grid.

Refinement and export: The generated DEM can be refined by removing outliers and smoothing the surface. The final DEM can be exported in a variety of formats, including GeoTIFF and XYZ.

Texture Mapping: The 3D mesh is then textured with the original 2D images to give it color and detail. The software maps the pixels from the images onto the triangles of the mesh, creating a photo-realistic 3D model.

Model Editing: The final step is to edit the 3D model to remove any artifacts or errors. The software provides tools for smoothing the surface, filling holes, and removing unwanted elements.

In summary, Metashape uses photogrammetric techniques to create a dense point cloud from overlapping images and then generates a DEM by either triangulating the point cloud or using interpolation techniques. The accuracy of the DEM can be improved by adding ground control points, and the final output can be refined and exported in various formats. Another output of this process is a 3D model that can be used for various applications such as 3D printing, virtual reality, and animation. The stages of the process for laboratory heave measurement and field slope modelling and monitoring are shown in the schematics below (*Figure 35-36*) using a flowchart.

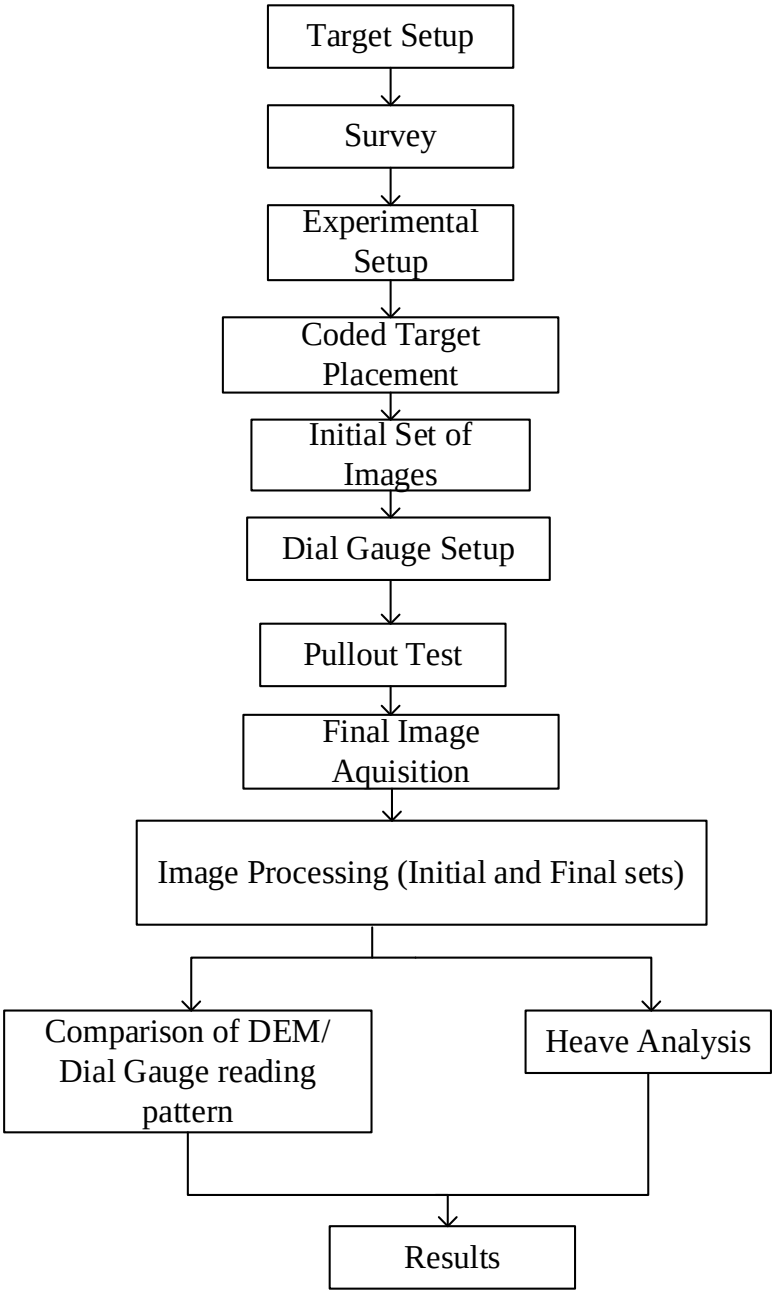

Figure 35: Flowchart for Heave Measurement and Analysis using Photogrammetry.

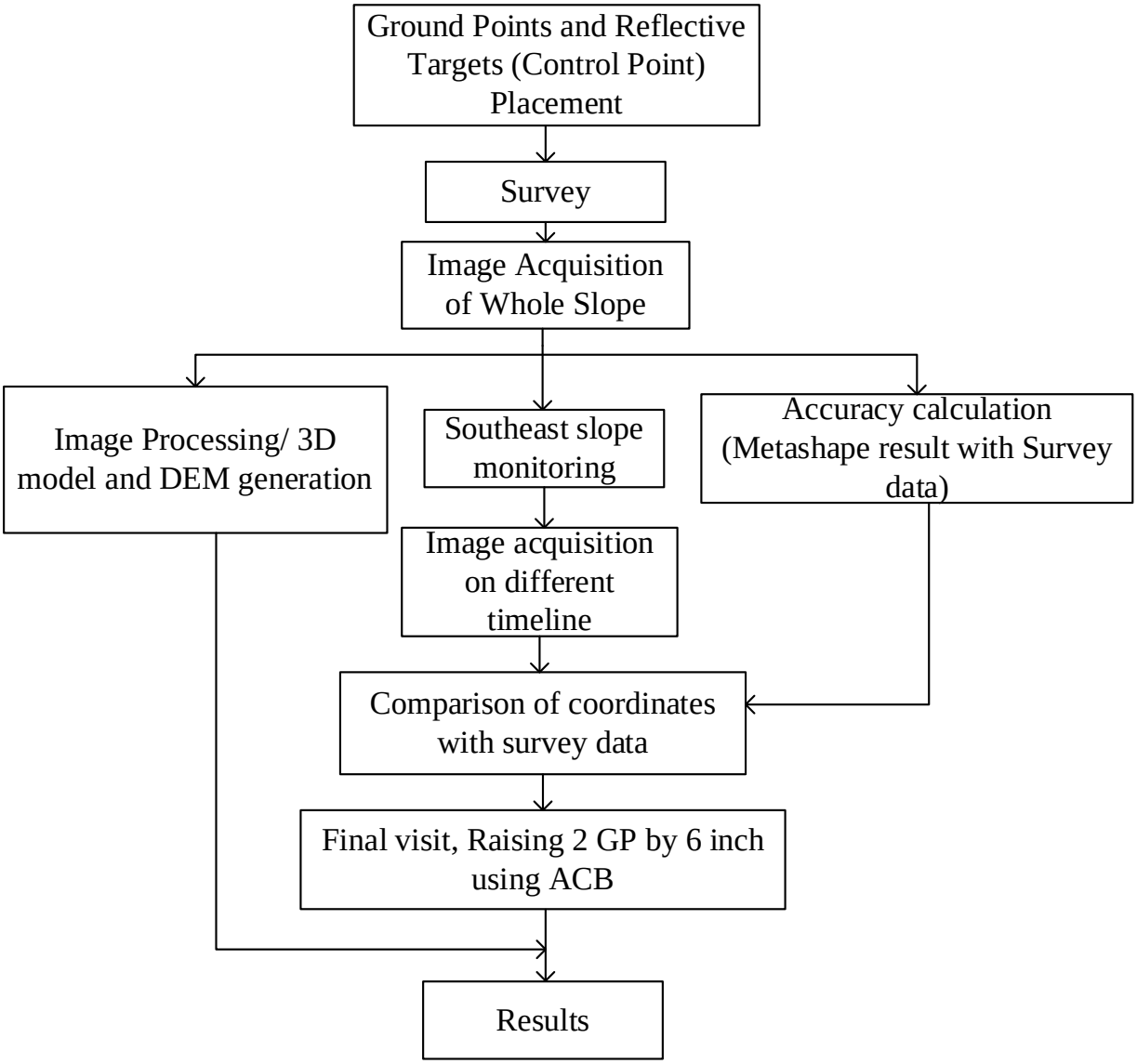

Figure 36: Flowchart for Field Application and Analysis of Photogrammetry

CHAPTER 4

RESULTS AND ANALYSIS

4.1 Heave Measurement in Lab

The application of photogrammetry in lab works for heave measurement was demonstrated through a series of four tests. The tests involved pulling the soil using anchors and measuring the heave using photogrammetry. To assess the accuracy of the photogrammetric approach, clayey soil was used to compare the dial gauge values with the photogrammetric values. Once the accuracy was established, the photogrammetric approach was used to measure the heave in sandy soil in the same box where minimal movement was expected. The results of the tests are expected to provide insights into the potential of using photogrammetry as a tool for measuring heave in soil samples in lab works.

4.1.1 Survey

Permanent markers were strategically placed in the column of the testing frame to ensure accuracy and consistency in surveying. These markers were square reflective targets measuring 60mm in length, with eight evenly distributed across the column (four per column) and two in the metal frame of the wooden box. The Leica 405D total station was used for surveying, with arbitrary coordinates assigned and a survey conducted to establish a benchmark. This survey was conducted with a level of accuracy of 0.01 ft. The coordinates of the points were recorded and presented in *Table 3* for reference.

Table 3: Coordinates of Markers for Lab Test

Point ID	X	Y	Z
Ref Tar 1	7.9	2.25	2.71
Ref Tar 2	8.56	6.04	2.73
Ref Tar 3	9.13	1.77	3.24
Ref Tar 4	9.13	1.6	3.64
Ref Tar 5	9.27	1.84	3.43
Ref Tar 6	9.29	2.09	3.19
Ref Tar 7	9.9	5.93	3.06
Ref Tar 8	9.91	6.09	3.4
Ref Tar 9	10.06	6.4	3.69
Ref Tar 10	10.06	6.24	3.63

4.1.2 Photogrammetry Output

To obtain precise measurements of heave in clayey soil, a series of four tests were performed using a combination of digital dial gauges and photogrammetric techniques. The gauges were placed on a metal platform and centered on coded targets on the soil surface. The number of strokes used to compact the soil was adjusted based on the depth of the anchor in the soil, and four markers were positioned around the cable and distributed across the center of the cable. Initial photos were taken and then, as the maximum heave on the surface of the dial gauge approached its displacement capacity, the reading was noted, and a final set of images was taken for further analysis. Camera calibration parameters were established, and Metashape was utilized to identify the printed coded targets on the soil surface. In the fourth test, heave was measured after each stroke, and the results were plotted against the pullout load.

The typical Sparse Cloud, Dense Cloud, 3D models textured image (before and after pullout test) and ortho mosaic of the surface is shown for the test with an embedment depth of 65cm (*Figure 37-40*).

Figure 37: Sparse cloud points of the surface (before pullout test), for test 1 (embedment depth 65cm).

Figure 38: Dense cloud points of the surface (before pullout test), for test 1 (embedment depth 65cm).

(a)

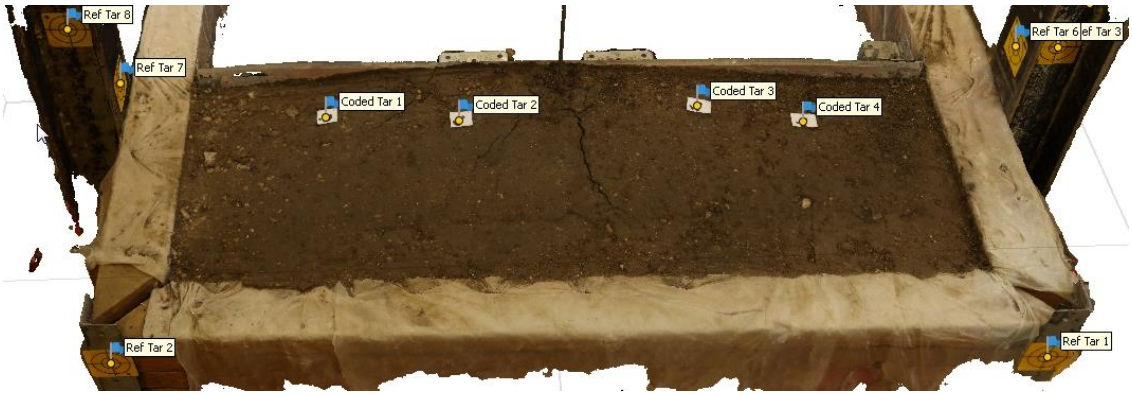

(b)

Figure 39: 3D textured image of surface (a) before test and (b) after test, for test 1 (embedment depth 65cm).

Figure 40: Orthophoto of surface, for test 1 (embedment depth 65cm).

4.1.3 Heave Measurement

The heave analysis involved analyzing the difference in elevation between the digital elevation models (DEMs) obtained from the initial and final set of images. Specifically, the difference in elevation for the center of the coded targets was noted and compared to the readings obtained from the digital dial gauges as seen in *Figure 41*. This comparison provided a means of validating the accuracy of the photogrammetric approach in measuring heave.

The lab pullout test involved testing the soil at different embedment depths of 55 cm, 65 cm, 75 cm, and 85 cm. The number of strokes required for each respective depth was adjusted accordingly, with 2 strokes required for the 55 cm depth, 2.4 strokes for the 65 cm depth, 4 strokes for the 75 cm depth, and 4.5 strokes for the 85 cm depth. The resulting heave in the surface was recorded and analyzed and summarized in *Table 4.*

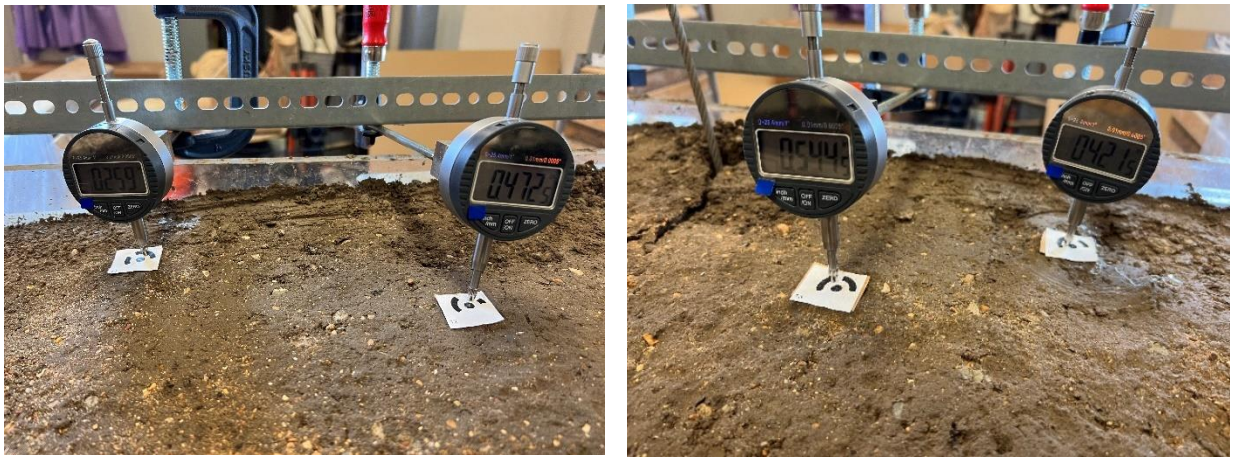

Figure 41: Dial gauge readings after the second test (point 1 on left)

Table 4: Comparison of Dial Gauge Reading with Elevation Difference from Metashape

Test ID	Embedment depth, cm	No of Strokes	Max Pullout Load, lbs.	Coded Target Point	Dial Gauge reading, inch (1)	Initial Elevation Metashape, inch (2)	Final Elevation Metashape, inch (3)	Heave from Metashape, inch (5) = (3-2)	Difference of Metashape and dial gauge, inch (5)-(1)
E65	65	2.4	514	1	0.802	34.092	34.848	0.756	-0.046
				2	0.905	34.008	34.944	0.936	0.031
				3	Limit exceed	34.26	35.208	0.948	-
				4	0.651	34.248	34.884	0.636	-0.015
E75	75	4	659	1	0.259	33.876	34.14	0.264	0.005
				2	0.472	33.984	34.536	0.552	0.08
				3	0.544	34.068	34.62	0.552	0.008
				4	0.421	33.936	34.392	0.456	0.035
E85	85	4.5	671	1	0.485	33.756	34.296	0.54	0.055
				2	Limit exceed	33.864	34.944	1.08	-
				3	0.796	33.972	34.8	0.828	0.032
				4	0.371	34.032	34.416	0.384	0.013
E55	55	2	619	1	0.11	34.752	34.884	0.132	0.022
				2	0.67	34.956	35.652	0.696	0.026
				3	0.392	35.028	35.424	0.396	0.004
				4	0.064	35.004	35.076	0.072	0.008

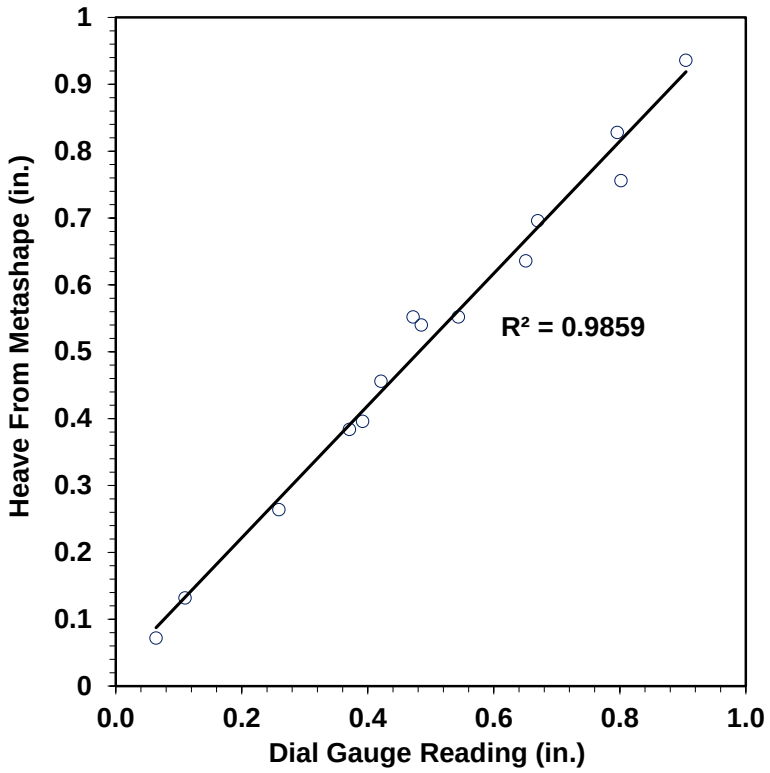

Figure 42: R-squared value from Dial gauge and Metashape Measurement

In this study, we compared the accuracy of photogrammetry with that of the dial gauge method for measuring heave in soil. We found that the average difference between the measurements obtained using the two methods was only 0.03 inches, with the maximum difference being 0.08 inches. However, it is worth noting that some of the data could not be compared as some of the readings from the dial gauge were lost due to the displacement limit of the gauge being reached during the pullout test. From the R-squared analysis (*Figure 42*) the value is found to be nearly 0.99 excluding the points where the dial gauge reading cannot be obtained. Despite this limitation, the results of this study indicate that photogrammetry is a reliable tool for measuring heave in soil with reliable accuracy, even in scenarios where the displacement limit of the dial gauges is limited to a few inches.

It is important to note that the potential applications of close-range photogrammetry in soil heave measurement are not limited to cases where the displacement limit of the dial gauges is reached. In fact, photogrammetry can be used to measure heave in scenarios where the displacement of the surface is greater than expected, making it a useful tool in geotechnical engineering. Moreover, photogrammetry offers several advantages over traditional methods such as dial gauges, including its ability to capture many data points in a short period of time, and its non-contact measurement approach, which eliminates the need for physical contact with the soil surface. Overall, the results of this study demonstrate the potential of photogrammetry as a reliable and efficient tool for measuring soil heave in geotechnical engineering applications.

In addition, for the test with a 55 cm embedment depth, the dial gauge readings were plotted against the corresponding pullout load recorded from the load cell (*Figure 43-45*). This provided additional insights into the behavior of the soil under different conditions, allowing for a more comprehensive analysis of the data obtained from the tests.

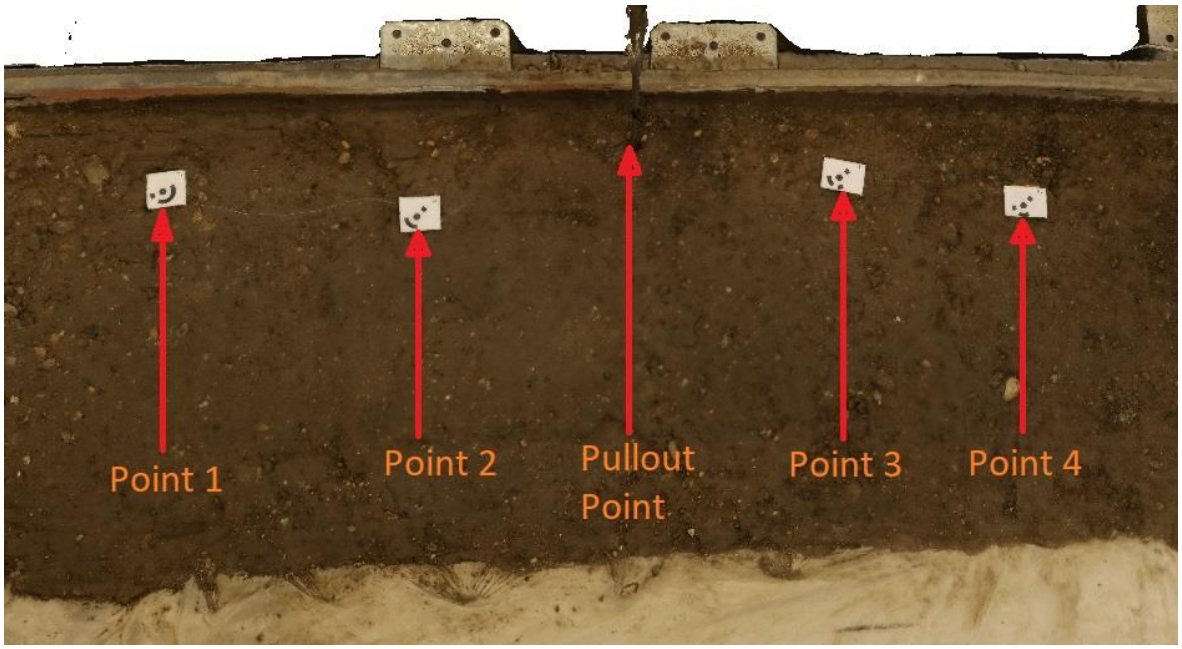

Figure 43: Location of points with respect to pullout location

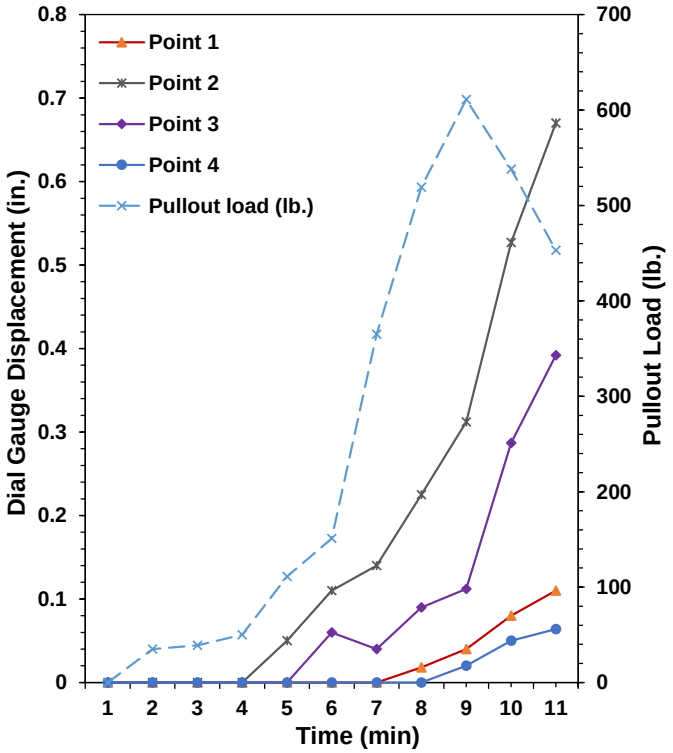

Figure 44: Plot of Load and Dial gauge reading for 55 cm embedment depth plotted with time

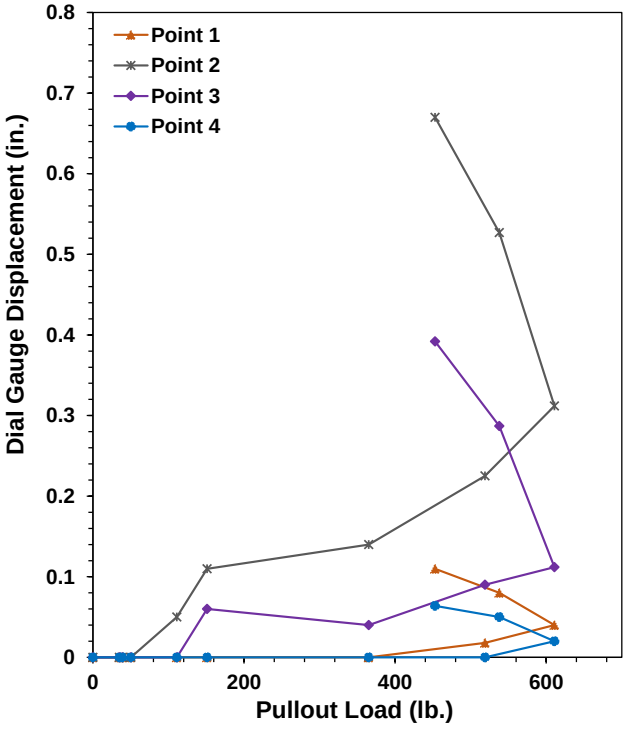

Figure 45: Surface Displacement plotted with Load

The figure presented above illustrates the correlation between the load and dial gauge reading during the pullout test. This test was conducted over a period of two strokes, with each stroke lasting 5 minutes. The coded targets were arranged from left to right, with points 1 and 4 located furthest from the cable and points 2 and 3 closer to the cable. At the end of the first stroke and with some pullout load, heave was observed in the central points (2 and 3), while the heave in points 1 and 4 was insignificant and only became apparent during the later stages of the test. As the pullout load decreased after reaching the maximum point, the heave on the surface continued to increase. The point in the test where the load began to decrease, and the heave increased exponentially can be considered the failure point.

This information is of great importance for understanding the behavior of the soil during the pullout test and can aid in predicting the potential for heave under various conditions. The differences in heave between the central and outer points emphasize the significance of the location of the measurement points when analyzing soil heave. By observing the behavior of the soil at different points during the test, we can better understand the mechanisms underlying soil heave and identify areas of potential instability.

4.1.4 Heave Pattern Analysis

The pattern of heave can be compared for different embedment depths. The comparison is eased by comparing DEMs before and after the end of the pullout test. Heave pattern can be seen by comparing the contour colors of the surface. While the heave in the surface varies depending upon the test setup, and number of strokes still we can have some relevant comparison of the results of DEM of different embedment depths.

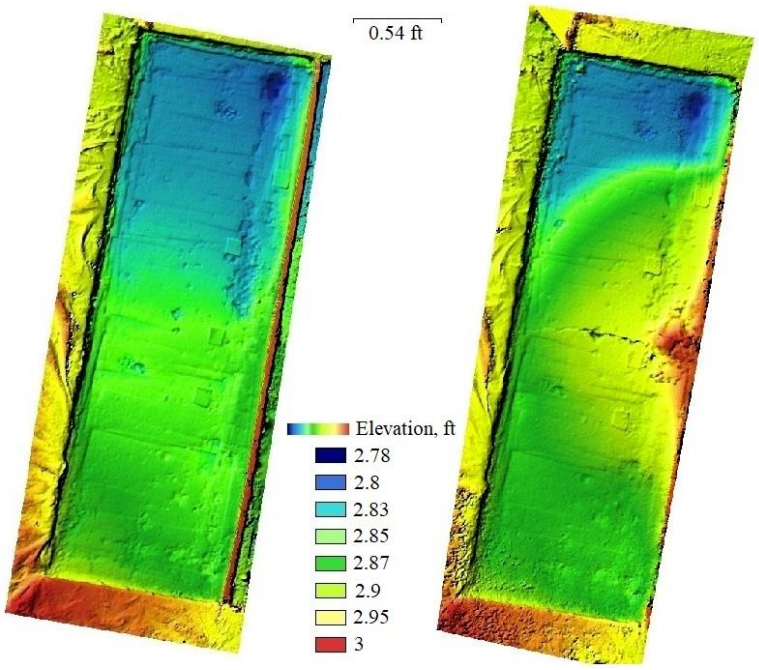

(a) (b)

Figure 46: DEM of 65cm embedment depth (a) before and (b) after pullout test

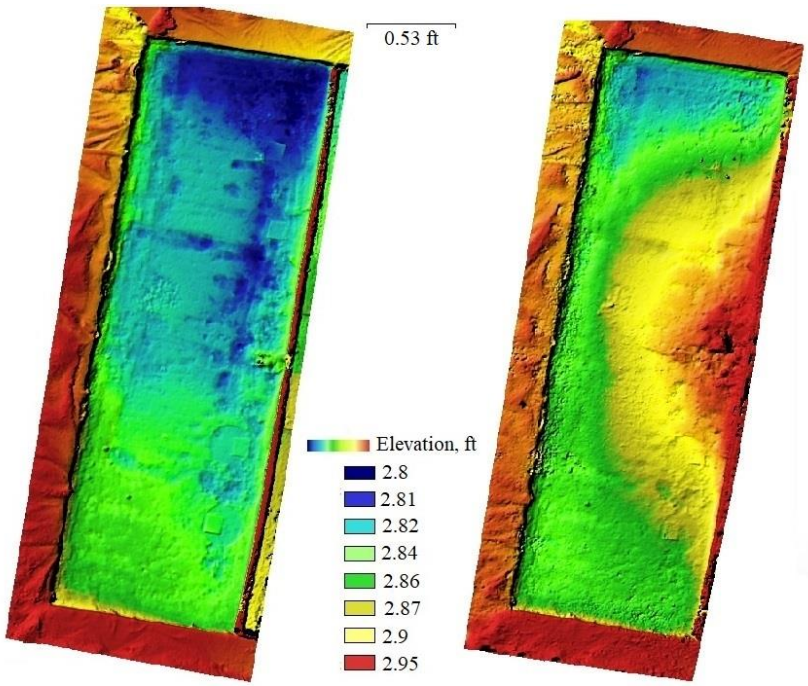

(a) (b)

Figure 47: DEM of 75cm embedment depth (a) before and (b) after pullout test

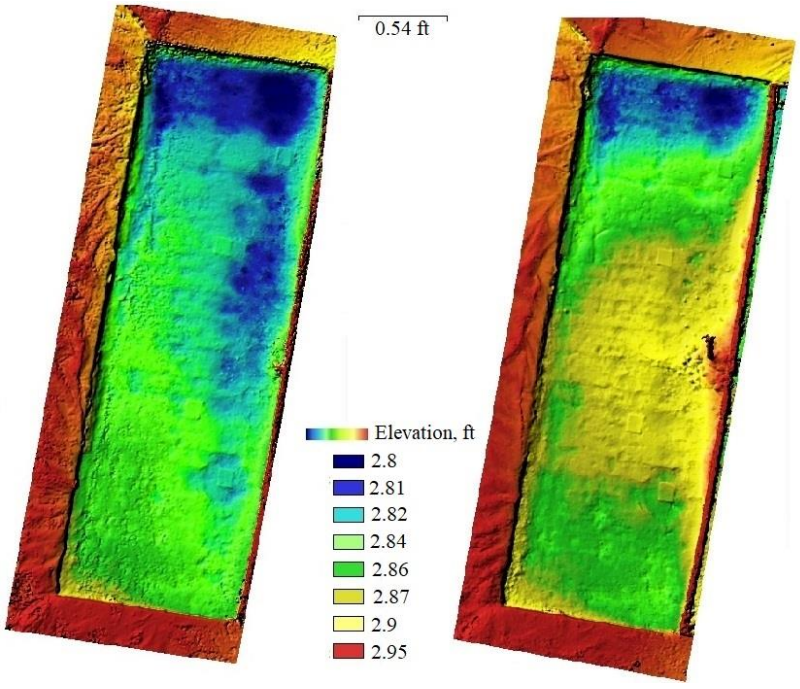

(a) (b)

Figure 48: DEM of 85cm embedment depth (a) before and (b) after pullout test

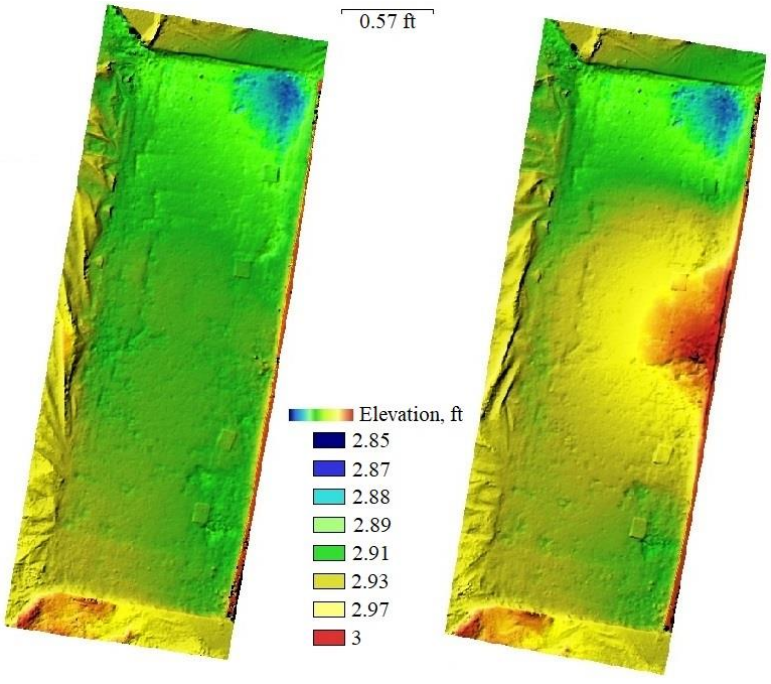

(a) (b)

Figure 49: DEM of 55cm embedment depth before (a) before and (b) after pullout test

Analyzing the contour of the heave generated from the difference of elevation of initial and final after pullout shown in *Figure 50*, the analysis shows that for the lesser embedment depths of 55 and 65 cm depths, the heave can be seen with a small radius. The heave was also acquired with a lesser number of hydraulic jack strokes. Similarly, for the 75 and 85-cm depth embedment, the heave had a greater radius on the surface. The stroke number for higher embedment was also higher to get the heave surface in the soil.

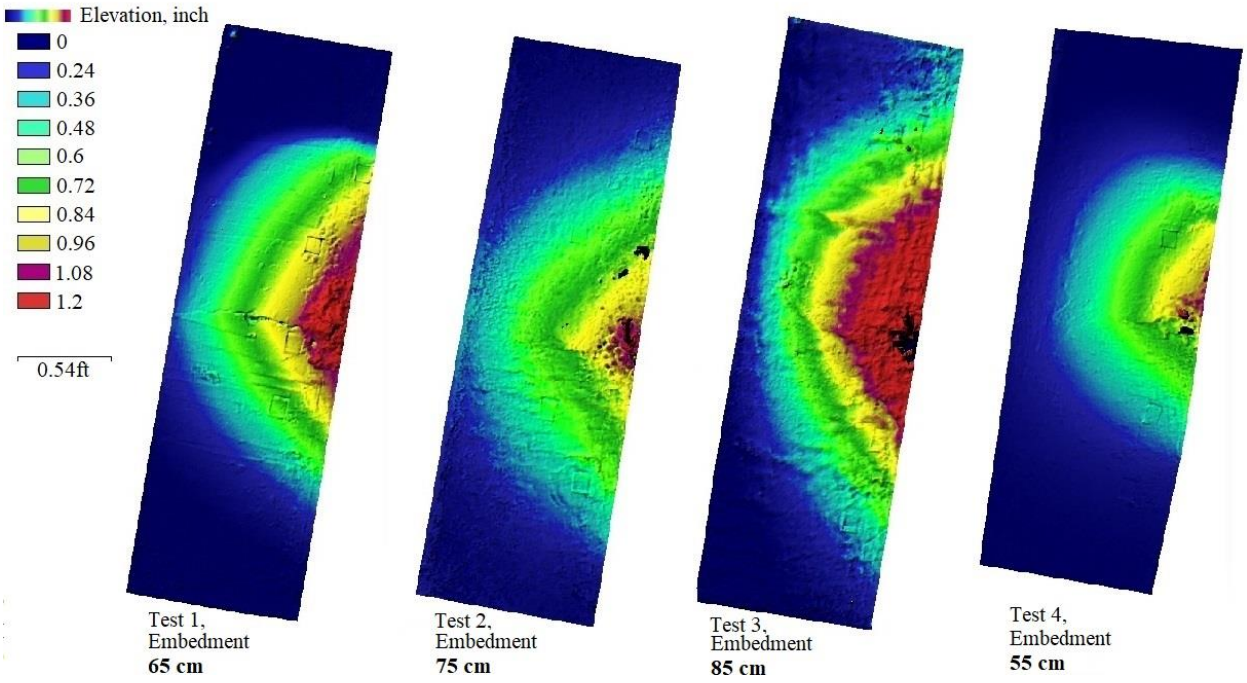

Figure 50: Heave surface contour of each test, calculated subtracting initial elevation from final elevation after pullout test.

In addition, the coordinates of the DEM are exported and plotted in MATLAB for better visualization. The coordinates can be extracted with ease to the desired format for further processing. In MATLAB we meshed and created the surface with the color pattern. The resulting

sample 3D surface of the heave and 2D map of the heave was generated and is presented for 65 cm embedment in *Figure 51*.

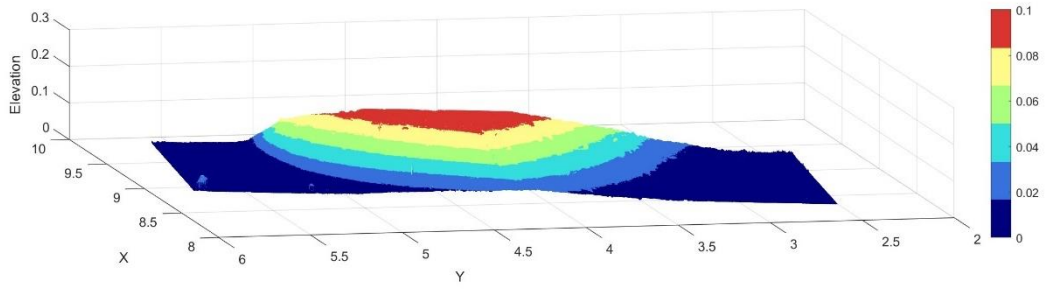

(a)

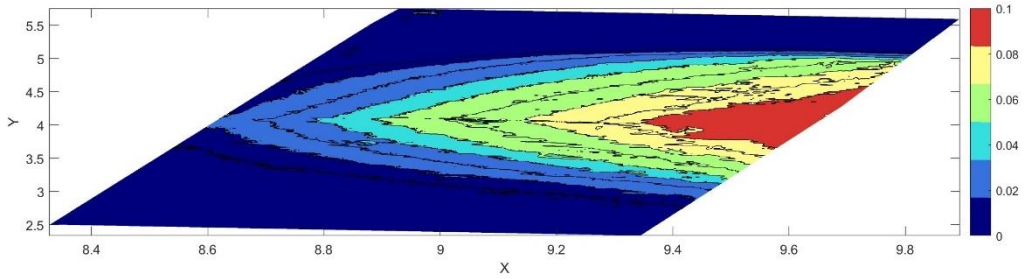

(b)

Figure 51: The plotted heave surface for the test E65 in MATLAB (a) 3D and (b) 2D (Dimensions in ft.)

4.2 Field 3D Modelling and Slope Monitoring

3D modeling is the creation of a three-dimensional representation of a surface or object using specialized software. Slope monitoring involves the use of sensors to measure the stability of slopes and detect potential hazards such as landslides.

4.2.1 Schedule of Activities

We conducted a total of 5 field visits to acquire the coordinates of the control and ground points necessary images for the 3D modelling and slope monitoring. The survey was conducted to determine the coordinate of the slope then followed by a series of image acquisitions. The summarized table for the site visits along with a brief description of works is tabulated below in *Table 5*.

Table 5: Schedule of Site Activities

Date	Purpose of Visit	Task Performed
January 27, 2023	Survey of Control Points and Ground Points	Survey coordinates of 15 control points and 6 GPs
January 28, 2023	Image Acquisition	Image acquisition for complete slope with 905 images
February 24, 2023	Image Acquisition	Image acquisition of southeast slope with 259 images
March 9, 2023	Image Acquisition	Image acquisition of southeast slope with total 305 images. Three GPs were added for higher accuracy.
March 24, 2023	Image Acquisition	Image acquisition of southeast slope with 275 images
April 6, 2023	Image Acquisition, Raising Elevation of GCP	Image acquisition of southeast slope with 264 images. Two GPs were raised using GPs 6 inches.

4.2.2 Survey Results

During the visit on January 27th, 2023, a survey of the ground points and reflective targets on the column was performed. The survey used a total of 9 reflective targets and 4 black and white ground check points on the east side of the slope, while the west side had 6 reflective targets and 2 ground checkpoints. To establish a reference point, we assumed an arbitrary point at the edge of the east slope as the zero point for the east and north coordinates. The elevation was also assumed to be 500 feet, and the coordinates were recorded based on the assumed benchmark.

The survey results for both the reflective targets and ground points are presented below for the east and west sides, respectively in *Table 6-7*. These measurements provided critical data that allowed us to accurately map and model the slope, aiding in the analysis and evaluation of its behavior and characteristics. By establishing a reference point and accurately measuring the reflective targets and ground points, we could ensure that their subsequent work was precise and reliable.

Table 6: Coordinates of Points of East Side

Point ID	Easting	Northing	Elevation
East 11 Ground Point south	-72.92	86.86	490.12
East 12 Ground Point	-41.39	51.93	494.89
East 13 Ground Point	30.06	41.83	487.71
East 14 Ground Point north	135.35	27.74	488.54
East 21 column outside south	-7.61	41.49	494.68
East 22 column outside mid	39.76	32.83	492.59
East 23 column outside north	174.24	23.68	490.41
East inside column 1 north	204.98	22.22	488.58
East inside column 2	146.05	33.42	486.57
East inside column 3	69.36	31.48	490.48
East inside column 4	40.28	36.93	489.97
East inside column 5	-7.33	46.09	491.66
East inside column 6 south	-27.48	49.94	493.47

Table 7: Coordinates of West Side

Point ID	Easting	Northing	Elevation
West inside column 1 south	85.48	123.00	490.74
West inside column 2 mid	125.54	115.91	489.07
West inside column 3 north	181.09	105.33	484.50
West Ground Point 11 North	110.58	111.49	482.96
West Ground Point 12 South	28.00	139.81	486.35
West column outside North	153.92	114.33	485.99
West Column Outside middle	125.49	119.80	487.73
West Column Outside South	107.10	122.68	489.69

The Leica TC405 has an angle measurement accuracy of 5 seconds, which is equivalent to 0.0014 degrees or 0.024 miles, according to the manufacturer's specifications. Additionally, the instrument's distance measurement accuracy is ± (0.0066 ft + 2 ppm), where ppm stands for parts per million. This means that for every 3,281 ft distance measured, there could be an error of up to 0.007 ft plus an additional 2 ppm. The precision of the Leica TC405, which is a mid-range total station, depends on various factors, including the operator's skill, the instrument's calibration, and the operating conditions. High-accuracy measurements with the Leica TC405 require careful consideration of these factors. The camera was not calibrated and had some minor reliability issues, which resulted in some errors. As a result, the error was calculated to be ± 0.015 ft.

4.2.3 3D Model Output

To generate a 3D model of the slopes for visualization of the slope profile, the images were processed using Metashape software. Due to the large area of both sides of the slopes, the images were divided into three chunks, namely the east section, middle section, and west section, for processing. Once the processing of these chunks was completed, they were merged to produce a complete 3D model of the slope.

The generated 3D model of the slope provided detailed information about the slope's surface features, which were enhanced through the mesh refining features of Metashape as seen in *Figures 52-60*. Additionally, 3D textured images of the east slope, west slope, and the combined slope were also generated to provide a comprehensive view of the slope. These images not only showcased the slope's physical characteristics but also provided a clear visualization of the slope profile, making it easier to understand and analyze.

Figure 52: Unfiltered sparse cloud of slope

Figure 53: Unfiltered dense cloud of slope

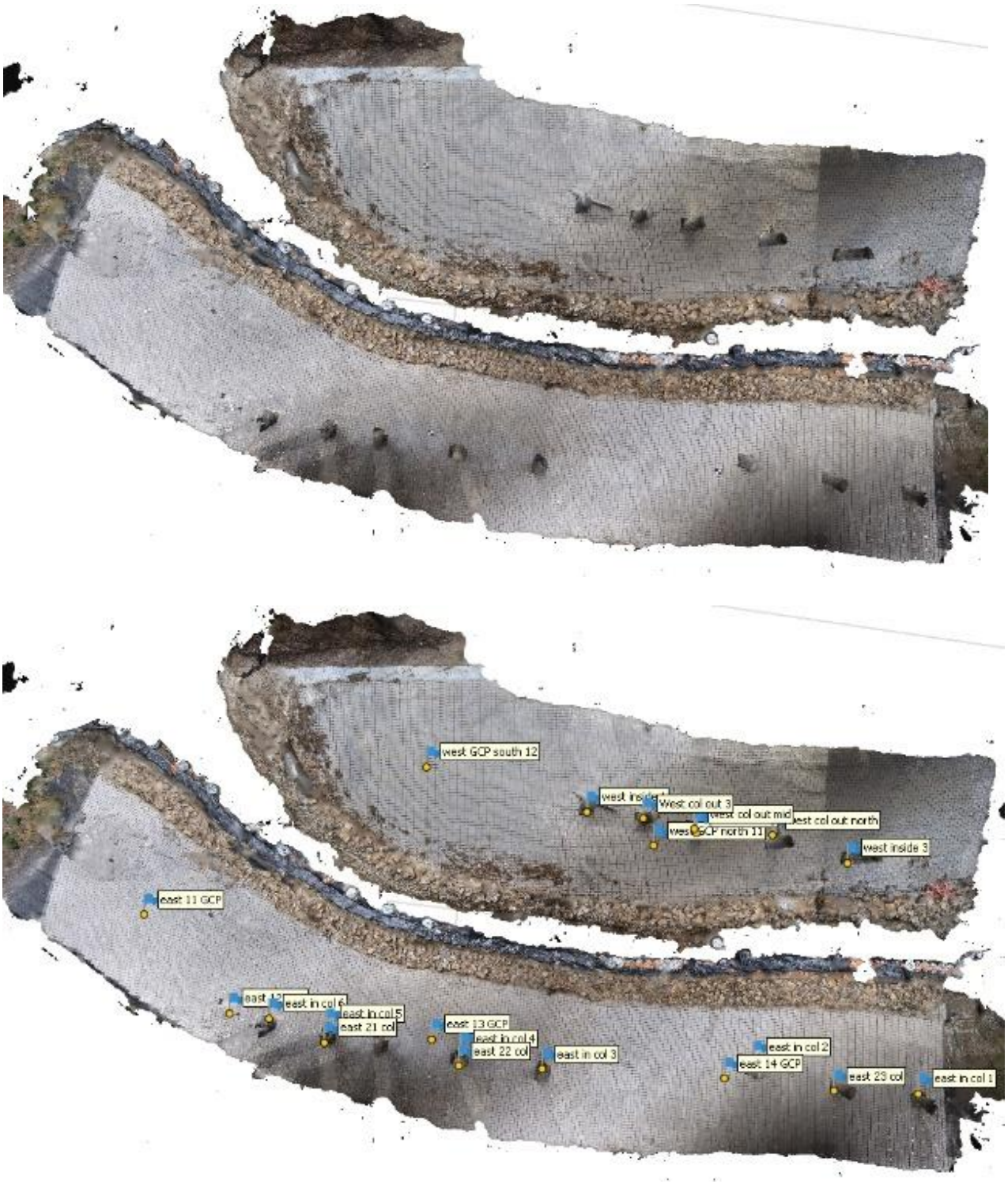

Figure 54: 3D Textured Model of the Slope Top view (Top) with placing of markers (Bottom)

Figure 55: 3D model of west side

Figure 56: East side 3D model

Figure 57: 3D model north to south (Top) and south to north (Bottom)

4.2.4 Digital Elevation Model and Orthomosiac

Figure 61 shows the generated digital elevation model (DEM) of the site through Metashape software. DEM can be generated via tie points, dense cloud, and generated mesh structures. In this study, the DEM was calculated from a dense cloud as it can culminate in more accurate results.

Orthophoto or ortho mosaic as an aerial photograph or viewpoint also was generated from the resulting DEM and mesh by rectifying the camera distortion making it a single high-resolution image. *Figure 62* presents the orthophoto of the combined slope. For further study, *Figure 63-64* shows 5 cross sections were generated to resemble the exact profile of the slope.

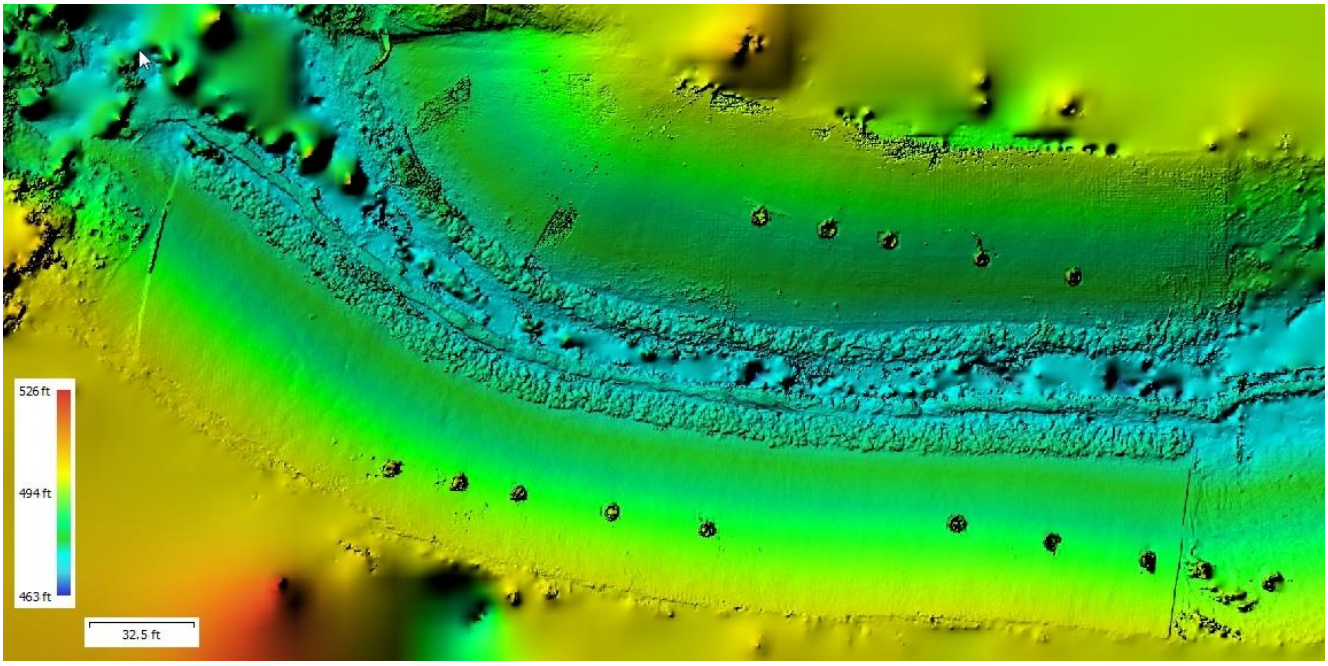

Figure 58: DEM of slope

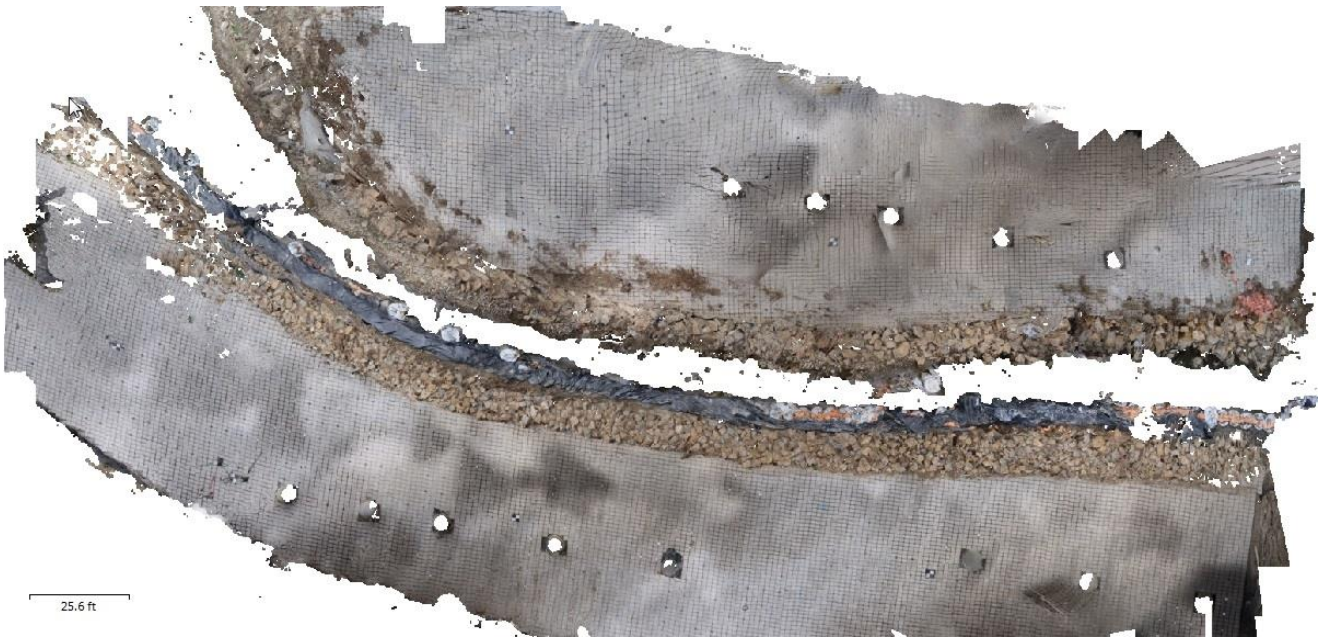

Figure 59: Orthophoto of slope

Based on the DEM of the profile (*Figure 61*), it was observed that the elevation of the slope ranged from 500 feet at the peak of the slope to around 475 feet close to the slope's valley. Furthermore, the software generated colored palettes of the DEM data for contour visualization.

To study the characteristics of the slope and compare it with the design, five cross-sections at different points were taken from the east side to the west side (*Figure 63*). These sections, numbered from 1 to 5 with section 1 on the north side until 5 at the south of the field provided a comprehensive understanding of the slope's nature.

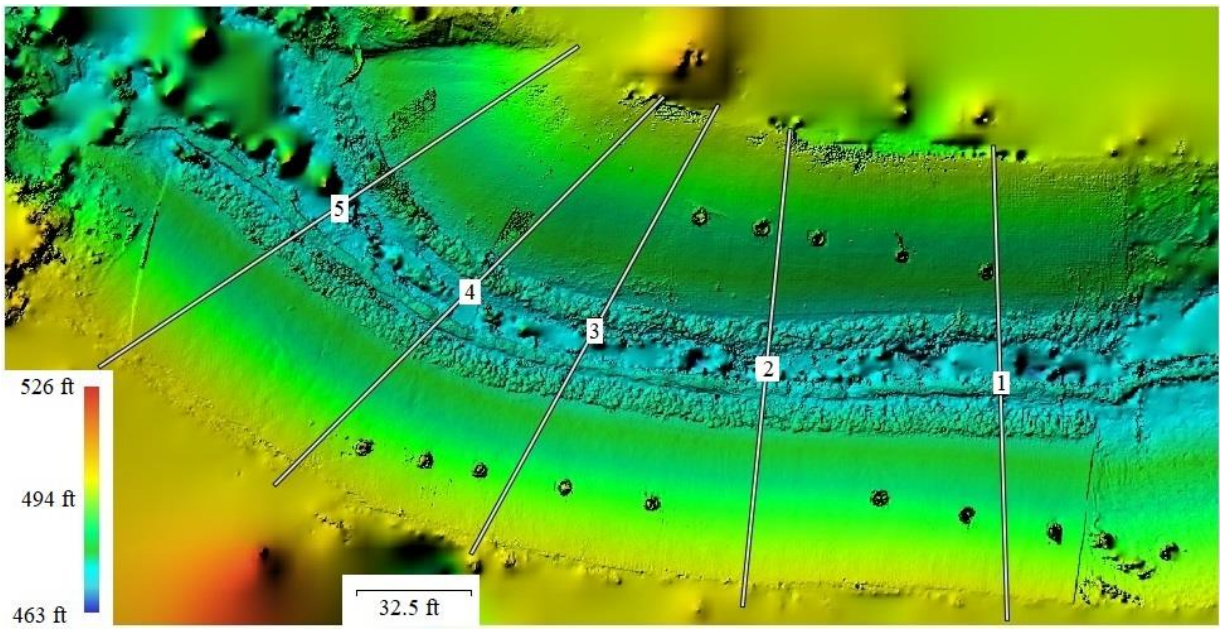

Figure 60: Location of Cross sections

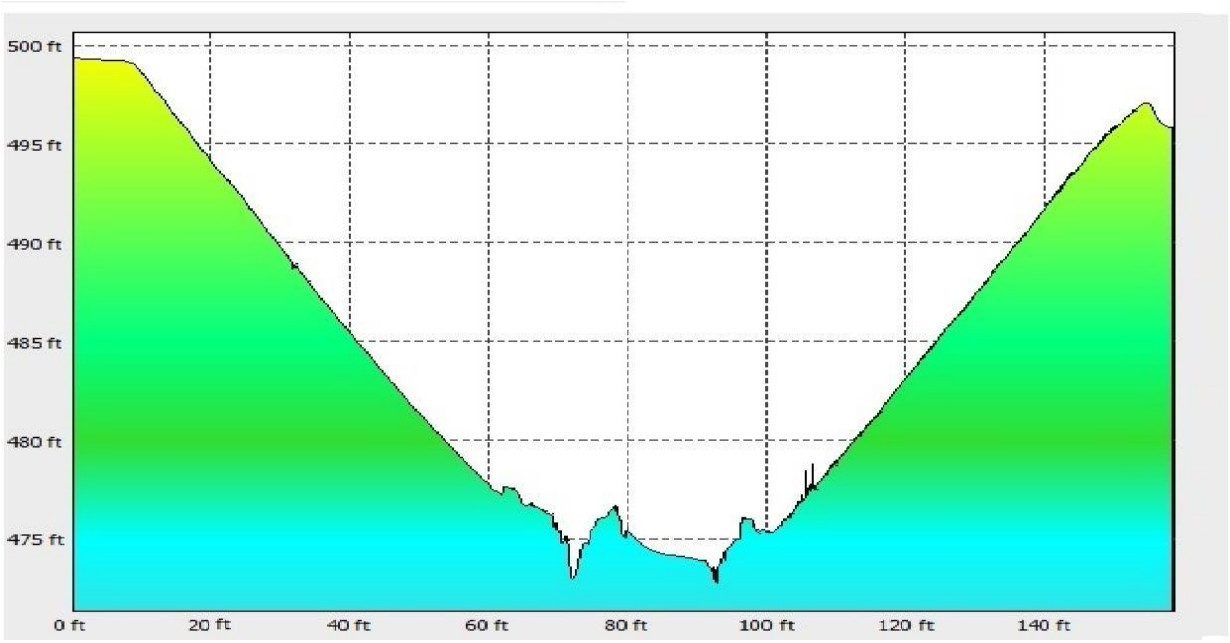

(a)

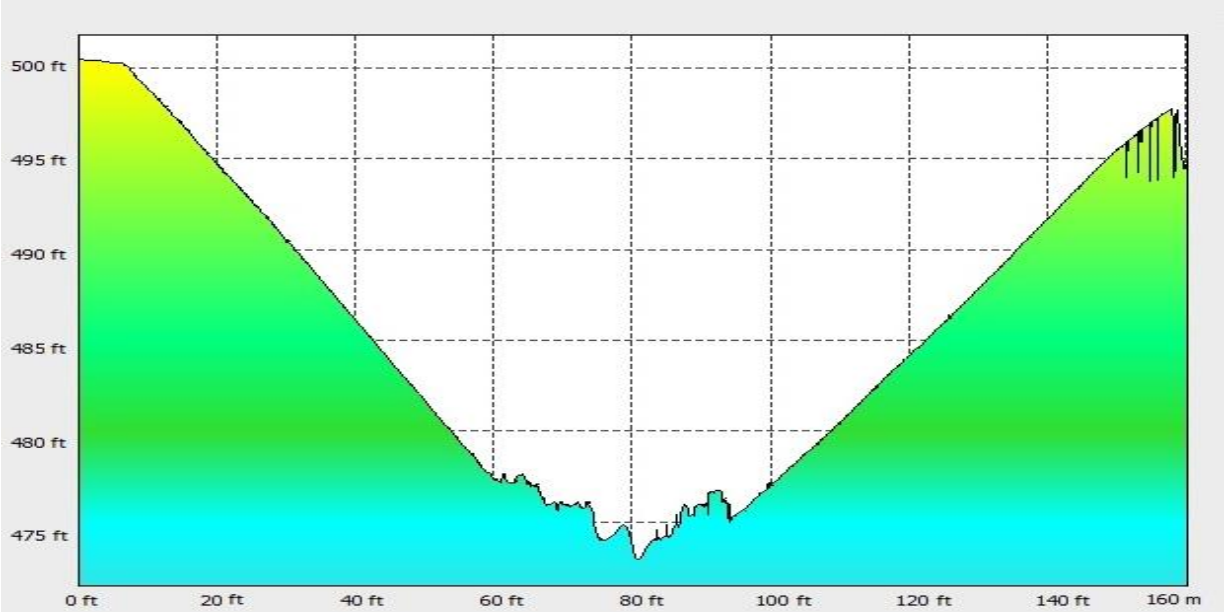
500 ft
495 ft
490 ft
485 ft
480 ft
475 ft
0 ft
20 ft
40 ft
60 ft
80 ft
100 ft
120 ft
140 ft
160 m

(b)

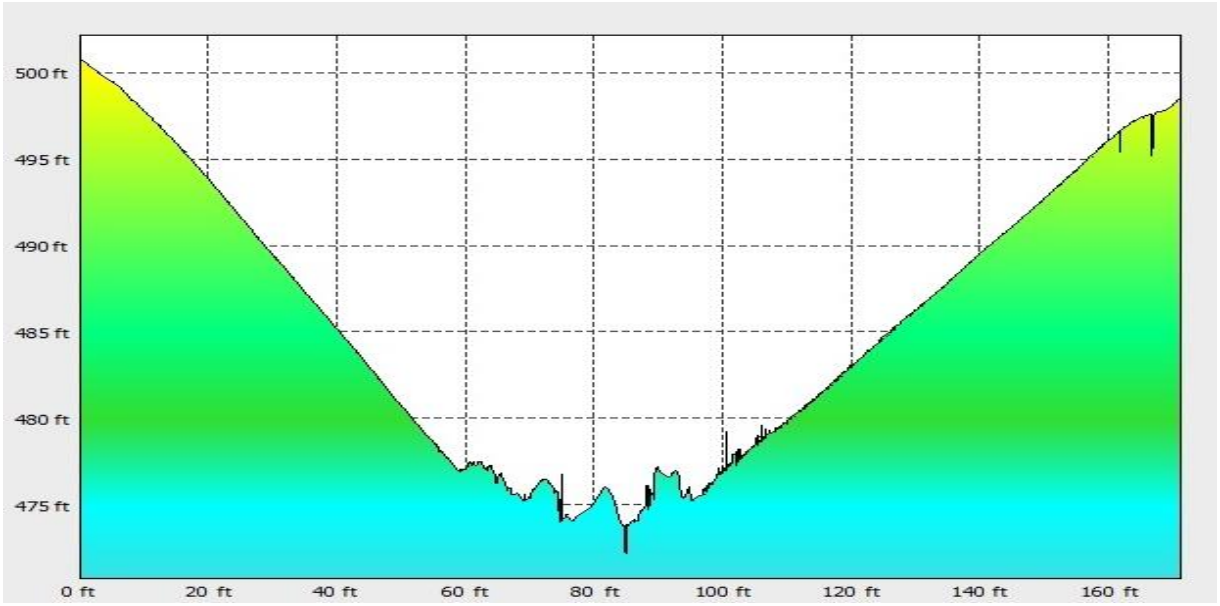
500 ft
495 ft
490 ft
485 ft
480 ft
475 ft
0 ft
20 ft
40 ft
60 ft
80 ft
100 ft
120 ft
140 ft
160 ft

(c)

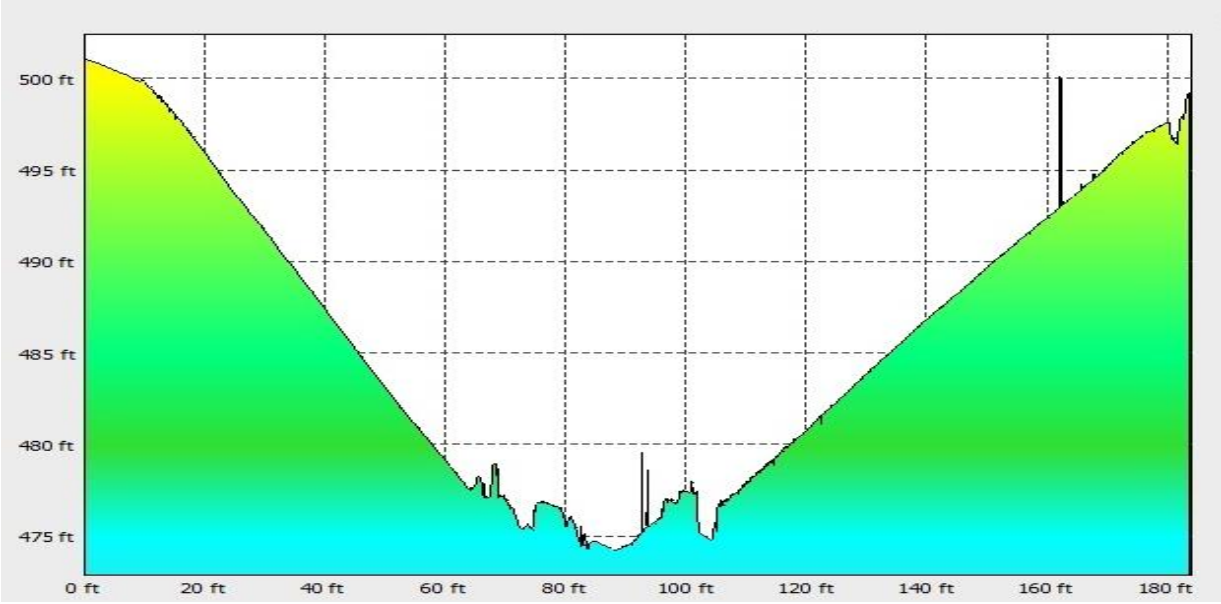

(d)

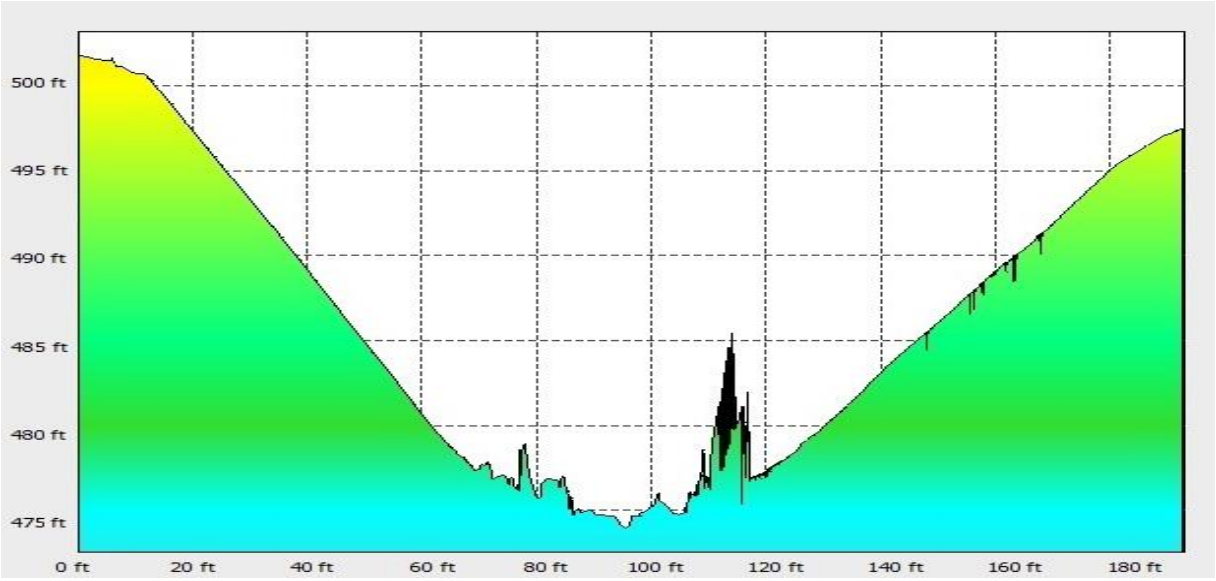

(e)

Figure 61: Cross section along 1 (a) to 5 (e)

After analyzing the cross sections of the riverbank slope, it was observed that the slope inclination is steeper on the east side compared to the west side. The average H: V ratios of the east and west sides were determined to be 2.5:1 and 3:1, respectively, based on the analysis of five cross-sections. The slope profile was found to be uniform across all sections, except for a slightly flatter

southern part in the west side. The water channel showed some noise during the analysis, and a peak was visible on the western side of section number 5 due to vegetation.

This analysis also verifies that the minimum 2:1 slope design in the contract was achieved. The eastern side of the slope is restricted due to the presence of the service road, which results in the slope becoming steeper with less space available.

The cross-section of the riverbank slope generated from Metashape can have various applications. It can be used to study the nature of the slope, assess the stability of the slope, and check against the design. The slope cross-section can also be used to calculate the volume of soil or rock needed to be removed or added for construction or maintenance purposes. In addition, it can aid in identifying potential hazards, such as areas of erosion or instability, and help develop strategies to mitigate them. Furthermore, the slope cross-section can be used to monitor changes in the slope over time and compare them to previous measurements to assess any changes or trends. Overall, the cross-section of the riverbank slope generated from Metashape can provide valuable information for various applications related to river management and engineering.

4.2.5 Accuracy of the Photogrammetric Application

To ensure accurate results from image processing, ground points' coordinates are used for accuracy testing, and compared with field survey data. Ground points, marked in images, serve as checkpoints to measure accuracy. In this case, there are four ground checkpoints in the east and two in the west. The coordinates of these checkpoints are calculated using Metashape and compared to survey data, which is displayed in *Table 8*.

Table 8: Comparison of Coordinates from Metashape with Survey Data Difference and Distance

Description	Survey Data			Metashape data			Difference			Difference Distance (ft.)
	X	Y	Z	X	Y	Z	ΔX	ΔY	ΔZ	
East 11 GCP south	-72.92	86.86	490.12	-73.02	86.82	490.20	0.104	0.036	0.077	0.134
East 12 GCP	-41.39	51.93	494.89	-41.39	51.92	494.90	0.003	0.007	0.008	0.011
East 13 GCP	30.06	41.83	487.71	29.94	41.80	487.76	0.124	0.031	0.050	0.137
East 14 GCP north	135.35	27.74	488.54	135.26	27.77	488.61	0.086	0.032	0.066	0.113
West GCP north 11	110.58	111.49	482.96	110.80	111.66	483.16	0.218	0.173	0.201	0.343
West GCP south 12	28.00	139.81	486.35	28.19	140.04	486.46	0.191	0.225	0.106	0.314

Table 9: Mean and Standard Deviation of Difference Coordinates

Location	Difference, ft			Difference Distance (ft.)	Difference, ft			Difference Distance (ft.)
	ΔX	ΔY	ΔZ		ΔX	ΔY	ΔZ	
	Mean				Standard Deviation			
Whole slope	0.121	0.084	0.085	0.175	0.07	0.083	0.06	0.116
East Side	0.079	0.026	0.05	0.099	0.046	0.011	0.026	0.052
West Side	0.205	0.199	0.154	0.328	0.014	0.026	0.048	0.015

To ensure the accuracy of Photogrammetry by Metashape, the difference between the X, Y, and Z values obtained from the Metashape and survey data is compared for the ground control points. The distance of the point from the survey coordinates was also calculated to determine the relative deviation from the actual location. The error values for the east and west sides of the slope are presented in a table, and it is observed that the mean and standard deviation (*Table 9*) in the error of survey data and values from Metashape in the east side is lower compared to the west side.

This can be explained by the fact that a higher number of distributed targets can lead to a more accurate model in image processing.

4.2.6 As-Built Slope Stability Analysis

The stability analysis of the complete slope was performed by selecting the steepest cross-section, and the soil properties were obtained from a combination of site investigation and lab tests. The analysis was carried out using GeoStudio software, and a factor of safety was calculated. The soil profile consisted of a top layer of Lean Clay, followed by clayey sand and Limestone. There was a thin layer of weathered limestone between the limestone and sandy layer. The piezometric head was found to be at a depth of 12 feet. The soil properties were illustrated in a diagram. The steepest part of the slope was observed to be at a slope of 2.5:1 (H: V).

The slope's natural stability was analyzed without any reinforcement or surcharge, and a factor of safety of 1.2 was obtained as shown in *Figure 65*, indicating that slope protection methods should be employed. Therefore, the slope was analyzed after applying a surcharge from ACB and reinforcement from PDEA (*Figure 66*). The factor of safety was increased to 1.8 after soil stabilization, which was found to be satisfactory for the slope's stability.

Color	Name	Slope Stability Material Model	Unit Weight (pcf)	Effective Cohesion (psf)	Effective Friction Angle (°)
	Clayey Sand / Clayey Gravel	Mohr-Coulomb	125	0	30
	Lean Clay	Mohr-Coulomb	125	100	22
	Limestone	Bedrock (Impenetrable)			
	Weathered Limestone	Mohr-Coulomb	145	0	45

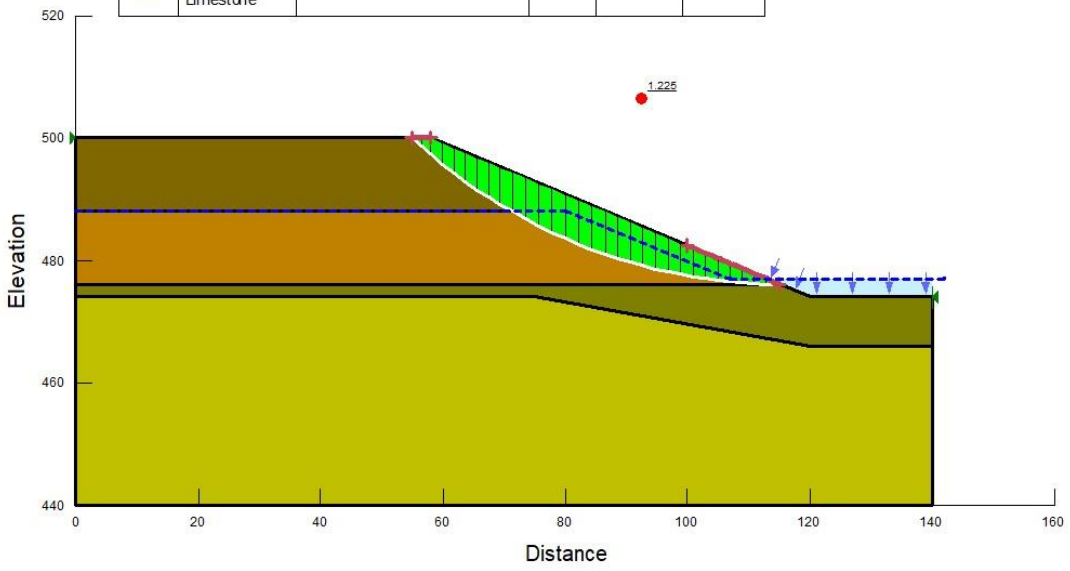

Figure 62: Slope without anchor and surcharge, FS=1.225 (Dimension in ft)

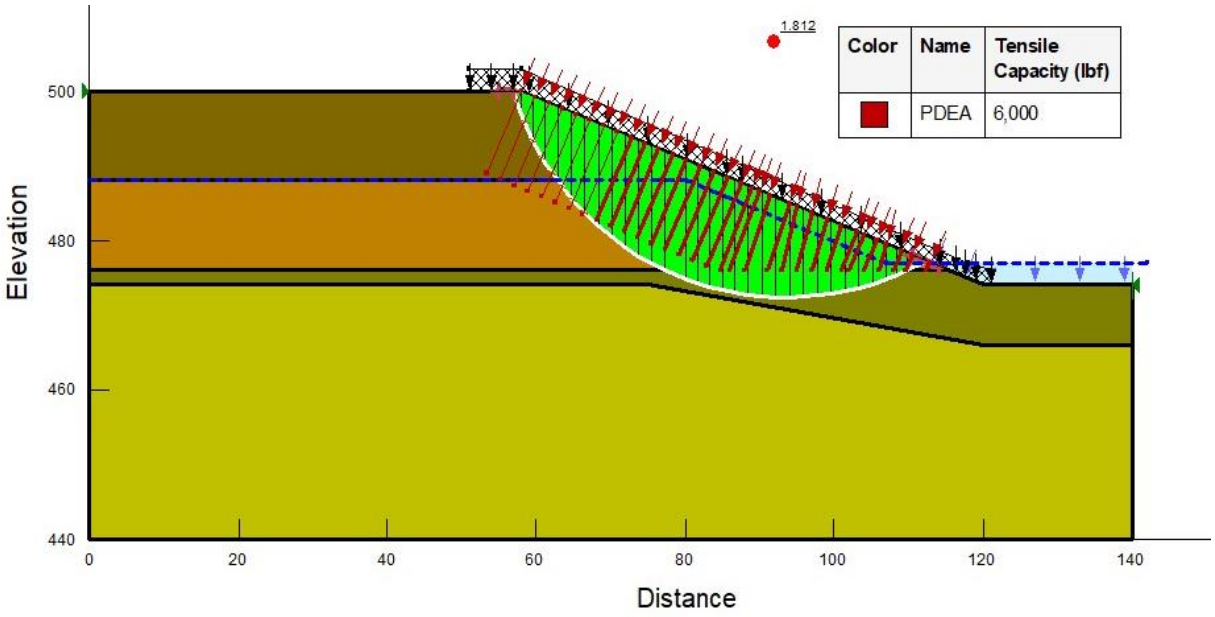

Figure 63: Slope with Anchor and Surcharge, FS=1.812 (Dimension in ft)

4.2.7 Analysis of the Inclinometer Section (Slope of South-East Section)

As a part of our photogrammetric application study, we have undertaken the task of monitoring the movement of a couple of points on a slope near the inclinometer installation site (*Figure 67-68*). The objective is to analyze and track any changes or movements in the slope over time from the coordinates obtained from DEM (*Figure 69-70*). To achieve this, five sets of images were captured at different time intervals, starting from December 2022 and continuing till April 2023. During this process, we focused on studying two ground points and their corresponding positions. By analyzing the images and comparing the positions of the ground points across different time intervals, we can gain insights into any changes that may have occurred in the slope as summarized in *Table 10* and plotted in *Figure 71-72*.

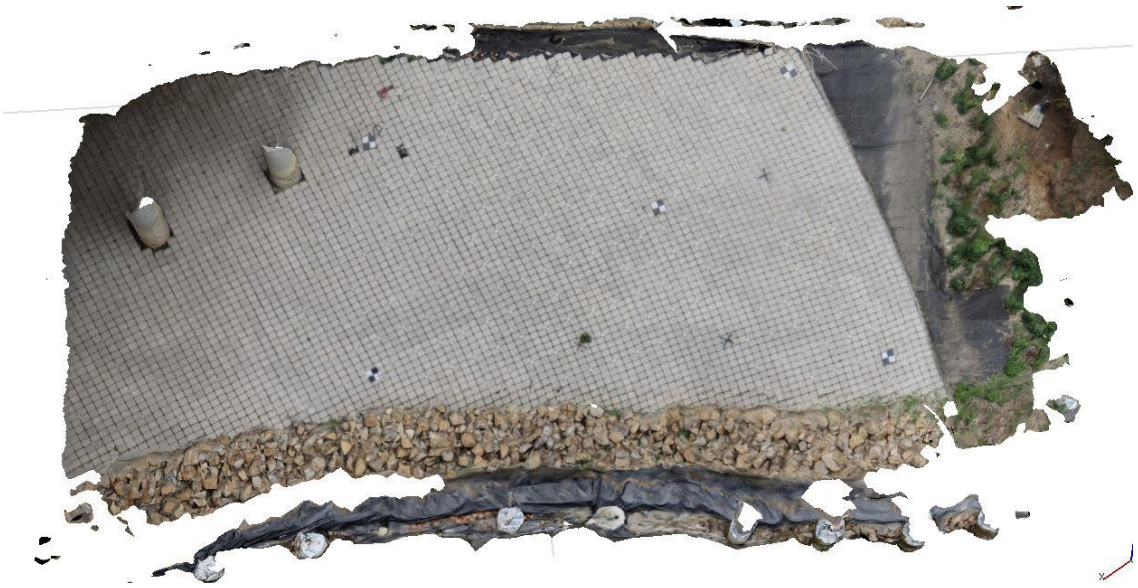

Figure 64: Textured model from March 9 of inclinometer part

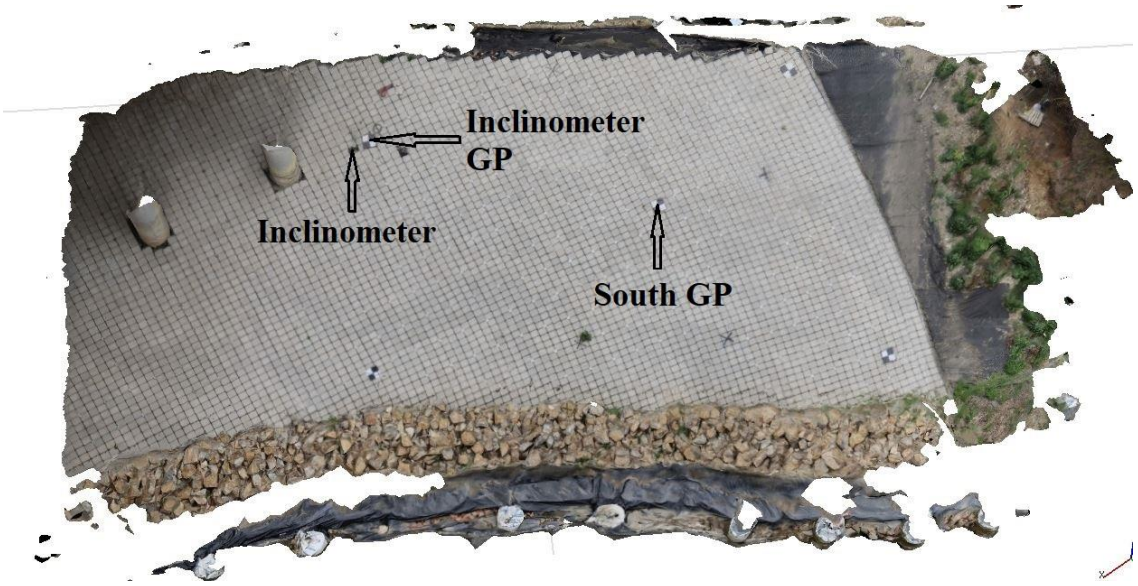

Figure 65: Selected Ground Points for Slope Monitoring

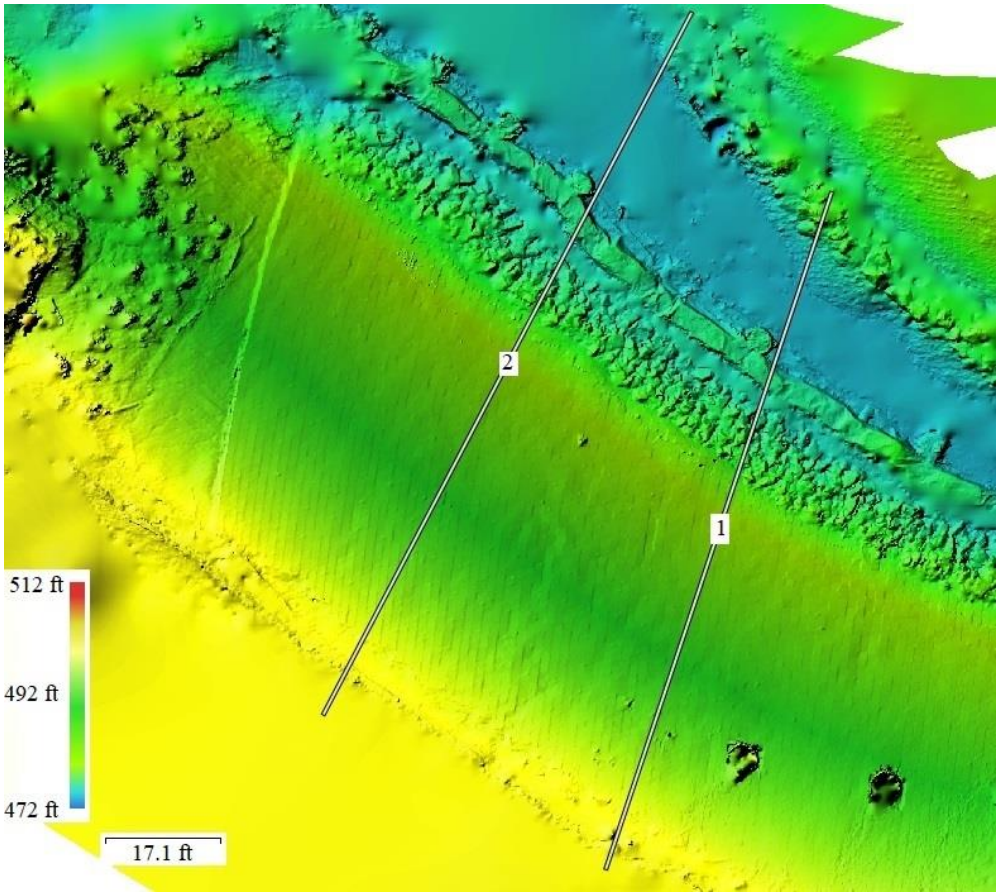

Figure 66: DEM of southeast section of slope with two sections passing from GP

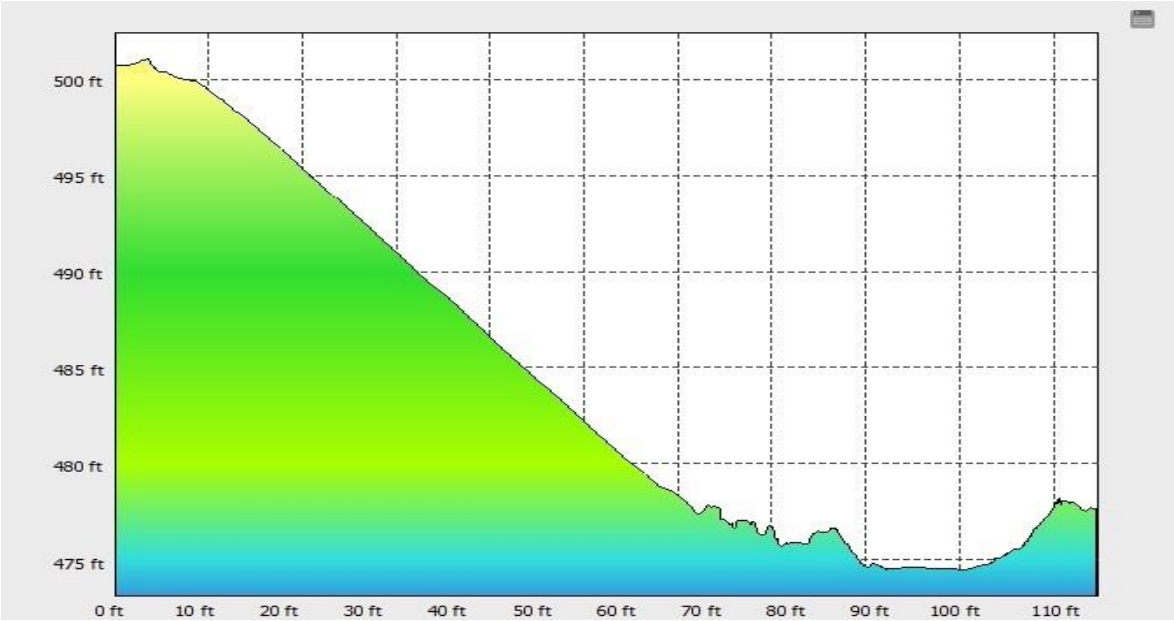

(a)

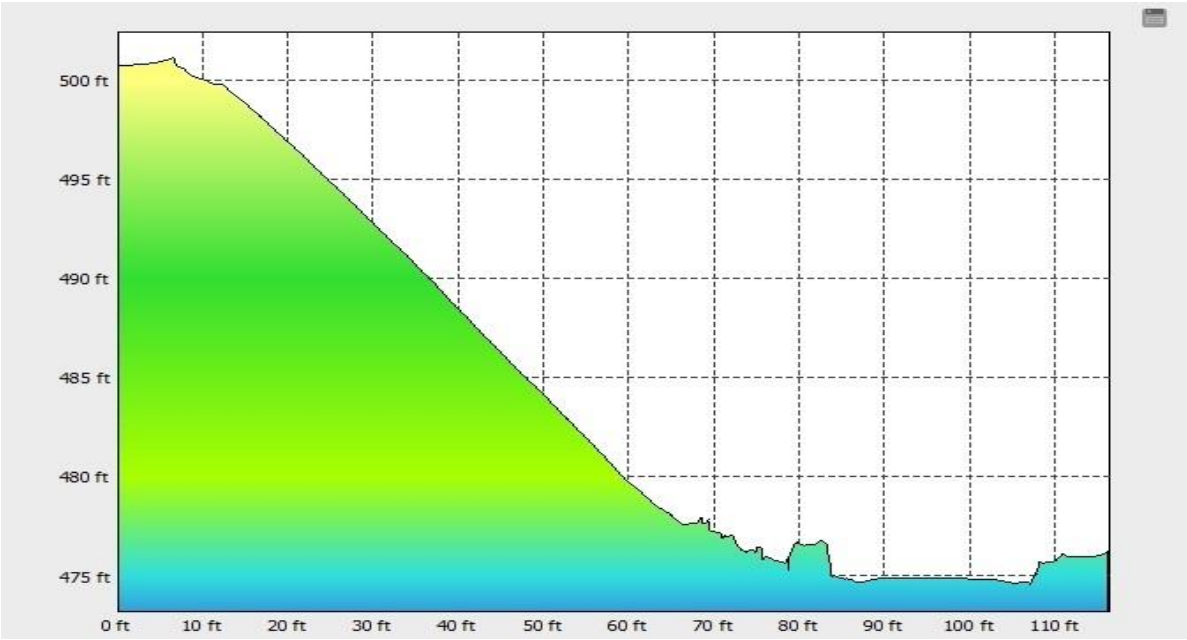

(b)

Figure 67: Cross section at (a) 1 and (b) 2

Table 10: GP Coordinates from Metashape compared with Survey Data

Source and Date	Coordinates (ft)				Difference with Survey Data			Distance with Survey Data, ft
	Point ID	X	Y	Z	ΔX	ΔY	ΔZ	
Survey 1/27	Inclinometer GP	-41.39	51.93	494.89	0	0	0	0
	South GP	-72.92	86.86	490.12	0	0	0	0
Metashape 1/28	Inclinometer GP	-41.398	51.97	495.009	0.008	0.04	0.119	0.126
	South GP	-72.807	86.97	490.107	0.113	0.1096	0.013	0.158
Metashape 2/24	Inclinometer GP	-41.167	51.741	494.932	0.223	0.189	0.042	0.295
	South GP	-72.826	86.884	490.179	0.094	0.0235	0.059	0.113
Metashape 3/9	Inclinometer GP	-41.37	51.939	494.921	0.02	0.009	0.031	0.038
	South GP	-72.919	86.885	490.134	0.001	0.025	0.014	0.029
Metashape 3/23	Inclinometer GP	-41.379	51.928	494.99	0.011	0.002	0.1	0.101
	South GP	-72.769	86.824	490.135	0.151	0.0364	0.015	0.156

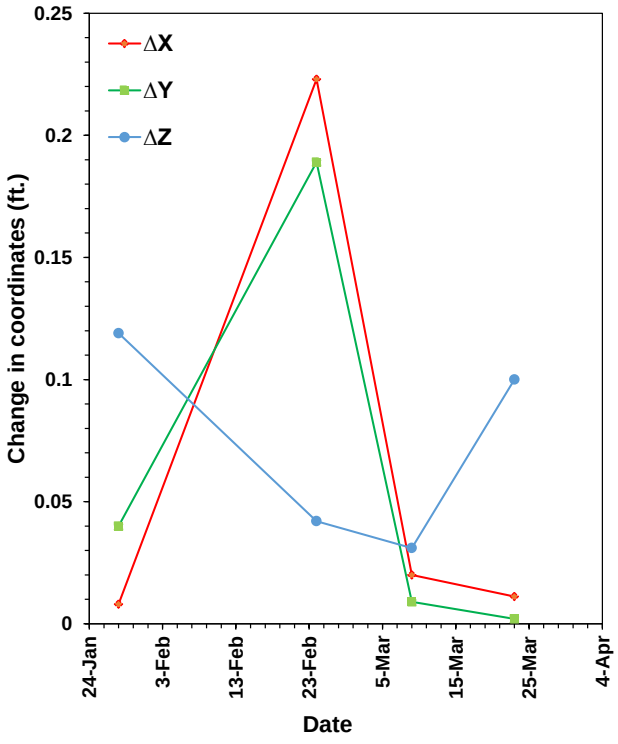

Figure 68: Plot for Change in Coordinates at GP near Inclinometer

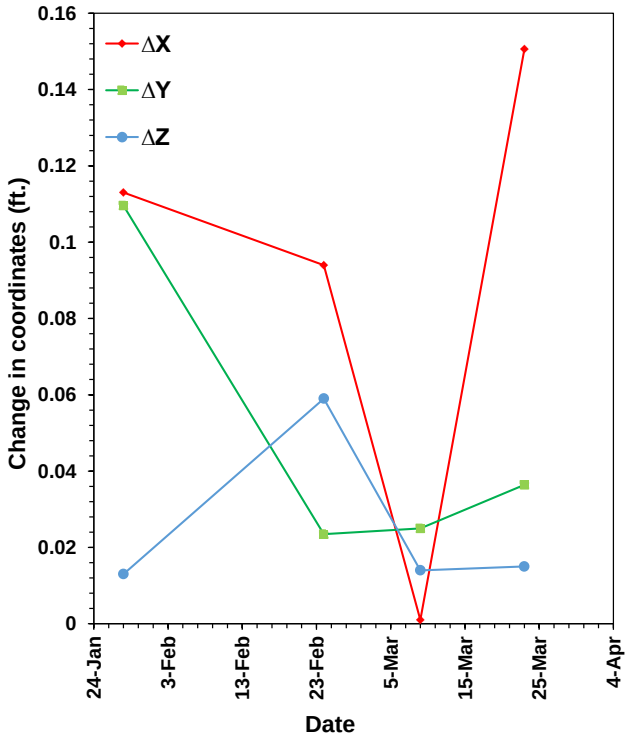

Figure 69: Plot for Change in Coordinates at South GP

Upon analyzing the data presented in the table and graphs, it was observed that there was little to no movement of the point of interest. The values of movement recorded by the inclinometer installed at the site of the slope were negligible and matched exactly with the output from the metashape.

Although, the South GP showed a higher degree of deviation, which can be attributed to the distribution of permanent control points. The permanent control points were placed only in the columns of bridges, which were further away from the South GP compared to the GP near the inclinometer.

Since no movement in the slope was observed, an additional ACB was added on top of the existing ACB for both ground points during the final site visit on April 6, 2023, for image acquisition to demonstrate the validity of the photogrammetry application as shown *in Figure 73*.

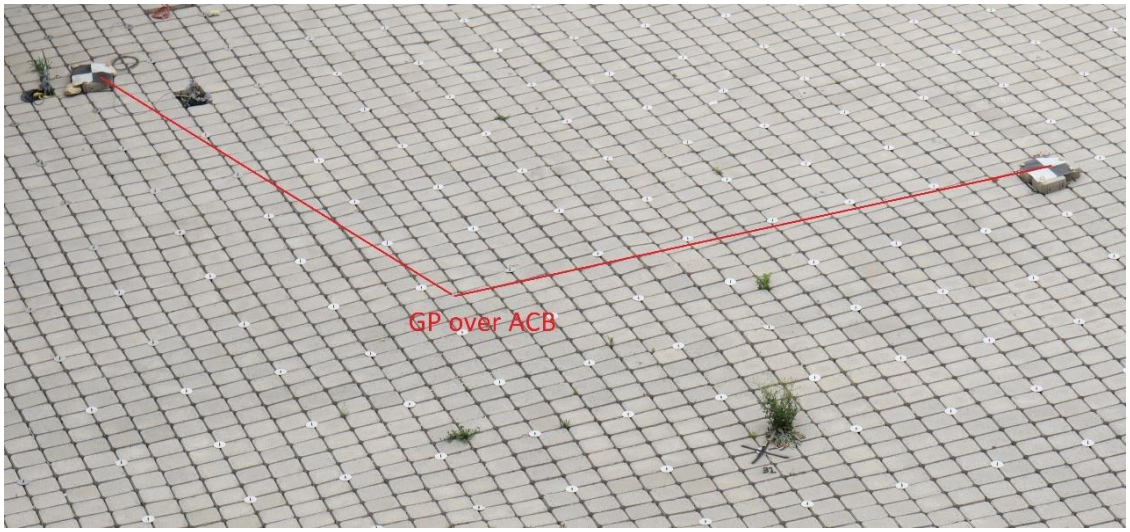

Figure 70: GPs Placed over 6-inch ACB

As seen in the figure the GPs were raised using ACB of an average thickness 6 inches. The calculation, the average X and Y coordinates from the last four site visit were used as shown in *Table 11*.

Table 11: Calculation for X and Y coordinates of GPs

Date/ Coordinates	GP near Inclinometer			South GP		
	X	Y	Z	X	Y	Z
28-Jan-23	-41.4	51.97	495.01	-72.81	86.97	490.11
24-Feb-23	-41.17	51.74	494.93	-72.83	86.88	490.18
9-Mar-23	-41.37	51.94	494.92	-72.92	86.89	490.13
23-Mar-23	-41.38	51.93	494.99	-72.77	86.82	490.14
Average	-41.33	51.9	494.96	-72.83	86.89	490.14

The X and Y coordinates for the ground points (GP) were calculated and used to derive the corresponding Z coordinates. The elevation difference between the computed Z coordinates and the survey data was then calculated. The results showed that there was a change in elevation of 6.4 inches and 6.9 inches for the GP located near the inclinometer and the South GCP, respectively when compared with the survey coordinates. In addition, when compared with the average value of elevation of the last 4 visits the change in elevation is 5.6 inches and 6.6 inches respectively. While the average change in elevation was slightly more than the average thickness of the ACB block used, it demonstrated the capability of photogrammetry to detect changes in slope surfaces with minimal error.

Despite the minor error that is inherent in photogrammetry, there were other factors that could have contributed to the elevation change. One possible factor was the placement of the GP. It was not completely glued to the surface of the ACBs, which could have resulted in some errors. Another possible factor was the natural movement of the surface caused by the swelling and shrinking properties of the topsoil. This phenomenon is often observed in slope monitoring, especially after a storm event that occurred in the week of image acquisition might cause soil to swell. While the exact cause of the error could not be fully determined, the results showed that photogrammetry can provide reliable measurements for monitoring slope surfaces.

CHAPTER 5

SUMMARY, CONCLUSION, AND RECOMMENDATION

5.1 Summary

Photogrammetry is a relatively new technique used in civil engineering and recently the application of photogrammetry in civil engineering is increasing because of its benefits in cost efficiency and other reasons. However, most of the research is concentrated on using sophisticated cameras and there is a lack of research and published documents regarding handheld cameras. Here the study tried to fill the gap by testing Canon 805D camera by using it for 3D modelling, slope monitoring, and heave measurement.

To evaluate the accuracy of photogrammetry, we conducted lab and field tests using traditional measurement methods as a comparison. In the lab, we successfully measured the heave on the surface of the soil using photogrammetry. By comparing the initial and final digital elevation models (DEMs) of the surface, the photogrammetric software was able to detect changes in the surface with a high level of accuracy. The maximum difference between the photogrammetric and dial gauge readings was only 0.08 inches, with an average difference of 0.03 inches. Additionally, the software enabled us to identify the heave pattern for different embedment depths and detect the overall movement of the soil surface with high accuracy.

In the field, we achieved successful 3D modeling of the slope with minimal error. The maximum deviation of a ground point in any direction on the east side was 0.12 feet, while on the west side, it was slightly higher, with a maximum deviation of 0.22 feet. The maximum error in distance computation was 0.14 feet on the east side and 0.34 feet on the west side. We monitored

the slope for nearly four months, and no significant movement was observed based on the four field data points collected. To test the reliability of photogrammetry, we raised a point by six inches during the final visit. The photogrammetric software detected a change in elevation of 6.4 inches and 6.9 inches, demonstrating the accuracy of photogrammetry for slope monitoring.

In short, our study provides evidence of the accuracy and potential of photogrammetry for civil engineering applications using handheld cameras.

5.2 Conclusion

After conducting laboratory and field investigations, the following conclusions can be drawn:

- Photogrammetry is an effective alternative for slope monitoring with reliable accuracy compared to traditional methods such as total station, especially with proper referencing of the site.
- Heave measurement can also be efficiently and accurately done using photogrammetry to replace traditional methods, such as dial gauges, during laboratory tests. It can detect soil surface deformation with a high accuracy of R square value of 0.99 in this study.
- Except for surface deformation measurement, the heave pattern and characteristics during pullout tests for different embedment depths can be analyzed by comparing the DEM model in the photogrammetric software, such as Metashape.
- A handheld camera such as the Canon 805D can also be used to create a 3D model with appropriate settings in photogrammetric software. This is a cost-effective solution compared to using sophisticated cameras.

However, there are some challenges that need to be considered when using photogrammetry:

- Although free photogrammetric software is available, advanced features require the purchase of software, which may not be feasible for short-term projects.
- Capturing images is challenging. The settings should remain the same throughout image capture to ensure consistency in the results.
- Lighting affects the accuracy of the results, meaning specific weather conditions, such as cloudy, are needed for capturing site photos, inconvenient for continuous monitoring.
- Some level of expertise is required for image acquisition and analysis, which can be tedious and time-consuming and cannot be carried if required immediately.

5.3 Recommendations

To further improve the usage of the photogrammetric application for soil movement, the following recommendations can be considered for future research:

- Investigate the impact of commonly used camera specifications on the accuracy of photogrammetric measurement.
- Examine the feasibility of using photogrammetry for monitoring different types of soil and soil movement such as settlement and lateral movement.
- Study the effect of camera angle and position on the accuracy of the photogrammetric measurement.

• Compare the accuracy and cost-effectiveness of photogrammetry with other monitoring techniques such as satellite imagery and laser scanning.

• Develop a comprehensive guideline for capturing images and processing them using photogrammetric software for optimal results.

• Conduct experiments to determine the best time of day to capture images for soil movement monitoring and compare the results for different weather conditions.

REFERENCES

Adams, A. (2018). The camera. Ansel Adams.

Alidoost, F., & Arefi, H. (2017). Comparison Of Uas-Based Photogrammetry Software For 3d Point Cloud Generation: A Survey Over A Historical Site. ISPRS Annals of Photogrammetry, Remote Sensing & Spatial Information Sciences, 4.

Asfaw, N. T., Lei, G., Azizian, M., Poudel, A., Hoyos, L., & Yu, X. (2023). Field Pull-Out Tests of Percussion Driven Earth Anchors (PDEAs). Applied Sciences, 13(4), 2132.

Asfaw, N. T., Azizan, M., Poudel, A., & Yu, X. Laboratory Pull-Out Test of a Percussion Driven Earth Anchor Installed in a Clayey Soil Compacted Inside a Soil Box. In Geo-Congress 2023 (pp. 281-291).

Baker, W. H., & Konder, R. L. (1966). Pullout load capacity of a circular earth anchor buried in sand. Highway Research Record, 108.

Ballesteros, R., Ortega, J. F., Hernández, D., & Moreno, M. Á. (2015). Characterization of Vitis vinifera L. canopy using unmanned aerial vehicle-based remote sensing and photogrammetry techniques. American Journal of Enology and Viticulture, 66(2), 120–129.

Balsa-Barreiro, J., & Fritsch, D. (2018). Generation of visually aesthetic and detailed 3D models of historical cities by using laser scanning and digital photogrammetry. Digital Applications in Archaeology and Cultural Heritage, 8, 57–64.

Baxter, D., Goma, S. R., & Aleksic, M. (2009). Applying image quality in cell phone cameras: lens distortion. Image Quality and System Performance VI, 7242, 389–399.

Becker, R. E., Galayda, L. J., & MacLaughlin, M. M. (2018). Digital photogrammetry software comparison for rock mass characterization. 52nd US Rock Mechanics/Geomechanics Symposium.

Bolognesi, M., Furini, A., Russo, V., Pellegrinelli, A., & Russo, P. (2014). Accuracy of cultural heritage 3D models by RPAS and terrestrial photogrammetry. The International Archives of Photogrammetry, Remote Sensing and Spatial Information Sciences, 40(5), 113.

Chowdhury, R., Flentje, P., & Bhattacharya, G. (2009). Geotechnical slope analysis. Crc Press.

Cleveland, L. J., & Wartman, J. (2006). Principles and applications of digital photogrammetry for geotechnical engineering. Site and Geomaterial Characterization, 128-135.

Elkhrachy, I. (2021). Accuracy Assessment of Low-Cost Unmanned Aerial Vehicle (UAV) Photogrammetry. Alexandria Engineering Journal, 60(6), 5579–5590. https://doi.org/https://doi.org/10.1016/j.aej.2021.04.011

Fraser, C. S., & Brown, D. C. (1986). Industrial photogrammetry: New developments and recent applications. The Photogrammetric Record, 12(68), 197–217.

Fryer, J. G., & Kniest, H. T. (1985). Errors in depth determination caused by waves in through-water photogrammetry. The Photogrammetric Record, 11(66), 745–753.

Grau, J., Liang, K., Ogilvie, J., Arp, P., Li, S., Robertson, B., & Meng, F.-R. (2021). Improved Accuracy of Riparian Zone Mapping Using Near Ground Unmanned Aerial Vehicle and Photogrammetry Method. Remote Sensing, 13(10), 1997.

Grenzdörffer, G. J., Engel, A., & Teichert, B. (2008). The photogrammetric potential of low-cost UAVs in forestry and agriculture. The International Archives of the Photogrammetry, Remote Sensing and Spatial Information Sciences, 31(B3), 1207–1214.

Grussenmeyer, P., & al Khalil, O. (2008). A comparison of photogrammetry software packages for the documentation of buildings.

Grussenmeyer, P., & Khalil, O. al. (2002). Solutions for exterior orientation in photogrammetry: a review. The Photogrammetric Record, 17(100), 615–634.

Guindon, B. (1997). Computer-based aerial image understanding: A review and assessment of its application to planimetric information extraction from very high resolution satellite images. Canadian Journal of Remote Sensing, 23(1), 38–47.

Hagerty, D. J., Spoor, M. F., & Ullrich, C. R. (1981). Bank failure and erosion on the Ohio River. Engineering Geology, 17(3), 141–158.

Hartley, R., & Zisserman, A. (2003). Multiple view geometry in computer vision. Cambridge university press.

Honarmand, M., & Shahriari, H. (2021). Geological mapping using drone-based photogrammetry: An application for exploration of vein-type Cu mineralization. Minerals, 11(6), 585.

Howland, M. D., Kuester, F., & Levy, T. E. (2014). Photogrammetry in the field: Documenting, recording, and presenting archaeology. Mediterranean Archaeology and Archaeometry, 14(4), 101–108.

Jaboyedoff, M., Oppikofer, T., Abellán, A., Derron, M.-H., Loye, A., Metzger, R., & Pedrazzini, A. (2012). Use of LIDAR in landslide investigations: a review. Natural Hazards, 61, 5–28.

Javadnejad, F., & Gillins, D. T. (2016). Unmanned aircraft systems-based photogrammetry for ground movement monitoring. In Pipelines 2016 (pp. 1000-1011).

Jensen, J. R., Hodgson, M. E., Garcia-Quijano, M., Im, J., & Tullis, J. A. (2009). A remote sensing and GIS-assisted spatial decision support system for hazardous waste site monitoring. Photogrammetric Engineering & Remote Sensing, 75(2), 169–177.

Kane, W. F., & Beck, T. J. (2000). Instrumentation practice for slope monitoring. Engineering Geology Practice in Northern California. Association of Engineering Geologists Sacramento and San Francisco Sections.

Lin, C.-S., Chen, C.-T., Wei, T.-C., Chen, W.-L., & Chang, C.-C. (2010). A positioning model of

a two CCD camera coordinate system with an alternate-four-matrix look-up table algorithm. Optics and Lasers in Engineering, 48(12), 1193–1199.

Lin, J. Y., & Shih-Hong, C. (2012). The accuracy influence of different camera calibration conditions to bundle adjsutment of closerange images. Proceedings of the 33rd Asian Conference on Remote Sensing, ACRS, 1672–1681.

Luhmann, T. (2010). Close range photogrammetry for industrial applications. ISPRS Journal of Photogrammetry and Remote Sensing, 65(6), 558–569.

Luhmann, T., Fraser, C., & Maas, H.-G. (2016). Sensor modelling and camera calibration for close-range photogrammetry. ISPRS Journal of Photogrammetry and Remote Sensing, 115, 37–46.

Luhmann, T., Robson, S., Kyle, S., & Boehm, J. (2013). Close-range photogrammetry and 3D imaging. Walter de Gruyter.

Maas, H.-G., & Hampel, U. (2006). Photogrammetric techniques in civil engineering material testing and structure monitoring. Photogrammetric Engineering and Remote Sensing, 72(1), 39.

Mandirola, M., Casarotti, C., Peloso, S., Lanese, I., Brunesi, E., Senaldi, I., Risi, F., Monti, A., & Facchetti, C. (2021). Guidelines for the use of Unmanned Aerial Systems for fast photogrammetry-oriented mapping in emergency response scenarios. International Journal of Disaster Risk Reduction, 58, 102207.

Manual, A. M. U. (2022). Professional Edition, Version 1.8. Agisoft LLC.

McWilliam, T., & Paramaguru, L. (2017). USE OF TEMPORARY ANCHORS IN REINFORCED SOIL WALL CONSTRUCTION FOR THE M4 MOTORWAY WIDENING. AUSTRALIAN GEOMECHANICS JOURNAL, 52(4), 79–88.

Nex, F., & Remondino, F. (2014). UAV for 3D mapping applications: a review. Applied Geomatics, 6, 1–15.

Parulski, K. A. (1985). Color filters and processing alternatives for one-chip cameras. IEEE Transactions on Electron Devices, 32(8), 1381–1389.

Puliti, S., Dash, J. P., Watt, M. S., Breidenbach, J., & Pearse, G. D. (2020). A comparison of UAV laser scanning, photogrammetry and airborne laser scanning for precision inventory of small-forest properties. Forestry: An International Journal of Forest Research, 93(1), 150–162.

Racek, O., Blahůt, J., & Hartvich, F. (2021). Observation of the rock slope thermal regime, coupled with crackmeter stability monitoring: initial results from three different sites in Czechia (central Europe). Geoscientific Instrumentation, Methods and Data Systems, 10(2), 203–218.

Ricolfe-Viala, C., & Sánchez-Salmerón, A.-J. (2010). Robust metric calibration of non-linear camera lens distortion. Pattern Recognition, 43(4), 1688–1699.

Rottensteiner, F., Sohn, G., Gerke, M., Wegner, J. D., Breitkopf, U., & Jung, J. (2014). Results of the ISPRS benchmark on urban object detection and 3D building reconstruction. ISPRS Journal of Photogrammetry and Remote Sensing, 93, 256–271. https://doi.org/https://doi.org/10.1016/j.isprsjprs.2013.10.004

Sagers, S., & Patterson, R. (2012). Shutter Speed in Digital Photography.

Shashi, M., & Jain, K. (2007). Use of photogrammetry in 3D modeling and visualization of buildings. ARPN Journal of Engineering and Applied Sciences, 2(2), 37–40.

Stylianidis, E., Patias, P., Tsioukas, V., Sechidis, L., & Georgiadis, C. (2003). A digital close-range photogrammetric technique for monitoring slope displacements. Proc. Of11th FIG Symp. Deform. Meas. Santorini, Greece.

Szeliski, R. (2010). Computer vision: algorithms and applications Springer Science & Business

Media.

Waltham, N. (2013). CCD and CMOS sensors. Observing Photons in Space: A Guide to Experimental Space Astronomy, 423–442.

Wang, C., Chung, J., & Lin, Y. (2015). Dem Measurements of A Gravel-Bed Surface Using Two Scales of Images. The Photogrammetric Record, 30(152), 387–401.

Wang, Q., Liu, Y., Guo, Y., Wang, S., Zhang, Z., Cui, X., & Zhang, H. (2022). A Robust and Effective Identification Method for Point-Distributed Coded Targets in Digital Close-Range Photogrammetry. Remote Sensing, 14(21). https://doi.org/10.3390/rs14215377

Westoby, M. J., Brasington, J., Glasser, N. F., Hambrey, M. J., & Reynolds, J. M. (2012). ‘'Structure-from-Motion’ Motion' photogrammetry: A low-cost, effective tool for geoscience applications. Geomorphology, 179, 300–314. https://doi.org/https://doi.org/10.1016/j.geomorph.2012.08.021

Wolf, P. R., Dewitt, B. A., & Wilkinson, B. E. (2014). Elements of Photogrammetry with Applications in GIS. McGraw-Hill Education.

Yang, C., Shropshire, G. J., & Peterson, C. L. (1997). Measurement of ground slope and aspect using two inclinometers and GPS. Transactions of the ASAE, 40(6), 1761–1776.

Zhang, H., Yang, J., Baartman, J. E. M., Li, S., Jin, B., Han, W., Yang, X., Gai, L., Ritsema, C. J., & Geissen, V. (2018). Quality of terrestrial data derived from UAV photogrammetry: A case study of Hetao irrigation district in northern China. International Journal of Agricultural and Biological Engineering, 11(3), 171–177.

Zhang, Z. (2000). A flexible new technique for camera calibration. IEEE Transactions on Pattern Analysis and Machine Intelligence, 22(11), 1330–1334.

Zhu, C., He, M., Karakus, M., Cui, X., & Tao, Z. (2020). Investigating toppling failure mechanism

of anti-dip layered slope due to excavation by physical modelling. Rock Mechanics and Rock Engineering, 53, 5029–5050.